Science and Technology of Nuclear Installations

Fast Reactors and Advanced Light Water Reactors for Sustainable Development

Guest Editors: Toshikazu Takeda, Massimo Salvatores, Giuseppe Palmiotti, Kazumi Aoto, and Katsuhisa Yamaguchi

Fast Reactors and Advanced Light Water Reactors for Sustainable Development

Science and Technology of Nuclear Installations

Fast Reactors and Advanced Light Water Reactors for Sustainable Development

Guest Editors: Toshikazu Takeda, Massimo Salvatores, Giuseppe Palmiotti, Kazumi Aoto, and Katsuhisa Yamaguchi

Editorial Board

Contents

Hindawi Publishing Corporation
Science and Technology of Nuclear Installations
Volume 2012, Article ID 373891, 2 pages
doi:10.1155/2012/373891

Editorial

Fast Reactors and Advanced Light Water Reactors for Sustainable Development

Toshikazu Takeda,[1] Massimo Salvatores,[2] Giuseppe Palmiotti,[3] Kazumi Aoto,[4] and Katsuhisa Yamaguchi[1]

[1] *Research Institute of Nuclear Engineering, University of Fukui, Tsuruga, Fukui 914-0055, Japan*
[2] *Commissariat à l'Energie Atomique de Cadarache, 13108 St. Paul-lés-Durance, France*
[3] *Idaho National Laboratory, Idaho Falls, ID 83415, USA*
[4] *Japan Atomic Energy Agency, O-arai, Ibaraki 311-1393, Japan*

Correspondence should be addressed to Toshikazu Takeda, t_takeda@u-fukui.ac.jp

Received 23 August 2012; Accepted 23 August 2012

The importance of nuclear energy, as a realistic option to solve the issues of the depletion of energy resources and the global environment, has been re-acknowledged worldwide. In response to this international movement, the papers compiling the most recent findings in the fields of fast reactors (FR) and advanced light water reactors (LWR) were gathered and published in this special issue.

This special issue compiles six articles, most of which are very meticulously performed studies of the multiyear development of design and assessment methods for large sodium-cooled FRs (SFRs), and two are related to the fuel cycle options that are leading to a greater understanding on the efficient utilization of energy resources.

The Japanese sodium-cooled fast reactor (JSFR) is addressed in two manuscripts. H. Yamano et al. reviewed the current design which adopts a number of innovative technologies in order to achieve economic competitiveness, enhanced reliability, and safety. Their safety assessments of both design basis accidents and severe accidents indicate that the devised JSFR satisfies well their risk target. T. Takeda et al. discussed the improvement of the modeling accuracy for the detailed calculation of JSFR's features in three areas: neutronics, fuel materials, and thermal hydraulics. The verification studies which partly use the measured data from the prototype FBR Monju are also described. Two of these manuscripts deal with those aspects of advanced design of SFR that have hitherto not been explored in great depth.

The paper by G. Palmiotti et al. explored the possibility of using the sensitivity methodologies in the reactor physics field. A review of the methods used is provided, and several examples illustrate the success of the methodology in reactor physics. A new application as the improvement of nuclear basic parameters using integral experiments is also described.

F. Baqué et al. reviewed the evolution of the in-service inspection and repair (ISI&R) capabilities for the SFR under development in France. Associated needs are being defined through an iterative method between designers and inspection specialists: adaptation of the SFR design to ISI&R requirements, validation of the ultrasonic transducers and associated ultrasonic nondestructive examination techniques, and validation of laser repair processes and associated robotic equipment.

F. Gao et al. and W. Ko et al. discussed how to treat the fuel cycle options for the efficient utilization of energy resources. Which type of reactor to be employed, and whether or not to adopt a reprocessing technique for spent fuel, are two key issues to be addressed. SFR and fuel recycling coupled to pyroprocessing gained considerable attention and shows promising advantages.

By compiling these papers, we hope to broaden the knowledge of our readers with respect to the presented subjects which are all of high importance for sustainable development.

Toshikazu Takeda
Massimo Salvatores
Giuseppe Palmiotti
Kazumi Aoto
Katsuhisa Yamaguchi

Hindawi Publishing Corporation
Science and Technology of Nuclear Installations
Volume 2012, Article ID 529623, 14 pages
doi:10.1155/2012/529623

Research Article

Developments in Sensitivity Methodologies and the Validation of Reactor Physics Calculations

Giuseppe Palmiotti[1] and Massimo Salvatores[2]

[1] *Nuclear Science and Engineering Division, Idaho National Laboratory, 2525 Fremont Avenue, Idaho Falls, ID 83415, USA*
[2] *CEA Cadarache, 13108 Saint-Paul-lez-Durance, France*

Correspondence should be addressed to Giuseppe Palmiotti, giuseppe.palmiotti@inl.gov

Received 25 January 2012; Revised 4 April 2012; Accepted 6 April 2012

Academic Editor: Toshikazu Takeda

The sensitivity methodologies have been a remarkable story when adopted in the reactor physics field. Sensitivity coefficients can be used for different objectives like uncertainty estimates, design optimization, determination of target accuracy requirements, adjustment of input parameters, and evaluations of the representativity of an experiment with respect to a reference design configuration. A review of the methods used is provided, and several examples illustrate the success of the methodology in reactor physics. A new application as the improvement of nuclear basic parameters using integral experiments is also described.

1. Introduction

Reactor physics calculations can be quite complex. The governing equation for neutronics is the differential-integral Boltzmann equation for neutron transport, which is a linear equation requiring the treatment of seven independent variables, three in space, two in angle, one in energy of the incident neutrons, and time. The difficulty in obtaining accurate solutions for problems in reactor core physics, shielding, and related applications is further aggravated by a number of factors. The nuclear data (i.e., the neutron cross-sections) frequently fluctuate rapidly over orders of magnitude in the energy variable. The neutron population is often sharply peaked in a particular angular direction, and those directions may vary strongly in space and energy. Finally, the geometric configurations that must be addressed are complex three-dimensional configurations, with many intricate interfaces resulting from arrays of fuel rods, coolant channels, and control rods, as well as reflectors and shielding penetrated by ducting and other irregularities. While a great deal of effort has been expended in developing computational methods to deal with these problems (they fall into two classes: Monte Carlo and deterministic), still a major hurdle exists connected with the scarce knowledge of the neutron cross sections. In the past many experiments have been performed in order to derive information that would reduce the uncertainties associated with the major neutronics design parameters. This would improve both the economical aspect of the design and the safety margins. The challenge that the reactor physicist is confronted with is how to transpose the experimental information to the reference design in order to reduce uncertainties. This has been done using several approaches including bias correcting factors, parameters that characterize systems, and data adjustment. One specific methodology, which makes use of sensitivity coefficients, has been particularly successful in reactor physics. Sensitivity coefficients are determined and assembled, using different methodologies, in a way that, when multiplied by the variation of the corresponding input parameter, they will quantify the impact on the targeted quantities whose sensitivity is referred to. Sensitivity coefficients can be used for different objectives like uncertainty estimates, design optimization, determination of target accuracy requirements, adjustment of input parameters, and evaluations of the representativity of an experiment with respect to a reference design configuration. In the following, first the theory of the methods used will be presented, and then some past applications will be shown to illustrate the remarkable success they have obtained

in the reactor physics field. Finally, some new applications will be also described as the improvement of nuclear basic parameters using integral experiments.

2. Theory

Sensitivity analysis and uncertainty evaluation are the main instruments for dealing with the sometimes scarce knowledge of the input parameters used in simulation tools [1]. For sensitivity analysis, sensitivity coefficients are the key quantities that have to be evaluated. They are determined and assembled, using different methodologies, in a way that, when multiplied by the variation of the corresponding input parameter, they will quantify the impact on the targeted quantities whose sensitivity is referred to. Sensitivity coefficients can be used for different objectives like uncertainty estimates, design optimization, determination of target accuracy requirements, adjustment of input parameters, and evaluations of the representativity of an experiment with respect to a reference design configuration.

In uncertainty evaluation, the sensitivity coefficients are multiplied by the uncertainties of the input parameters in order to obtain the uncertainty of the targeted parameter of interest. The origin and quality of the uncertainties of the input parameters can be different and vary quite a lot. In some cases, they are provided by the expert judgment of qualified designer. In some other cases more useful information is available, for instance from experimental values, and they are cast in more rigorous formalism. This is the case, for instance, of the covariance matrix for neutron cross-sections, where correlations in energy and among the different input parameters (reactions, isotopes) are also provided.

Target accuracy assessments are the inverse problem of the uncertainty evaluation. To establish priorities and target accuracies on data uncertainty reduction, a formal approach can be adopted by defining target accuracy on design parameter and finding out required accuracy on data. In fact, the unknown uncertainty data requirements can be obtained by solving a minimization problem where the sensitivity coefficients in conjunction with the existing constraints provide the needed quantities to find the solutions.

Sensitivity coefficients are also used in input parameter adjustments. In this case, the coefficients are used within a fitting methodology (e.g., least square fit and Lagrange's multipliers with most likelihood function) in order to reduce the discrepancies between measured and calculational results. The resulting adjusted input parameters can be subsequently used, sometimes in combination with bias factors, to obtain calculational results to which a reduced uncertainty will be associated.

A further use of sensitivity coefficients is, in conjunction with a covariance matrix, a representativity analysis of proposed or existing experiments. In this case the calculation of correlations among the design and experiments allows to determine how representative is the latter of the former and, consequently, to optimize the experiments and to reduce their numbers. Formally one can reduce the estimated uncertainty on a design parameter by a quantity that represents the knowledge gained by performing the experiment.

There are two main methodologies developed for sensitivity and uncertainty analysis. One is the forward (direct) calculation method based either on the numerical differentiation or on a stochastic method (Monte Carlo type), and the other is the adjoint method based on the perturbation theory and employs adjoint importance functions. In general, the forward approach is preferable when there are few input parameters that can vary and many output parameters of interest. The contrary is true for the adjoint methodology. The adjoint methodology has been the one mainly adopted in rector physics, as the source of uncertainty is mainly related to the neutron cross-sections that can represent a very notable number of variables (up to several hundred thousand). Moreover, the linear property of the Boltzmann equation makes the adjoint approach even more attractive.

2.1. Historical Notes. The perturbation theory has been introduced in reactor physics in the 50s, and one can find a classical presentation in the Weinberg and Wigner book [2] (see also [3]). This is the perturbation theory applied to the k_{eff} of the critical reactor, and Usachev gave a comprehensive development in an article published at the Geneva conference of 1955 [4].

It is interesting to note that the perturbation theory applied to reactor makes use of a definition of a function (the adjoint flux), which has a specific physical meaning if one is dealing with a nonconservative system as in the case of a nuclear reactor. This physical interpretation of the adjoint flux has been the focus of extensive studies, during the 1960s, in particular by Lewins [5, 6].

The perturbation theory, mostly developed and applied for reactivity coefficient studies, was readily used [7] for an application, sensitivity studies, which had a spectacular development in the 1970s and 1980s. This development was made possible by a generalization of the perturbation theory (thanks again to Usachev), which deals with the general problem of a variation of any kind of a neutron flux functional. Usachev derived an explicit formulation that relates the functional variation to any change of the Boltzmann operator [8].

This development and its further generalization by Gandini, to the case of any kind of linear and bilinear functional of the real and adjoint flux [9], opened a new territory for the perturbation theory. It was now possible to relate explicitly the variation of any type of integral parameter (multiplication factor, reaction rates, reactivity coefficients, source values, etc.) to any kind of change of the operator that characterizes the system.

The application of the generalized perturbation theory to real life problems led to new interesting developments that allowed clarification of specific characteristics of the new theory with implications for the computation of the generalized importance functions introduced by the theory [10].

Starting from the early 1970s, the generalized perturbation methods, which were essentially developed and used in Europe, became popular also in the rest of the world and in particular with new developments in several U.S. laboratories, ANL [11, 12] and ORNL [13], and in Japan [14].

The perturbation methods, and their main application in the field of sensitivity analysis, have been used mostly in their first-order formulation. Actually, as for any perturbation theory, the power of the method is particularly evident when one considers small perturbations (for instance, for cross-sections σ) that therefore induce little changes of the functions (e.g., the neutron flux φ), which characterize the system and for whom one can neglect the second-order product (for instance $\delta\sigma\delta\varphi$). However, there have been theoretical developments that take into accounts higher-order effects without losing all the advantages typical of the first-order formulations [15–17].

Among the theoretical developments after the 1970s that had significant practical impact, one has to mention the extension of the perturbation theory to the nuclide field that allows study of the burnup due to irradiation in the reactor at the first order [18–21] and to higher orders [22]. Subsequently, a new formulation, the "equivalent generalized perturbation theory" EGPT [23], allowed treatment, in a very simple and efficient way, of the perturbation and sensitivity analyses for reactivity coefficients.

Among the most recent development, it is worth mentioning those related to the ADS (accelerator driven systems) case with functionals that allow to calculate the sensitivity of the source importance (φ^*) and the inhomogeneous reactivity [24].

Finally, one should remember that, beside the neutronic field, there have been several studies for extending the perturbation theory developed for reactor physics to other domains (thermal-hydraulics, safety, etc.) with very interesting theoretical developments [25–28].

2.2. Sensitivity Coefficients and Perturbation Theories. The variations of any integral parameter Q due to variations of cross-sections σ can be expressed using perturbation theories [29, 30], to evaluate sensitivity coefficients S:

$$\frac{\delta Q}{Q} = \sum_j S_j \frac{\delta\sigma_j}{\sigma_j}, \tag{1}$$

where the sensitivity coefficients S_j are formally given by

$$S_j = \frac{\partial Q}{\partial \sigma_j} \cdot \frac{\sigma_j}{Q}. \tag{2}$$

For practical purposes, in the general expression of any integral parameter Q, the explicit dependence from some cross-sections (e.g., σ_i^e) and the implicit dependence from some other cross-sections (e.g., σ_j^{im}) are kept separated:

$$Q = f\left(\sigma_j^{im}, \sigma_i^e\right). \tag{3}$$

As an example, we consider a reaction rate:

$$R = \langle \underline{\sigma}^e, \underline{\Phi} \rangle, \tag{4}$$

where brackets $\langle , \rangle$ indicate integration over the phase space. In the case of a source-driven system, $\underline{\Phi}$ is the inhomogeneous flux driven by the external source and the homogeneous flux in the case of critical core studies. In (4), $\underline{\sigma}^e$ can be an energy dependent detector cross-section; R is "explicitly" dependent on the $\underline{\sigma}^e$ and "implicitly" dependent on the cross-sections which characterize the system, described by the flux $\underline{\Phi}$. In other terms, R depends on the system cross-sections via $\underline{\Phi}$. Equation (1) can be rewritten as follows:

$$\frac{\delta Q}{Q} = \sum_j S_j \frac{\delta\sigma_j^{im}}{\sigma_j^{im}} + \left(\frac{\partial Q}{\partial \sigma^e} \cdot \frac{\sigma^e}{Q}\right) \cdot \frac{\delta\sigma^e}{\sigma^e}, \tag{5}$$

where we have the hypothesis of an explicit dependence of Q on only one σ^e. If we drop the index "im",

$$\frac{\delta Q}{Q} = \sum_j S_j \frac{\delta\sigma_j}{\sigma_j} + \left(\frac{\partial Q}{\partial \sigma^e} \cdot \frac{\sigma^e}{Q}\right) \cdot \frac{\delta\sigma^e}{\sigma^e} = I + D, \tag{6}$$

where the term I is generally called "indirect" effect and the term D is called "direct" effect. While the direct effects can be obtained with explicit expressions of the derivatives of Q, the indirect effect (i.e., the sensitivity coefficients S) can be obtained with perturbation expression, most frequently at the first order [29, 30].

2.2.1. Reactivity Coefficients. A reactivity coefficient (like the Doppler effect) can be expressed as a variation of the reactivity of the unperturbed system (characterized by a value K of the multiplication factor, a Boltzmann operator M, a flux $\underline{\Phi}$, and an adjoint flux $\underline{\Phi}^*$):

$$\Delta\rho = \left(1 - \frac{1}{K_p}\right) - \left(1 - \frac{1}{K}\right) = \frac{1}{K} - \frac{1}{K_p}, \tag{7}$$

where K_p corresponds to a variation of the Boltzmann operator such that

$$\begin{aligned} M &\longrightarrow M_p\left(= M + \delta M_p\right), & \underline{\Phi} &\longrightarrow \underline{\Phi}_p\left(= \underline{\Phi} + \delta\underline{\Phi}_p\right), \\ \underline{\Phi}^* &\longrightarrow \underline{\Phi}_p^*\left(= \underline{\Phi}^* + \delta\underline{\Phi}_p^*\right), & K &\longrightarrow K_p\left(= K + \delta K_p\right). \end{aligned} \tag{8}$$

The sensitivity coefficients (at first order) for $\Delta\rho$ to variations of the σ_j are given as in [23]:

$$S_j^{\Delta\rho} = \frac{\partial(\Delta\rho)}{\partial\sigma_j} \cdot \frac{\sigma_j}{\Delta\rho} = \left\{ \frac{1}{I_f^p} \left\langle \underline{\Phi}_p^*, \sigma_j \underline{\Phi}_p \right\rangle - \frac{1}{I_f} \left\langle \underline{\Phi}^*, \sigma_j \underline{\Phi} \right\rangle \right\}, \tag{9}$$

where $I_f = \langle \underline{\Phi}^*, F\underline{\Phi} \rangle$ and $I_f^p = \langle \underline{\Phi}_p^*, F\underline{\Phi}_p \rangle$, F being the neutron fission production part of the $M(= F - A)$ operator.

2.2.2. Reactivity Rates. The classical formulations found, for example, in [29, 30], can be applied to the case of, for example, damage rate or He-production in the structures, or to the power peak factor in the core:

$$R = \langle \underline{\Phi}, \underline{\Sigma}_R \rangle. \tag{10}$$

The sensitivity coefficients are given by

$$S_j^R = \left\langle \underline{\Psi}_R^*, \sigma_j \underline{\Phi} \right\rangle, \tag{11}$$

where $\underline{\Phi}$ has been defined above, and $\underline{\Psi}_R^*$ is the solution of

$$M^* \underline{\Psi}_R^* = \underline{\Sigma}_R, \tag{12}$$

and M^* is the adjoint of the operator M. In the specific case of the power peak, this parameter can be expressed as the ratio:

$$R = \frac{\left\langle \Sigma_p \underline{\Phi} \right\rangle_{\text{MAX}}}{\left\langle \Sigma_p \underline{\Phi} \right\rangle_{\text{Reactor}}}, \tag{13}$$

with Σ_p the power cross-section, essentially represented by $E_f \cdot \Sigma_f$, E_f being the average energy released per fission. The sensitivity coefficients are defined as

$$S_j = \left\langle \underline{\Psi}^*, \sigma_j \underline{\Phi} \right\rangle, \tag{14}$$

and $\underline{\Psi}^*$ is the importance function solution of

$$M^* \underline{\Psi}^* = \frac{\Sigma_{p,\text{MAX}}}{\left\langle \Sigma_p \underline{\Phi} \right\rangle_{\text{MAX}}} - \frac{\Sigma_{p,\text{Reactor}}}{\left\langle \Sigma_p \underline{\Phi} \right\rangle_{\text{Reactor}}}, \tag{15}$$

where $\Sigma_{p,\text{MAX}}$ is the Σ_p value at the spatial point, where $< \Sigma_p \underline{\Phi} > \equiv < \Sigma_p \underline{\Phi} >_{\text{MAX}}$, and $\Sigma_{p,\text{Reactor}}$ is the Σ_p value at each spatial point of the reactor. In (15) effects due to $\Sigma_{p,\text{MAX}}$ and $\Sigma_{p,\text{Reactor}}$ variations are assumed to be negligible.

2.2.3. Nuclide Transmutation. The generic nuclide K transmutation during irradiation can be represented as the nuclide density variation between time t_0 and t_F. If we denote n_{Fi}^K the "final" density, the appropriate sensitivity coefficient is given by

$$S_j^K = \frac{\partial n_F^K}{\partial \sigma_j} \cdot \frac{\sigma_j}{n_F^K} = \frac{1}{n_F^K} \int_{t_0}^{t_F} \underline{n}^* \sigma_j \underline{n} \, dt, \tag{16}$$

where the time-dependent equations to obtain $\underline{n}^*$ and $\underline{n}$, together with their boundary conditions, are defined in [18–21]

Uncertainty Analysis, Experiment Representativity, and Target Accuracy Assessment. Uncertainty evaluation and experiment representativity factors are computed in ERANOS with covariance matrices provided in different general formats. The uncertainties associated to the cross-section can be represented in the form of a variance-covariance matrix:

$$D_\sigma = \begin{pmatrix} d_{11} & d_{12} & \cdots & d_{1J} \\ d_{12} & d_{22} & \cdots & d_{2J} \\ \cdots & \cdots & \cdots & \cdots \\ d_{1J} & d_{2J} & \cdots & d_{JJ} \end{pmatrix}, \tag{17}$$

where the elements d_{ij} represent the expected values related to the parameters σ_j and σ_i.

The variance of Q can then be obtained as

$$\text{var}(Q) = \sum_{j \cdot i}^{J} S_j S_i d_{ij}. \tag{18}$$

In order to plan for specific experiments able to reduce uncertainties on selected design parameters, a formal approach, initially proposed by Usachev and Bobkov [31], has been applied by Palmiotti and Salvatores [32] and further developed in by Gandini [33].

In the case of a reference parameter R, once the sensitivity coefficient matrix S_R and the covariance matrix D are available, the uncertainty on the integral parameter can be evaluated by the equation:

$$\Delta R_0^2 = S_R^+ D' S_R. \tag{19}$$

We can consider an integral experiment conceived in order to reduce the uncertainty ΔR_0^2. Let us indicate by S_E the sensitivity matrix associated with this experiment. If we give "representativity factor" the following expression:

$$r_{RE} = \frac{(S_R^+ D S_E)}{\left[(S_R^+ D S_R)(S_E^+ D S_E) \right]^{1/2}}, \tag{20}$$

it can be shown [31] that the uncertainty on the reference parameter R_0 is reduced by

$$\Delta R_0'^2 = \Delta R_0^2 \cdot (1 - r_{RE}^2). \tag{21}$$

If more than one experiment is available, (21) can be generalized. In the case of two experiments, characterized by sensitivity matrices S_{E1} and S_{E2}, the following expression [33] can be derived:

$$\Delta R_0'^2 = S_R^+ D' S_R = \Delta R_0^2 \left[1 - \frac{1}{1 - r_{12}^2} (r_{R1} - r_{R2})^2 - \frac{2}{1 + r_{12}} r_{R1} r_{R2} \right], \tag{22}$$

where D' is the new covariance matrix and

$$r_{12} = \frac{(S_{E1}^+ D S_{E2})}{\left[(S_{E1}^+ D S_{E1})(S_{E2}^+ D S_{E2}) \right]^{1/2}},$$
$$r_{R1} = \frac{(S_R^+ D S_{E1})}{\left[(S_R^+ D S_R)(S_{E1}^+ D S_{E1}) \right]^{1/2}}, \tag{23}$$
$$r_{R2} = \frac{(S_R^+ D S_{E2})}{\left[(S_R^+ D S_R)(S_{E2}^+ D S_{E2}) \right]^{1/2}}.$$

The approach outlined here can be used to plan optimized integral experiments to reduce uncertainties on a set of integral parameters of a reference system.

A successive step is the assessment of target accuracy requirements. Target accuracy assessment [32] is the inverse problem of the uncertainty evaluation. To establish priorities and target accuracies on data uncertainty reduction, a formal approach can be adopted by defining target accuracy on design parameters and finding out required accuracy on data in order to meet them. In fact, the unknown uncertainty

data requirements can be obtained by solving a minimization problem where the sensitivity coefficients in conjunction with the constraints on the integral parameters provide the needed quantities for finding the solutions.

The unknown uncertainty data requirements d_i can be obtained by solving the following minimization problem for the functional Q:

$$Q = \sum_i \frac{\lambda_i}{d_i^2} = \min \quad i = 1 \cdots I, \tag{24}$$

with the following constraints:

$$\sum_i S_{ni}^2 d_i^2 + \sum_{ii'} S_{ni} d_i \mathrm{Corr}_{ii'} d_{i'} S_{ni'} \le \left(R_n^T\right)^2 \quad n = 1 \cdots N, \tag{25}$$

where N is the total number of integral design parameters, S_{ni} are the sensitivity coefficients for the integral parameter R_n, and R_n^T are the required target accuracies on the N integral parameters, λ_i are "cost" parameters related to each σ_i and should give a relative figure of merit of the difficulty of improving that parameter (e.g., reducing uncertainties with an appropriate experiment), and $\mathrm{Corr}_{ii'}$ are the correlation values between variable i and i'.

2.2.4. Data Assimilation. Uncertainty and sensitivity analysis can be used to effectively combine nuclear data covariance information, integral experiments, their "representativity," and their associated experimental uncertainties in order to reduce a priori uncertainties on performance parameters (like k_{eff} or reactivity coefficients) that characterize a reference design configuration. Several approaches (usually called "bias factor" methods; see, e.g., [33]) have been attempted. A more rigorous approach is the so-called data assimilation (called also adjustment, calibration, tuning).

If we define B_p the "a priori" nuclear data covariance matrix and S_B the sensitivity matrix of the performance parameters $B(B = 1 \cdots B_{\mathrm{TOT}})$ to the J nuclear data, the "a priori" covariance matrix of the performance parameters is given by

$$B_B = S_B B_p S_B^T. \tag{26}$$

It can be shown that, using a set of I integral experiments A characterized by a sensitivity matrix S_A, beside a set of statistically adjusted cross-section data, a new ("a posteriori") covariance matrix $\widetilde{B}_p$ can be obtained (see, e.g., [34]):

$$\widetilde{B}_p = B_p - B_p S_A^T \left(S_A B_p S_A^T + B_A\right)^{-1} S_A B_p, \tag{27}$$

where B_A is the integral experiment uncertainty matrix. In the case of I experiments $(i = 1 \cdots I)$:

$$B_A = \begin{vmatrix} b_{11} & b_{12} & \cdots & b_{1I} \\ b_{21} & b_{22} & & \\ \vdots & & \ddots & \\ b_{I1} & & & b_{II} \end{vmatrix}, \tag{28}$$

(b_{ii} are the experimental uncertainties of each experiment i) and S_A is the sensitivity matrix of the I experiments to the J nuclear parameters (cross-sections by energy group, isotope, and reaction type):

$$S_A = \begin{vmatrix} s_{11} & s_{12} & \cdots & s_{1J} \\ s_{21} & s_{22} & & \\ \vdots & & \ddots & \\ s_{I1} & & & s_{IJ} \end{vmatrix}. \tag{29}$$

This matrix can then be used to define a new ("a posteriori") covariance matrix $\widetilde{B}_B$ for the performance parameters:

$$\begin{aligned} \widetilde{B}_B = S_B \widetilde{B}_p S_B^T &= \left\{ B_B - S_B B_p S_A^T \left(S_A B_p S_A^T + B_A\right)^{-1} S_A B_p S_B^T \right\} \\ &= B_B \left\{ 1 - \left(S_B B_p S_B^T\right)^{-1} \left(S_A B_p S_A^T + B_A\right)^{-1} \right. \\ &\qquad \left. \times \left(S_A B_p S_B^T\right)^2 \right\}. \end{aligned} \tag{30}$$

If we consider only one performance parameter B and only one experiment "i" and if we put $B_A = 0$, we obtain from (26) the expression of the "representativity" of one integral experiment, as defined in [32]:

$$r_{iB} = \frac{\left(S_B B_p S_i^T\right)}{\left[\left(S_i B_p S_i^T\right)\left(S_B B_p S_B^T\right)\right]^{1/2}}. \tag{31}$$

Then, we can consider (30) as a generalized expression for the reference parameter uncertainty reduction as given in [32]. This generalized expression accounts for more than one experiment and allows estimating the impact of any new experiment in the reduction of the "a priori" uncertainty of the design performance parameters [35].

In fact, we can define an "assimilated" representativity factor that characterizes the uncertainty reduction obtained through the assimilation process. Let us first define the uncertainties on an integral parameter (e.g., K_{eff}) for a specific design target system (e.g., a reactor to be designed) using the nuclear data covariances before, B_p, and after, $\widetilde{B}_p$, assimilation:

$$\begin{aligned} \Delta R_0^2 &= S_R^+ B_p S_R, \\ \Delta R_0'^2 &= S_R^+ \widetilde{B}_p S_R; \end{aligned} \tag{32}$$

then using (21) we can derive the "assimilated" representativity factor r_{RE}^{2A} associated with the assimilation process:

$$r_{RE}^{2A} = 1 - \frac{\Delta R_0'^2}{\Delta R_0^2}. \tag{33}$$

If we define the uncertainty reduction factor UR as,

$$\mathrm{UR} = \frac{\Delta R_0}{\Delta R_0'}, \tag{34}$$

we can obtain using (33)

$$r_{RE}^{A} = \sqrt{1 - \frac{1}{\mathrm{UR}^2}}. \tag{35}$$

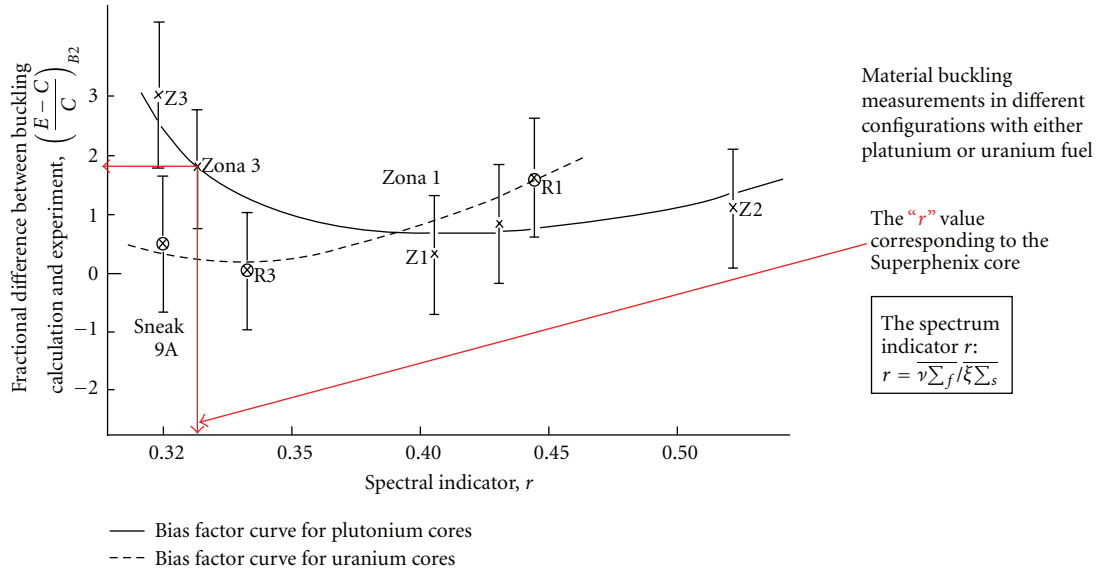

FIGURE 1: $(E - C)/C$ trend following the spectrum indicator r for different experiments.

3. An Example from the Past: Superphenix

In the 1960s and 1970s, there has been the development in France of a "practical" (and powerful) method of nuclear data assimilation (or adjustment) and bias factors assessment together with associated uncertainties. The method was based on the following steps.

(i) Conceive and perform simple, "clean" integral experimental configurations in zero-power critical assemblies, each of them characterized by a meaningful parameter "r" (as a "spectrum indicator"). In each configuration, several integral parameters i (e.g., K_{eff}, critical buckling, reaction rate ratios, etc.) are measured.

(ii) The observed experimental to calculation ratio E_i/C_i for each specific integral parameter was interpreted in terms of nuclear data statistical adjustments (see later).

(iii) The adjusted data are associated to a new calculated value C_i' Residual E_i/C_i' values are displayed as function of the "r" parameter (see Figure 1).

(iv) The reference design core is also characterized by a specific value of "r". Its integral parameters R are calculated with the adjusted nuclear data.

(v) Deduction by interpolation (see Figure 1) of the expected E_R/C_R' on the reference design core and use of it as "bias factor" for the calculated value of the reference design core parameter C_R.

In Europe, this approach was preferred to the "mock-up" approach, mainly used in the USA.

A milestone was reached in 1984 when this approach allowed prediction of the critical mass of Superphenix to approximately 3 (out of ~300) subassemblies (corresponding to ~0.3% $\Delta k/k$).

4. Target Accuracy Requirements: The OECD/NEA Subgroup 26

The first and most significant recent initiative aiming to a systematic nuclear data uncertainty impact assessment was taken by the Working Party on Evaluation Cooperation (WPEC) of the OECD Nuclear Energy Agency Nuclear Science Committee when it established a subgroup (called 26) to develop a systematic approach to define data needs for advanced reactor systems and to make a comprehensive study of such needs for Generation-IV (Gen-IV) reactors. This subgroup was established at the end of 2005, and a final report was published in 2008 [36]. A comprehensive sensitivity and uncertainty study was performed to evaluate the impact of neutron cross-section uncertainty on the most significant integral parameters related to the core and fuel cycle of a wide range of innovative systems, even beyond the Gen-IV range of systems. In particular, results have been obtained for the sodium-cooled advanced breeder reactor (ABR), the sodium-cooled low conversion ratio fast reactor (SFR), the sodium-cooled European fast reactor (EFR), the gas-cooled fast reactor (GFR), the lead-cooled fast reactor (LFR), and the accelerator driven lead-cooled minor actinide burner (ADMAB). These systems correspond to current studies within the Generation-IV initiative, the advanced fuel cycle initiative (AFCI), and the advanced fuel cycle and partitioning/transmutation studies in Japan and Europe.

The integral parameter uncertainties were initially calculated using covariance data developed in a joint effort of several laboratories contributing to the subgroup activity. This set of covariance matrices was referred to as BOLNA [37].

The calculated integral parameter uncertainties, resulting from the initially assessed uncertainties on nuclear data of the BOLNA set were found rather acceptable for the early phases of design feasibility studies. In fact, the uncertainty

Table 1: Summary of highest-priority target accuracies for fast reactors from subgroup 26.

	Energy range	Current (BOLNA) Accuracy (%)	Target accuracy (%)
σ_{inel}	6.07 ÷ 0.498 MeV	10 ÷ 20	2 ÷ 3
σ_{capt}	24.8 ÷ 2.04 keV	3 ÷ 9	1.5 ÷ 2
σ_{fiss}	1.35 MeV ÷ 454 eV	8 ÷ 20	2 ÷ 3 (SFR, GFR, LFR) 5 ÷ 8 (ABTR, EFR)
σ_{capt}	498 ÷ 2.04 keV	7 ÷ 15	4 ÷ 7
σ_{fiss}	1.35 ÷ 0.498 MeV	6	1.5 ÷ 2
ν	1.35 ÷ 0.498 MeV	4	1 ÷ 3
σ_{fiss}	2.23 ÷ 0.498 MeV	19 ÷ 21	3 ÷ 5
σ_{fiss}	1.35 ÷ 0.183 MeV	17	3 ÷ 5
σ_{fiss}	1.35 MeV ÷ 67.4 keV	17	3 ÷ 4
σ_{fiss}	6.07 ÷ 2.23 MeV	12	3
σ_{fiss}	1.35 ÷ 0.498 MeV	50	5
σ_{fiss}	183 ÷ 67.4 keV	47	7
σ_{fiss}	2.23 ÷ 0.498 MeV	16 ÷ 25	3 ÷ 6
σ_{fiss}	1.35 ÷ 0.498 MeV	28	4 ÷ 10
σ_{fiss}	2.23 ÷ 1.35 MeV	14	3
σ_{fiss}	1.35 ÷ 0.498 MeV	11	3
σ_{fiss}	6.07 ÷ 1.35 MeV	14 ÷ 50	3 ÷ 6
σ_{fiss}	19.6 ÷ 6.07 MeV	53	6

on k_{eff} was found to be less than 2% for all systems (with the exception of the ADS) and reactivity coefficient uncertainties below 20%. Power distributions uncertainties are also relatively small, except in the case of the ADS.

However, later conceptual and design optimization phases of selected reactor and fuel cycle concepts will need improved data and methods in order to reduce margins, both for economical and safety reasons. For this purpose, a compilation of preliminary "Design Target Accuracies" was put together, and a target accuracy assessment was performed to provide an indicative quantitative evaluation of nuclear data improvement requirements by isotope, nuclear reaction, and energy range in order to meet the Design Target Accuracies. First priorities were formulated on the basis of common needs for fast reactors and, separately, thermal systems. These priority items (see Table 1) were included in the High Priority Request List (HPRL) of the OECD-NEA Data Bank.

5. A More Recent Example of Data Assimilation

The purpose of the work performed in this example [38] was to provide a first series of guidelines to improve methods and data used in the preliminary study of a sodium-cooled fast spectrum "advanced burner" reactor, as defined within the GNEP initiative and the AFCI program [39]. The reference 1000 MWt ABR core concepts were developed with ternary metal and mixed oxide fuels. Compact core concepts of medium TRU conversion ratio (~0.8 for the start-up core and ~0.7 for the recycled equilibrium core) were developed by tradeoff between the burn-up reactivity loss and the TRU conversion ratio. Two enrichment zones are used for the metal core, whereas three enrichment zones are used for the oxide core. In both cases, there is a steel reflector surrounding the core and no fertile blanket.

The selected integral experiments should meet a series of requirements: (a) low and well-documented experimental uncertainties, (b) enabling to separate effects (e.g., capture and fission), and (c) allowing validating global energy- and space-dependent effects.

As for the point (b) above, irradiation experiments, in particular of separate isotope samples, allow very significant information on capture data, while fission rate experiments in well-characterized spectra provide high-accuracy information on fission data. As for the point (c), the global energy validation should be envisaged using as far as possible "representative" experiments, according to the definition given below, while specific spatial effects (as reflector effects in the ABR cores) should be singled out with appropriate experiments (e.g., experiments with or without blankets, to underline possible specific effects due to the presence of a steel reflector).

A series of experiments following the indicated requirements was selected to the purpose of reducing the current uncertainties on the targeted cores (ABR with metal or oxide fuels). Table 2 shows the list of significant experiments that have been chosen in the present study together with the main integral parameters that have been measured and that have been calculated. These experiments allow covering a wide range of fuel types, including the reference system

Table 2: List of integral experiments to be used in the statistical adjustment.

Experiment	Parameter to be analyzed			Fuel type	Pu/(U + Pu)
	Critical mass	Reaction rates	Irradiation experiment		
GODIVA	Yes	Yes	—	U metal	0.0
JEZEBEL^{239}	Yes	Yes	—	Pu metal	1.0
JEZEBEL^{240}	Yes	—	—	Pu metal	1.0
ZPR-3/53	Yes	Yes	—	PuC-UC	0.42
ZPR-3/54	Yes	Yes	—	PuC-UC	0.42
ZPPR-15	Yes	Yes		Pu-U metal	0.13
COSMO[a]	—	Yes	—	PuO_2-UO_2	0.27
CIRANO[a]	Yes	-s	—	PuO_2-UO_2	0.27
PROFIL[b]	—	—	Yes	PuO_2-UO_2	0.27
TRAPU[b]	—	—	Yes	PuO_2-UO_2	0.27

[a] Experiments performed in the MASURCA facility.
[b] Irradiation experiments performed in the Phenix reactor.

fuels (oxide, metal): a wide range of Pu/(Pu + U) ratios and corresponding spectrum types (including both fission spectrum-type experiments and softer spectra), separated capture (PROFIL irradiation experiments in PHENIX, [40]) and fission rate effects for TRU (COSMO fission rate experiments, [41]), combined capture and fission effects (TRAPU irradiated fuels in PHENIX with different Pu vectors), and finally reflector versus blanket effects (ZPR3-53 with blanket and ZPR3-54 with reflector, CIRANO with reflector [42]).

As far as representativity, we considered a range of different ZPPR and ZPR experiments, in particular assemblies ZPPR-2, ZPPR-9, and ZPR6-7 with Pu oxide fuel, ZPPR-15 with Pu metal fuel, and ZPR6-6 with enriched UO_2 fuel. We performed a representativity study on the criticality of these experiments with respect to the two ABR cores. We added, for comparison purposes, the ZPR3-53 and 54 experiments. The results shown in Table 3 indicate that the ZPPR-15 experiment is the best suited to "represent" both ABR reference cores and that the other cores will not add significant information. In fact if we consider the extra information brought by, for example, ZPPR-9 with respect to ZPPR-15, we find, using (20), that adding ZPPR-9 there is only a very limited impact on the ABR k_{eff} uncertainty reduction, since the r_{12} value relative to ZPPR-15 and ZPPR-9 is too close to 1 (0.978).

Table 4 gives the *C/E* values with associated uncertainties before and after adjustment for the 44 integral experiments used in this study. The first remark is that ENDF/B-VII performs in general rather well. However, for a number of parameters (higher Pu isotopes and some minor actinides), there is a clear need for substantial improvements.

After adjustment, the "a posteriori" *C/E*s show a definite improvement, and with a few exceptions all residual calculation versus experiment discrepancies are reduced within the "a posteriori" experimental uncertainties. To obtain this result and in order to obtain a statistically sound adjustment (i.e., as indicated by a χ^2 test), it has been necessary in very few cases to modify (i.e., increase) the diagonal uncertainty values of the BOLNA covariance matrix for a specific reaction of a specific isotope.

Table 3: Representativity factors for k_{eff}.

Experiment	ABR metal	ABR oxide
ZPPR-15	0.814	0.738
ZPPR-2	0.780	0.740
ZPPR-9	0.796	0.723
ZPR3-53	0.435	0.434
ZPR3-54	0.065	0.115
ZPR6-6	0.190	0.175
ZPR6-7	0.792	0.739

After the adjustment we have applied the new cross-section covariance matrix to evaluate the "a posteriori" uncertainty on the k_{eff} of the two reference systems (ABR with metal or oxide fuel). The results are given in Table 5. The uncertainty on the k_{eff} of two reference ABR configurations is reduced significantly, from ~1.5% to ~0.6% in both cases. One interesting ancillary result is given by the "assimilated" representativity factors. As reported in Table 5 they are significantly higher than those of Table 3 and indicate the global representativity of the 44 experiments used in the data assimilation process with respect to the target systems for the K_{eff} parameter. As for the nuclear-data-related uncertainty, it is possible to further reduce the value obtained here (~0.6%), by including in the adjustment more nuclear data (e.g., more structural material data) and including few more integral experiments, carefully selected for that purpose and using more extensively the "representativity" approach outlined previously.

Finally, it is interesting to note that the proposed adjustment will reduce uncertainties not only of the k_{eff} but also uncertainties on the local TRU nuclide densities after irradiation and, as a consequence, the uncertainty on the reactivity loss per cycle.

Table 4: C/E and associated uncertainties (σ) before and after adjustment.

Type of experiment	Old $C/E \pm \sigma$	New $C/E \pm \sigma$	Type of experiment	Old $C/E \pm \sigma$	New $C/E \pm \sigma$
U235 Capture PROFIL1[a]	0.977 ± 0.020	1.009 ± 0.009	Cm244 TRAPU2[b]	0.872 ± 0.023	0.978 ± 0.021
U238 Capture PROFIL1[a]	1.004 ± 0.023	1.005 ± 0.010	U238 Fission Rate COSMO[c]	0.988 ± 0.015	1.006 ± 0.010
Pu238 Capture PROFIL2[a]	1.744 ± 0.040	1.015 ± 0.036	Np237 Fission Rate COSMO[c]	0.960 ± 0.015	0.979 ± 0.011
Pu239 (N,2N) PROFIL1[a]	0.752 ± 0.150	0.949 ± 0.133	Pu238 Fission Rate COSMO[c]	1.083 ± 0.025	1.005 ± 0.023
Pu239 Capture PROFIL1[a]	0.963 ± 0.030	1.021 ± 0.015	Pu239 Fission Rate COSMO[c]	0.983 ± 0.013	0.984 ± 0.003
Pu240 Capture PROFIL1[a]	1.001 ± 0.022	0.995 ± 0.013	Pu240 Fission Rate COSMO[c]	1.034 ± 0.023	1.016 ± 0.016
Pu241 Capture PROFIL1[a]	0.847 ± 0.041	0.871 ± 0.013	Pu241 Fission Rate COSMO[c]	0.998 ± 0.020	1.013 ± 0.017
Pu242 Capture PROFIL1[a]	1.092 ± 0.035	1.128 ± 0.019	Pu242 Fission Rate COSMO[c]	1.000 ± 0.023	1.002 ± 0.022
Am241 Capture PROFIL1[a]	1.000 ± 0.020	1.003 ± 0.015	Am241 Fission Rate COSMO[c]	1.074 ± 0.023	1.003 ± 0.022
Np237 Capture PROFIL2[a]	0.988 ± 0.036	1.009 ± 0.022	Am243 Fission Rate COSMO[c]	1.059 ± 0.023	1.008 ± 0.021
U236 TRAPU2[b]	0.965 ± 0.010	0.995 ± 0.009	k_{eff} GODIVA[d]	1.000 ± 0.001	0.999 ± 0.001
Np237 TRAPU2[b]	0.880 ± 0.033	0.954 ± 0.026	U238 Fission Rate GODIVA[d]	0.955 ± 0.012	0.965 ± 0.004
Pu238 TRAPU2[b]	0.942 ± 0.010	1.000 ± 0.006	Np237 Fission Rate GODIVA[d]	0.991 ± 0.016	1.003 ± 0.010
Pu239 TRAPU2[b]	1.006 ± 0.005	1.001 ± 0.004	Pu239 Fission Rate GODIVA[d]	0.986 ± 0.017	0.987 ± 0.003
Pu240 TRAPU2[b]	0.982 ± 0.006	1.000 ± 0.006	k_{eff} JEZEBEL9[e]	1.000 ± 0.002	1.001 ± 0.001
Pu241 TRAPU1[b]	1.005 ± 0.006	1.001 ± 0.003	U238 Fission Rate JEZEBEL9[e]	0.974 ± 0.009	0.984 ± 0.004
Pu242 TRAPU1[b]	0.998 ± 0.008	1.012 ± 0.004	Np237 Fission Rate JEZEBEL9[d]	1.009 ± 0.017	1.021 ± 0.010
Am241 TRAPU2[b]	0.985 ± 0.039	0.986 ± 0.005	k_{eff} JEZEBEL0[e]	1.000 ± 0.002	0.999 ± 0.002
Am242 TRAPU2[b]	1.029 ± 0.043	1.032 ± 0.013	k_{eff} CIRANO[f]	1.007 ± 0.002	1.002 ± 0.001
Am243 TRAPU1[b]	0.939 ± 0.026	0.974 ± 0.020	k_{eff} ZPPR-15	0.999 ± 0.002	0.999 ± 0.001
Cm242 TRAPU1[b]	1.003 ± 0.039	0.971 ± 0.013	k_{eff} ZPR-3/53	1.009 ± 0.002	1.001 ± 0.001
Cm243 TRAPU2[b]	0.462 ± 0.031	0.999 ± 0.031	k_{eff} ZPR-3/54	1.008 ± 0.002	1.000 ± 0.001

Isotope A/B atom density ratio at the end of irradiation of a sample of isotope A.
[a]Isotope atom density at the end of irradiation of TRAPU fuel pins with different initial Pu vectors.
[b]Normalized fission rates and k_{eff} in the COSMO critical experiment at MASURCA.
[c]JEZEBEL9: Pu-239 Sphere.
[d]JEZEBEL0: Pu-239 Sphere with high Pu-240 content.
[e]k_{eff} of the critical experiment CIRANO (high Pu content) at MASURCA.

6. The New Approach: Consistent Data Assimilation

The major drawback of the classical adjustment method is the potential limitation of the domain of application of the adjusted data since adjustments are made on multigroup data, and the multigroup structure, the neutron spectrum used as weighting function, and the code used to process the basic data file are significant constraints.

A new approach [43] has been developed in order to adjust physical parameters and not multigroup nuclear data, the objective being now to correlate the uncertainties of some basic parameters that characterize the neutron cross-section description, to the discrepancy between calculation and experimental value for a large number of clean, high-accuracy integral experiments.

This new approach is the first attempt to build up a link between the wealth of precise integral experiments and basic theory of nuclear reactions. A large amount of exceptionally precise integral measurements has been accumulated over last 50 years. These experiments were driven by the necessities of nuclear applications but were never fully exploited for improving predictive power of nuclear reaction theory. Recent advances in nuclear reaction modeling and neutron transport calculations, combined with sensitivity analyses methods, offer a reasonable possibility of deconvoluting results of the integral experiments in a way to obtain feedback on parameters entering nuclear reaction models. Essential ingredients of such a procedure will be covariances for model parameters and sensitivity matrices. The latter will provide direct link between reaction theory and integral experiments. By using integral reactor physics experiments (meter scale), information is propagated back to the nuclear level (femtometers) covering a range of more than 13 orders of magnitude.

The assimilation procedure results in more accurate and more reliable evaluated data files that will be of universal validity rather than tailored to a particular application. These files will naturally come with cross-section covariances incorporating both microscopic and integral measurements as well as constrains imposed by the physics of nuclear reactions. Thus, these covariances will encompass the entire relevant knowledge available at the time of evaluation.

On the physics side, the assimilation improves knowledge of model parameters, increasing the predictive power of nuclear reaction theory, and it would bring a new quality into nuclear data evaluation as well as refinements in nuclear reaction theory.

Table 5: k_{eff} Uncertainties (pcm) calculated with BOLNA and adjusted covariance.

Reactor	BOLNA (current)	Adjusted covariance	"Assimilated" represent
ABR Oxide	1438.7	639.1	0.896
ABR Metal	1460.4	638.7	0.899

6.1. Consistent Data Assimilation Approach. The classical "statistical adjustment" techniques [34] provide adjusted multigroup nuclear data for applications, together with new, improved covariance data and reduced uncertainties for the required design parameters, in order to meet target accuracies.

One should, however, set up a strategy to cope with the drawbacks of the methodology, which are related to the energy group structure and energy weighting functions adopted in the adjustment.

In fact, the classical statistical adjustment method can be improved by "adjusting" reaction model parameters rather than multigroup nuclear data. The objective is to associate uncertainties of certain model parameters (such as those determining neutron resonances, optical model potentials, level densities, and strength functions) and the uncertainties of theoretical nuclear reaction models themselves (such as optical model, compound nucleus, preequilibrium, and fission models) with observed discrepancies between calculations and experimental values for a large number of integral experiments.

The experiments should be clean (i.e., well documented with high QA standards) and high accuracy (i.e., with as low as possible experimental uncertainties and systematic errors), and carefully selected to provide complementary information on different features and phenomena, for example, different average neutron spectrum energy, different adjoint flux shapes, different leakage components in the neutron balance, different isotopic mixtures and structural materials.

In the past, a few attempts were made [44–46] to apply a consistent approach for improving basic nuclear data, in particular to inelastic discrete levels and evaporation temperatures data of ^{56}Fe for shielding applications, and to resolved resonance parameters of actinides (e.g., Γ and total widths and peak positions). This effort indicated not only the validity of the approach but also challenges to be overcome for its practical application. This was mainly related to the way of getting the sensitivity coefficients and to the need of reliable covariance information.

The consistent data assimilation methodology allows overcoming both difficulties, using the approach that involves the following steps.

(i) Selection of the appropriate reaction mechanisms along with the respective model parameters to reproduce adopted microscopic cross section measurements with the EMPIRE [47] code calculations. Use of coupled channels, quantum-mechanical preequilibrium theories, and advanced statistical model accounting for width fluctuations and full gamma cascade ensures state of the art modelling of all relevant reaction mechanisms.

(ii) Determination of covariance matrices for the set of nuclear reaction model parameters obtained in the previous step. This is achieved by combining initial estimates of parameter uncertainties, with uncertainties/covariances for the adopted experimental data through the KALMAN [48] code. This way, the resulting parameter covariances will contain constraints imposed by nuclear reaction theory and microscopic experiments. Several parameters have been considered, including resonance parameters for a few dominating resonances, optical model parameters for neutrons, level density parameters for all nuclei involved in the reaction, parameters entering preequilibrium models, and parameters determining gamma-strength functions.

(iii) Sensitivity of cross-sections to the perturbation of the above-mentioned reaction model parameters are calculated with the EMPIRE code.

(iv) Use of the adjoint technique to evaluate sensitivity coefficients of integral reactor parameters to the cross-section variations, as described in the previous step. To perform this task, the ERANOS code system [49], which computes sensitivity coefficients based on generalized perturbation theory, is employed.

(v) Performing analysis of selected experiments using the best calculation tools available (in general Monte Carlo codes like MCNP).

(vi) Performing consistent data assimilation on basic nuclear parameters using integral experiment analysis with best methodology available to provide discrepancies between calculation and measured quantities. After the C/Es are available, they are used together with the sensitivity coefficients coming from the previous step in a data assimilation code.

(vii) Constructing new ENDF/B type data files based on modified reaction theory parameters for use by neutronic designers.

6.2. Evaluation of Nuclear Physics Parameter Covariances. As indicated in the outline of the methodology, the first step is to provide estimated range of variation of nuclear physics parameters, including their covariance data. To this end the code EMPIRE [47] coupled to the KALMAN [48] code is employed.

KALMAN code is an implementation of the Kalman filter technique based on minimum variance estimation. It naturally combines covariances of model parameters, of experimental data and of cross-sections. This universality is

a major advantage of the method. KALMAN uses measurements along with their uncertainties to constrain covariances of the model parameters via the sensitivity matrix. Then, the final cross-section covariances can be calculated from the updated covariances for model parameters. This procedure consistently accounts for the experimental uncertainties and the uncertainties of the nuclear physics parameters. We emphasize that, under the term "reaction model," we mean also the resonance region described by models such as the multilevel Breit-Wigner formalism.

6.3. Evaluation Sensitivity Coefficients for Integral Experiments. In order to evaluate the sensitivity coefficients of the nuclear parameters to the integral parameters measured in a reactor physics experiment, a folding procedure is applied, where the sensitivities calculated by EMPIRE are folded with those calculated by ERANOS (i.e, multigroup cross-section sensitivity coefficient to integral parameters).

Following this procedure, the sensitivities of integral experiments to nuclear parameters p_k are defined as

$$\frac{\Delta R}{\Delta p_k} = \sum_j \frac{\Delta R}{\Delta \sigma_j} \times \frac{\Delta \sigma_j}{\Delta p_k}, \tag{36}$$

where R is an integral reactor physics parameter (e.g., K_{eff}, reaction rates, and reactivity coefficient) and σ_j a multigroup cross section (the j index accounts for isotope, cross section type, and energy group).

In general to compute σ_j one can use (a) EMPIRE with an appropriate set of parameters p_k to generate first (b) an ENDF/B file for that specific isotope and, successively, (c) to use NJOY, to obtain multigroup cross sections.

As specified in the previous section, one can compute the variation of the cross sections $\Delta\sigma_j$ resulting from a variation of each parameter p_k variation.

Specifically, the procedure would consist in the generation of the $\Delta\sigma_j$ corresponding to fixed, well-chosen variations of each p_k taken separately and therefore generating the $\Delta\sigma_j/\Delta p_k$. Following each EMPIRE calculation, an ENDF/B file for the isotope under consideration is generated and a subsequent run of NJOY on this file generates multigroup cross sections in the same energy structure used for the computation of the reactor physics integral parameters. The multigroup cross section variations associated to the individual fundamental parameter that has been varied in the corresponding EMPIRE calculation are readily computed by difference with the reference NJOY calculation for the isotope under consideration.

In parallel, the cross section sensitivity coefficients to integral parameter R,

$$\frac{\Delta R}{\Delta \sigma_j}, \tag{37}$$

are provided, using the standard generalized perturbation theory in the ERANOS code system.

Folding the two contributions (from EMPIRE and ERANOS), one obtains the sensitivity coefficients of the nuclear physics parameters to the integral measured parameters; see (36).

Table 6: C/E before and after statistical adjustment.

Detector	C/E before adj.	C/E after adj.
EURACOS ^{32}S	0.770 ± 0.085	0.997 ± 0.057
EURACOS ^{197}Au	0.954 ± 0.102	0.946 ± 0.010
JANUS-8 ^{32}S	0.538 ± 0.022	1.000 ± 0.022
JANUS-8 ^{197}Au	1.010 ± 0.033	0.959 ± 0.028
JANUS-8 ^{55}Mn	1.158 ± 0.025	1.028 ± 0.023
JANUS-8 ^{103}Rh	0.960 ± 0.106	0.976 ± 0.047

Finally, as far as data adjustment (or data "assimilation"), the methodology makes use of

(i) quantified uncertainties and associated variance-covariance data,

(ii) well-documented, high-accuracy, and "representative" integral experiments,

(iii) sensitivity coefficients for a variety of integral parameters.

6.4. ^{23}Na Consistent Data Assimilation. As a practical example we have considered the case of the ^{23}Na isotope. For this case we have used propagation experiments of neutrons in a medium dominated by this specific isotope. These kinds of experiments were specifically intended for improving the data used in the shielding design of fast reactors. Two experimental campaigns taken from the SINBAD database [50] have been used in this practical application: the EURACOS campaign and the JANUS-8 campaign.

In order to perform the consistent data assimilation on the ^{23}Na, a set of 136 nuclear parameters was selected, and sensitivities to them in terms of multigroup cross section were calculated ([51] provides the details of this step). The selected parameters include: scattering radius, bound level and 33 resonances (for each one: E_n resonance peak energy, Γ_n neutron width, Γ_g radiative width, for a total of 102 parameters), 33 parameters in fast region (21 Optical model parameters, 7 Statistical Hauser-Feshbach model parameters, and 5 Preequilibrium Exciton model parameters).

For what concerns the experiments, a set of reaction rate slopes (one for each detector in the two experiment campaigns) was selected. The selection was based, on low experimental and calculation uncertainty, good depiction of the neutron attenuation for the energy range to be characterized by the corresponding detector, complement of information (obtained by correlation calculations using the sensitivity coefficients), and good consistency among the C/E on the selected slopes. The selected slopes were the ratios of the fourth position to the first one for both detectors in the EURACOS experiment, while for the JANUS-8 experiment we selected the fourth to first position ratio for the ^{32}S and ^{197}Au detectors, fourth to second position for the ^{55}Mn (there was no measurement in the first position), and third to first for the ^{103}Rh (the fourth position has a very large experimental uncertainty).

Table 7: Parameter variations and standard deviations obtained by data assimilation.

Parameter	Variation (%)	Init. stand. dev. (%)	Final stand. dev. (%)
Scat. Rad.[a]	1.9	4.1	1.7
Γ_n Bou. Lev.[b]	−6.4	8.0	6.4
Γ_n 2.8 Kev[c]	0.6	1.9	1.9
Γ_γ 2.8 Kev[c]	10.5	11.8	10.5
Γ_n 538 Kev[c]	−57.2	65.9	58.4
R. Vol. Rad.[d]	−1.8	2.8	1.6
R. Surf. Dif.[e]	−0.8	5.0	4.7
R. Vol. Dif.[f]	−0.4	2.1	2.1
TOTRED[g]	−1.1	3.5	3.2
FUSRED[h]	−0.8	5.0	4.0

[a]Nuclear scattering radius.
[b]Bound-level resonance.
[c]Resonance peak energy.
[d]Optical model real volume radius for target nucleus.
[e]Optical model real surface diffuseness for target nucleus.
[f]Optical model real volume diffuseness for target nucleus.
[g]Optical model scaling of total cross-sections due to intrinsic model uncertainty.
[h]Optical model scaling of absorption cross-sections due to intrinsic model uncertainty.

A 41-group energy structure was adopted specifically to better describe the resonance structure of the ^{23}Na. The ERANOS code was used to calculate the multigroup sensitivity for the selected reaction rate slopes.

A specific code was written in order to manipulate the two sets of sensitivities (nuclear parameters and integral experiments to multigroup cross sections), check their consistency, calculate uncertainties on measured parameters, and perform the folding of (36).

Once obtained the sensitivity of nuclear parameters to the integral experiments, they were used together with the *C*/*E* of the computational analysis shown in Section 3 for a statistical adjustment. Table 6 shows the *C*/*E* after the adjustments for the selected reaction rates slopes.

As it can be observed, except for the gold detectors that did already show good *C*/*E* agreement, a remarkable improvement is obtained after the adjustments.

The corresponding variations of the nuclear parameters that are needed for obtaining such improvement are shown in Table 7. Only the parameters that require at least 0.3% of variation are reported, and for the meaning of the parameter name we refer to [51].

All the variations are in less than 1σ of the initial uncertainties and, therefore, look acceptable. Some important parameters show a significant improvement in the "a posteriori" standard deviation (e.g., scattering radius) that would translate in reduced uncertainties on design parameters when the "assimilated" cross sections will be used.

The χ^2 test after adjustment provided a value of 5.95, which is quite good in view of the fact that, for the statistical adjustment methodology adopted, the degrees of freedom of the problem are those of the number of experiments used in the adjustment, in this case 6.

7. Conclusions

We have shown that the sensitivity methodologies have been a remarkable success story when adopted in the reactor and fuel cycle physics field. Beside providing a unique tool to gain physics insight in reactor design and experiment analysis, sensitivity coefficients have been used for different objectives like uncertainty estimates, design optimization, determination of target accuracy requirements, adjustment of input parameters, and evaluations of the representativity of an experiment with respect to a reference design configuration. Several key examples of importance for fast reactor assessment have been provided for corroborating the success of the methodology in "real life" and its impact in industrial applications.

Even though so much success has been achieved by the validation methodology in reactor physics, still new challenges lay down the road. One of the current major hurdles that reactor physicists are confronted to is how to provide effective feedback, coming from the results of integral experiments, to nuclear physicists. As explained previously, in the past, through the multigroup adjustment, the reactor physicist would produce ad hoc nuclear data, needed for his specific reactor design, neglecting the fact of giving a feedback to evaluators. Of course, this approach limits the range of applicability of any findings coming out from integral experiments.

We have illustrated, by proposing the consistent method, a comprehensive approach that would cope with this problem. However, the consistent method is still in its infancy. In fact, for the moment it is restricted to single isotope experiments and to limited energy range applicability. Systematic for nuclear parameters of isotope families should be the next frontier; as well the extension of energy ranges to cover all the neutron spectrum of interest for different type of reactors.

In the same category, it is the problem of the new correlations created after adjustment. In fact (30), which defines the new a posteriori covariance matrix after adjustment, is a full matrix that correlates all the cross sections (isotopes, reactions, and energy groups) while the initial one, provided by evaluators, is quite sparse, and, in practice, only energy correlation is provided with a few reaction cross-correlations. Do the new correlations calculated by the adjustment provide physically sound indications or are they just the result of a mathematical procedure? In the former case, how one should use the information to improve evaluated nuclear data? This question is currently tackled by the OECD/NEA Subgroup 33 on "methods and issues for the combined use of integral experiments and covariance data" and surely deserves the attention of the reactor physics validation community. The Subgroup 33 has already provided a comprehensive assessment of current adjustment methodologies [52].

Finally, it should be reminded that reactor and fuel cycle physics is not the only field where sensitivity methods have been developed in the nuclear energy domain. We like to mention that there are books, not only journal articles, which present applications of adjoint sensitivity and uncertainty analysis to large-scale thermal hydraulics and thermomechanics; see, for example, [53–55], mostly due to the pioneering and systematic work of Professor D. Cacuci and coworkers.

In summary, sensitivity and validation methodologies in the nuclear energy domain are expected to play an even wider role in the future developments of nuclear energy in particular if advanced fuel cycles and innovative reactors will be implemented.

Acknowledgment

This paper prepared for the US Department of Energy through the INL LDRD Program under the DOE Idaho Operations Office Contract DE-AC07-05ID14517.

References

[1] G. Palmiotti et al., "Requirements for Advanced Simulation of Nuclear Reactor and Chemical Separation Plants," ANL-AFCI-168, Argonne National Laboratory, May 2006.

[2] A. Weinberg and E. Wigner, *The Physical Theory of Neutron Chain Reactors*, The University of Chicago Press, 1958.

[3] H. Brooks, "Perturbation Theory for Boltzmann Equation," KAPL-304, 1950.

[4] L. N. Usachev, "Equation for the value of neutrons, reactor kinetics and perturbation theory," in *Proceedings of the International Conference on the Peaceful Uses of Atomic Energy*, vol. 5, p. 503, Geneva, Switzerland, 1955.

[5] J. Lewins, "Time dependent importance of neutrons and precursors," *Nuclear Science and Engineering*, vol. 7, p. 268, 1960.

[6] J. Lewins, *Importance - The Adjoint Function*, Pergamon Press, 1965.

[7] A. Gandini, "Study of the sensitivity of calculations for Fast Reactors to Uncertainties in Nuclear Data," ANL-6608, 1962.

[8] L. N. Usachev, "Perturbation theory for the breeding factor, and other ratios of a number of different processes in a reactor," *Atomic Energy*, vol. 15, no. 6, p. 472, 1963.

[9] A. Gandini, "A generalized perturbation method for bi-linear functionals of the real and adjoint neutron fluxes," *Journal of Nuclear Energy*, vol. 21, no. 10, pp. 755–765, 1967.

[10] G. P. Cecchini and M. Salvatores, "Advances in the Generalized Perturbation Theory," *Nuclear Science and Engineering*, vol. 46, pp. 304–309, 1971.

[11] W. M. Stacey Jr., *Variational Methods in Nuclear Reactor Physics*, Academic Press, 1974.

[12] W. M. Stacey, "Variational estimates of reactivity worths and reaction rate rations in critical nuclear reactors," *Nuclear Science and Engineering*, vol. 48, p. 444, 1972.

[13] The Oak Ridge group, "Sensitivity and uncertainty analysis of reactor performance parameters," *Advances in Nuclear Science & Technology*, vol. 14, 1982.

[14] M. Mitani, "Higher order perturbation method in reactor calculations," *Nuclear Science and Engineering*, vol. 51, p. 180, 1973.

[15] A. Gandini, "Generalized perturbation theory for nonlinear systems for the importance conservation principle," *Nuclear Science and Engineering*, vol. 77, no. 3, pp. 316–343, 1981.

[16] E. Greenspan, D. Gilai, and E. M. Oblow, "Second-order generalized perturbation theory for source-driven systems," *Nuclear Science and Engineering*, vol. 68, no. 1, pp. 1–9, 1978.

[17] D. G. Cacuci, C. F. Weber, E. M. Oblow, and J. H. Marable, "Sensitivity theory for general systems of nonlinear equations," *Nuclear Science and Engineering*, vol. 75, no. 1, pp. 88–110, 1980.

[18] A. Gandini, "Time-dependent generalized perturbation methods for burn-up analysis," Tech. Rep. CNEN RT/FI (75) 4, Rome, Italy, 1975.

[19] J. M. Kallfelz, G. Bruna, G. Palmiotti, and M. Salvatores, "Burn-up calculations with time-dependent generalized perturbation theory," *Nuclear Science and Engineering*, vol. 62, p. 304, 1977.

[20] A. Gandini, M. Salvatores, and L. Tondinelli, "New developments in generalized perturbation methods in the nuclide field," *Nuclear Science and Engineering*, vol. 62, no. 2, pp. 339–345, 1977.

[21] M. L. Williams, "Development of depletion perturbation theory for coupled neutron/nuclide fields," *Nuclear Science and Engineering*, vol. 70, p. 20, 1979.

[22] G. Palmiotti, M. Salvatores, J. C. Estiot, and G. Granget, "Higher order effects in time-dependent sensitivity problems," *Nuclear Science and Engineering*, vol. 84, no. 2, pp. 150–155, 1983.

[23] A. Gandini, G. Palmiotti, and M. Salvatores, "Equivalent generalized perturbation theory (EGPT)," *Annals of Nuclear Energy*, vol. 13, no. 3, pp. 109–114, 1986.

[24] G. Palmiotti, P. J. Finck, I. Gomes, B. Micklich, and M. Salvatores, "Uncertainty assessment for accelerator-driven systems," in *Proceedings of the International Conference on Future Nuclear Systems (Global '99)*, Jackson, Wyo, USA, August-September 1999.

[25] E. M. Oblow, "Sensitivity theory for reactor thermal-hydraulic problems," *Nuclear Science and Engineering*, vol. 68, no. 3, pp. 322–337, 1978.

[26] C. V. Parks and P. J. Maudlin, "Application of differential sensitivity theory to a neutronic/thermal-hydraulic reactor safety code," *Nuclear Technology*, vol. 54, p. 38, 1981.

[27] D. G. Cacuci and C. F. Weber, "Applications of sensitivity theory for extrema of functionals to a transient reactor,"

Transactions of the American Nuclear Society, vol. 34, p. 312, 1980.

[28] A. Gandini, "GPT methods for fuel evolution and shuffling studies," *Transactions of the American Nuclear Society*, vol. 53, p. 265, 1986.

[29] A. Gandini, "Uncertainty analysis and experimental data transposition methods based on perturbation theory," in *Uncertainty Analysis*, Y. Ronen, Ed., CRC Press, Boca Raton, Fla, USA, 1988.

[30] E. Greenspan, "Developments in perturbation theory," in *Advances in Nuclear Science and Technology*, J. Lewins and A. Becker, Eds., vol. 14, Plenum, 1982.

[31] L. N. Usachev and Y. Bobkov, "Planning on Optimum Set of Microscopic Experiments and Evaluations to Obtain a Given Accuracy in Reactor Parameter Calculations," INDC CCP-19U, IAEA Int. Nucl. Data Committee, 1972.

[32] G. Palmiotti and M. Salvatores, "Use of integral experiments in the assessment of large liquid-metal fast breeder reactor basic design parameters," *Nuclear Science and Engineering*, vol. 87, no. 3, pp. 333–348, 1984.

[33] A. Gandini, *Uncertainty Analysis and Experimental Data Transposition Methods in Uncertainty Analysis*, Y. Ronen, Ed., CRC Press, 1988.

[34] A. Gandini and M. Petilli, "AMARA: A Code Using the Lagrange Multipliers Methods of Nuclear Data Adjustment," RT/FI(73)39, Comitato Nazionale per l'Energia Nucleare (1973).

[35] M. Salvatores, G. Aliberti, and G. Palmiotti, "Nuclear data validation and fast reactor design performances uncertainty reduction," in *Annual Meeting on American Nuclear Society*, pp. 519–522, Boston, Mass, USA, June 2007.

[36] "OECD/NEA WPEC Subgroup 26 Final Report: Uncertainty and Target Accuracy Assessment for Innovative Systems Using Recent Covariance Data Evaluations," 2008.

[37] D. Rochman, M. Herman, P. Oblozinsky, and S. F. Mughabghab, "Preliminary Cross-Section Covariances for WPEC Subgroup 26," Tech. Rep. BNL-77407-2007-IR, Brookhaven National Laboratory, 2007.

[38] G. Palmiotti, M. Salvatores, G. Aliberti et al., "A global approach to the physics validation of simulation codes for future nuclear systems," *Annals of Nuclear Energy*, vol. 36, no. 3, pp. 355–361, 2009.

[39] W. S. Yang, T. K. Kim, and R. N. Hill, "Performance Characteristics of Metal and Oxide Fuel Cores for a 1000 MWt Advanced Burner Reactor," in *Proceedings of the Workshop on Advanced Reactors With Innovative Fuels (ARWIF '08)*, Fukui, Japan, February 2008.

[40] A. D'Angelo, F. Cleri, P. Marimbeau, M. Salvatores, and J. P. Grouiller, "Analysis of sample and fuel pin irradiation experiments in phenix for basic nuclear data validation," *Nuclear Science and Engineering*, vol. 105, no. 3, pp. 244–255, 1990.

[41] NEA, "Benchmark on Computer Simulation of MASURCA Critical and Subcritical Experiments," NEA/NSC/DOC(2005) 23, 2005.

[42] P. J. Finck et al., "The CIRANO Experimental Program in Support of Advanced Fast Reactor Physics," in *Proceedings of the International Conference on the Physics of Reactors (PHYSOR '96)*, Mito, Japan, September 1996.

[43] G. Palmiotti, M. Salvatores et al., "Use of Covariance matrices in a consistent (Multiscale) data assimilation for improvement of basic nuclear parameters in nuclear reactor applications: from meters to femtometers," in *Proceedings of the International Conference on Nuclear Data for Science and Technology*, Jeju, South Korea, April 2010.

[44] A. Gandini and M. Salvatores, "Nuclear data and Integral Measurements Correlation for Fast reactors-Part 3: The Consistent Method," RT/FI(74)3, Comitato per l'Energia Nucleare, 1974.

[45] A. D'Angelo, A. Oliva, G. Palmiotti, M. Salvatores, and S. Zero, "Consistent utilization of shielding benchmark experiments," *Nuclear Science and Engineering*, vol. 65, no. 3, pp. 477–491, 1978.

[46] M. Salvatores, G. Palmiotti et al., "Resonance parameter data uncertainty effects on integral characteristics of fast reactors," in *Proceedings of the IAEA Specialist's Meeting on Resonance Parameters*, Vienna, Austria, September-October 1981.

[47] M. Herman, R. Capote, B. V. Carlson et al., "EMPIRE: nuclear reaction model code system for data evaluation," *Nuclear Data Sheets*, vol. 108, no. 12, pp. 2655–2715, 2007.

[48] T. Kawano and K. Shibata, "Covariance Evaluation System," JAERI-Data/Code 97-037, Japan Atomic Energy Research Institute, 1997.

[49] G. Rimpault et al., "The ERANOS code and data system for fast reactor neutronic analyses," in *Proceedings of the PHYSOR 2002*, Seoul, South Korea, October 2002.

[50] "SINBAD-2009.02: Shielding Integral Benchmark Archive and Database," Version February 2009, RSICC DATA LIBRARY DLC-237, ORNL.

[51] M. T. Pigni, M. Herman, C. M. Mattoon et al., "Evaluation of 23-Na neutron cross sections for nuclear data assimilation," in *Proceedings of the 2nd International Workshop on Nuclear Data Evaluation for Reactor Applications (Wonder '09)*, Cadarache, France, September-October 2009.

[52] C. de Saint-Jean, E. Dupont, M. Ishikawa, G. Palmiotti, and M. Salvatores, "Assessment of Existing Nuclear Data Adjustment Methodologies," A report by Working Party on International Evaluation Cooperation NEA/NSC/ DOC(2010)429, OECD, 2010.

[53] D. G. Cacuci, M. Ionescu-Bujor, and M. I. Navon, *Sensitivity and Uncertainty Analysis: Applications to Large Scale Systems*, vol. 2, Chapman & Hall/CRC, Boca Raton, Fla, USA, 2005.

[54] Y. Y. Azmy and E. Sartori, Eds., *Nuclear Computational Science: A Century in Review*, Kluwer Academic Publishers, Dordrecht, The Netherlands, 2008.

[55] D. G. Cacuci, Ed., *Handbook of Nuclear Engineering*, Springer, Berlin, Germany, 2010.

Hindawi Publishing Corporation
Science and Technology of Nuclear Installations
Volume 2012, Article ID 293467, 10 pages
doi:10.1155/2012/293467

Research Article

Economic Analysis of Different Nuclear Fuel Cycle Options

Won Il Ko and Fanxing Gao

Korea Atomic Energy Research Institute, Yuseong, Daejeon 305-353, Republic of Korea

Correspondence should be addressed to Won Il Ko, nwiko@kaeri.re.kr

Received 2 February 2012; Accepted 13 April 2012

Academic Editor: Katsuhisa Yamaguchi

An economic analysis has been performed to compare four nuclear fuel cycle options: a once-through cycle (OT), DUPIC recycling, thermal recycling using MOX fuel in a pressurized water reactor (PWR-MOX), and sodium fast reactor recycling employing pyroprocessing (Pyro-SFR). This comparison was made to suggest an economic competitive fuel cycle for the Republic of Korea. The fuel cycle cost (FCC) has been calculated based on the equilibrium material flows integrated with the unit cost of the fuel cycle components. The levelized fuel cycle costs (LFCC) have been derived in terms of mills/kWh for a fair comparison among the FCCs, and the results are as follows: OT 7.35 mills/kWh, DUPIC 9.06 mills/kWh, PUREX-MOX 8.94 mills/kWh, and Pyro-SFR 7.70 mills/kWh. Due to unavoidable uncertainties, a cost range has been applied to each unit cost, and an uncertainty study has been performed accordingly. A sensitivity analysis has also been carried out to obtain the break-even uranium price (215$/kgU) for the Pyro-SFR against the OT, which demonstrates that the deployment of the Pyro-SFR may be economical in the foreseeable future. The influence of pyrotechniques on the LFCC has also been studied to determine at which level the potential advantages of Pyro-SFR can be realized.

1. Introduction

Economics is an essential criterion to be considered in the future deployment of nuclear power. Today, the cost of electricity from nuclear power plants is, in most cases, highly competitive with other electricity-producing means, and is generally lower in cost than fossil fuel, wind, or solar energy. However, a closer look at nuclear power production brings an insight that the cost varies within a wide range, depending on the nuclear fuel cycle option. With the current trend toward competition in the power market, the option of nuclear fuel cycle is an important determinant in terms of economics.

Four nuclear fuel cycle options can be considered in the foreseeable future under the nuclear power situation in the Republic of Korea: a once-through cycle (OT), DUPIC recycling (DUPIC), thermal recycling using MOX fuel in a PWR (PWR-MOX), and SFR recycling employing pyroprocessing (Pyro-SFR). A comprehensive comparison among the proposed fuel cycle options necessitates an economic analysis for each option based on the material flow estimation. The objective of this work is to provide a systematic cost comparison among these nuclear fuel cycles.

FCC includes a front-end cost and back-end cost as well as costs associated with fuel recycling in the cases of recycling options. An economic analysis of FCC is a subject of great interest, which not only concentrates on the cost differences among these four fuel cycle options but also efficiently avoids the large uncertainties of the Generation IV reactor capital costs.

The levelized cost is a fundamental calculation principle in the energy and power industry. It is particularly appropriate for an estimate of the costs of energy given the various technologies. LFCC has offered an effective indicator for an economic comparison among nuclear fuel cycles and was adopted to compare the four fuel cycle options considered in this study [1].

The material flow is the basis used to obtain the LFCC. There are mainly two models to calculate the material flows [2–5]. One is an equilibrium model, and the other is a dynamic model. The equilibrium model focuses on a batch study with the assumptions that the whole system is in a steady state and that the mass flow as well as electricity production throughout the fuel cycle is in an ideal equilibrium state, which calculates the material flow

for the production of a certain amount of electricity to obtain the LFCC with reference to unit cost. The dynamic model takes the timing into consideration to simulate a relatively realistic case. The dynamic model offers a better way to simulate the complement process of a fuel cycle, which may take several decades. Comparatively, the equilibrium model enables a clear and direct comparison to suggest which optimized system should be complemented in the future. In particular, while the current research and development of certain technologies such as SFR and pyroprocessing are still underway, an equilibrium model offers a way to avoid large uncertainties of the future development and deployment. In this study, an equilibrium model was therefore built to calculate the material flow on a batch basis. With the unit costs being determined, the cost of each step of the fuel cycle could be obtained as an approach to obtain the LFCC.

The change of each key component due to the uncertainties can result in considerable differences in LFCCs among the fuel cycle scenarios. To take these unavoidable uncertainties into account, a wide range was applied to each unit cost, and the distribution of LFCC was obtained.

2. Reference Fuel Cycle and Material Flows

The four fuel cycle options considered in this study are specified by the breakdown structures consisting of a series of components (or steps), as shown in Figure 1. Figure 1(a) describes the OT material flow, which utilizes low-enriched uranium in a PWR without reprocessing of the spent fuels (SFs).

PWR SFs still contain fissile materials, approximately 0.9 w% U-235 and 0.5 w% Pu-239, depending on a 3.5% U-235 enrichment of the initial fuel and a burnup of 35 GWd/tHM, and therefore can be used as the fuel for CANDU reactors after the removal of some fission products (FPs). This PWR-CANDU symbiotic fuel cycle is referred to as DUPIC recycling [6], and the material flow is described in Figure 1(b).

Some Pu isotopes such as Pu-239 and Pu-241 are fissile, such as U-235, and can be burned using a thermal neutron spectrum. In the PWR-MOX option shown in Figure 1(c), a commercial PUREX technology is used for recovering U and Pu from the PWR SFs. The reprocessed materials can be fabricated into the mixed oxide (MOX) fuels of UO_2 and PuO_2 and then loaded into PWRs, while the MOX SFs would be permanently disposed of without further recycling.

A fast reactor utilizes fast neutrons of which a higher energy can burn both U-235 and transuranic elements (TRUs). This aspect makes it possible to transmute the TRUs and extract energy at the same time. In Pyro-SFR recycling shown in Figure 1(d), the PWR SFs are to be reprocessed to obtain TRU-bearing fuels for fast reactors, while the remaining uranium partitioned from the PWR SF would be disposed of as low- and intermediate-level radioactive waste. In this cycle, a sodium-cooled fast reactor (SFR) with a conversion ratio of 0.6067 is considered as the reference fast reactor [7]. Pyroprocessing has been developed to reprocess the oxide fuels discharged from PWRs and to fabricate metallic fuels containing TRU for future SFRs [8]. The metal fueled SFR using alloys of actinides zirconium (AcZr) has a high potential for recycling actinides by being integrated with the pyroprocessing. The TRU fuel after burning in the SFR would be repeatedly reprocessed through pyroprocessing, and the recovered TRUs would be recycled into an SFR to close the fuel cycle. However, it should be noted that practically some nasty TRU isotopes have to be separated and treated as HLW.

The material flow values in Figure 1 were calculated using the equilibrium model based on an output of 1 TWh of electricity, a detailed description of which refers to the previous material flow study [9].

3. Unit Cost Specification

The cost data in this paper are presented in 2010 US dollars. Cost data reported at different times were converted into the 2010 values using an escalation rate of 3% [10, 11]. It is difficult to estimate the absolute value of each of the components specified in Figure 1 because many uncertainties exist. Therefore, a range of unit cost (i.e., lower bound, nominal value, and upper bound) was applied in regard to these uncertainties. The nominal value refers to the best estimated unit cost. The lower bound means the low cost case, and the upper bound means the high cost case [5, 11]. It should be noted that the reactor capital and operating costs were not included in the FCC, which was calculated based on the premise introduced by the GEN IV program, in which the targets of the GEN IV reactor capital costs are to be comparable with those of the GEN III reactors [12]. It should be acknowledged that the capital cost taking around 80% of the total electricity cost [13]. Taking no account of the reactor capital cost, therefore, largely reduces the uncertainty of the SFR, and therefore enhances and emphasizes the contribution of the fuel cycle to the total electricity cost.

The main sources of the unit cost data used in this study were from an OECD/NEA study [1, 5, 11] and Advanced Fuel Cycle Cost Basis (short for AFCCB) [14–16], and engineering judgments were used when certain data were not available. The summarized data before converting to the 2010 values are listed in Table 1. Some specifications of the key components are described as follows. It should be noted that the cost difference of MOX fabrication for LWR is dramatically big between the OECD study and AFCCB study. For the OECD 2006 study [5], the cost is 1250$/kgHM. However, for the Advanced Fuel Cycle Cost Basis study, the cost is 3200$/kgHM [15]. The difference mainly lies in the technical readiness and the considerations on proliferation resistance (PR) as stated in the AFCCB reports. In our study, we admit the big gaps among different countries concerning the status of MOX fuel fabrication technique. In addition, the PR is definitely important for the future deployment of the fuel cycle, and therefore, the bigger unit cost from the US study was adopted.

3.1. Uranium Price. The uranium cost generally takes around 40% of the NFCs. The nominal value of the natural uranium

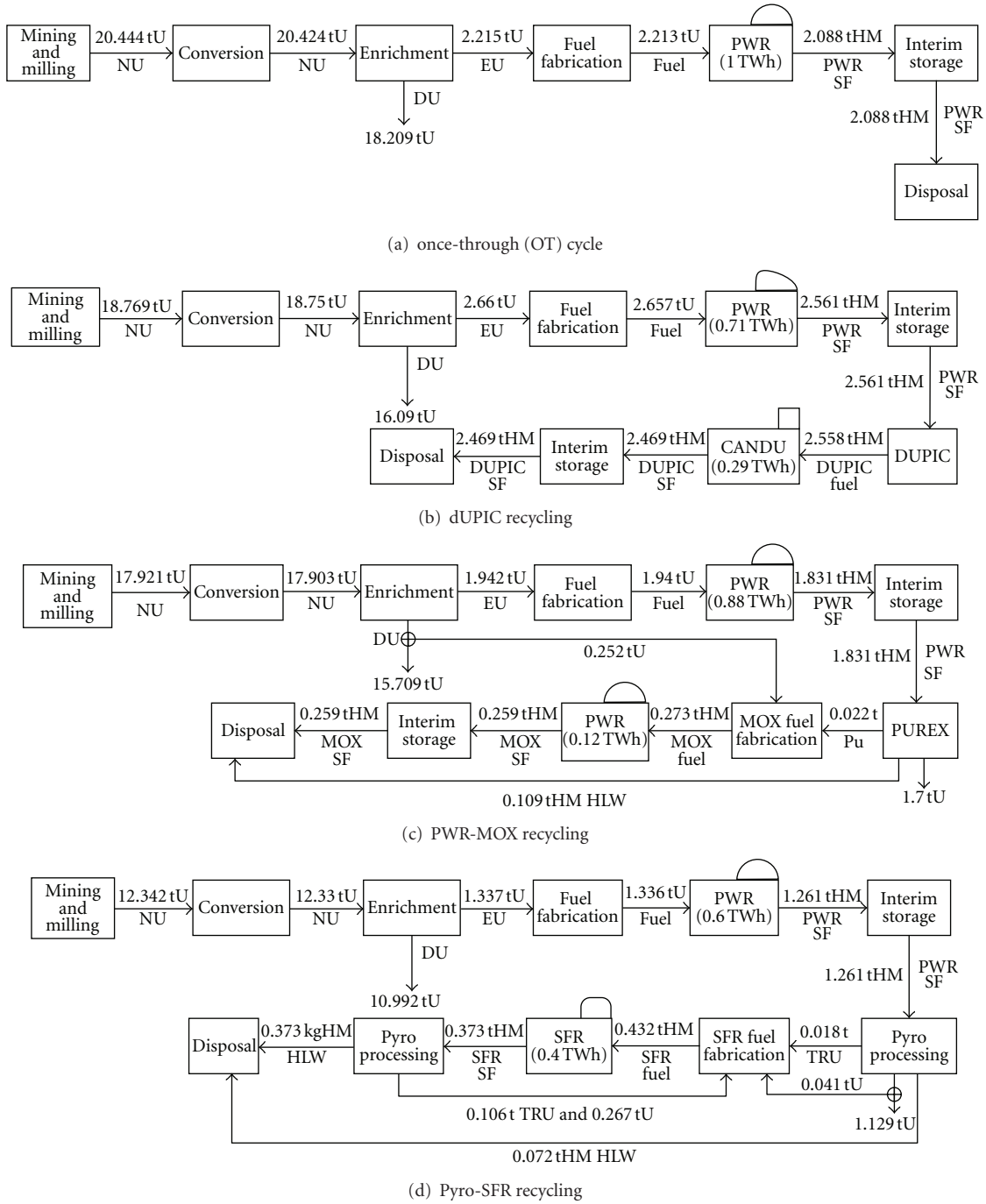

Figure 1: Main components in the nuclear fuel cycles.

price (158$/kgU) was from the monthly average price of December 2010 [17]. The upper bound value of the uranium price was based on the spot price of the historical peak value of June 2007, as shown in Figure 2 [17], which was much higher than the reference data of OECD/NEA and AFCCB. It is challenging to project the future uranium price due to the complexity of the price determinants, such as supply and demand. The uranium price reported in AFCCB was higher than those published by OECD/NEA in 2006. AFCCB reported the uranium price to be a low cost of 50$/kgU, nominal cost of 100$/kgU, and high cost of 150$/kgU in April 2007 (based on the values at 2007), but in March 2008, it was reported as a low cost of 25$/kgU, nominal cost of 60$/kgU, and high cost of 240$/kgU (based on the values at 2007), respectively. However, these costs were changed into a low cost of 30$/kgU, nominal cost of 75$/kgU, and high cost

Table 1: Unit costs for nuclear fuel cycle steps.

Cost items	Units	Low	Nominal	High
Uranium	\$/kgU	30	158	354
Conversion	\$/kgU	5	12	15
Enrichment	\$/SWU∗	80	155	180
Reprocessing				
PUREX	\$/kgHM	700	800	900
Pyro-UO_2	\$/kgHM	500	1,500	2,500
Fuel fabrication				
UO_2 fuel	\$/kgHM	200	240	300
MOX fuel	\$/kgHM	2,000	3,200	4,000
DUPIC fuel	\$/kgHM	500	700	900
Pyro. and SFR metal fuel fab.	\$/kgHM	2,500	5,000	7,500
Long-term storage				
Depleted U	\$/kgHM	2.6	3.6	4.6
Reprocessed U	\$/kgHM	2.6	3.6	40.0
Transport and storage				
DUPIC SF	\$/kgHM	50	100	250
UO_2 SF	\$/kgHM	105	125	145
MOX SF	\$/kgHM	145	218	580
Decay storage	\$/kgHM	10,000	22,500	35,000
HLW	\$/m^3	80,060	120,090	200,240
Disposal				
Packaging				
UO_2 SF	\$/kg	100	200	350
DUPIC SF	\$/kg	80	150	250
MOX SF	\$/kg	200	400	700
HLW of PUREX	\$/m^3	100,000	200,000	400,000
HLW of others	\$/m^3	100,000	200,000	400,000
Underground cost	\$/m^3	600	1,200	2,000

∗ SWU stands for separative work unit.

of 260\$/kgU in December 2009 based on the values of that year. It seems to be obvious that the newer reports suggest a wider range of uranium price.

It is reasonable to doubt the relatively lower prediction of the uranium price. However, the reason for the adoption of the peak value in this study is to enlarge the possible range of the uranium price to better reflect the high uncertainty of the future uranium price.

3.2. Conversion and Enrichment. The nominal price of conversion and the enrichment processes are from the monthly price of December of 2010. Low and high estimates are referred from the OECD/NEA report [5] and the AFCCB reports [14–16]. The high estimated cost of enrichment of OECD/NEA in 2000 is smaller than the spot price based on 2010, and thus an estimated value of 180\$/SWU was proposed.

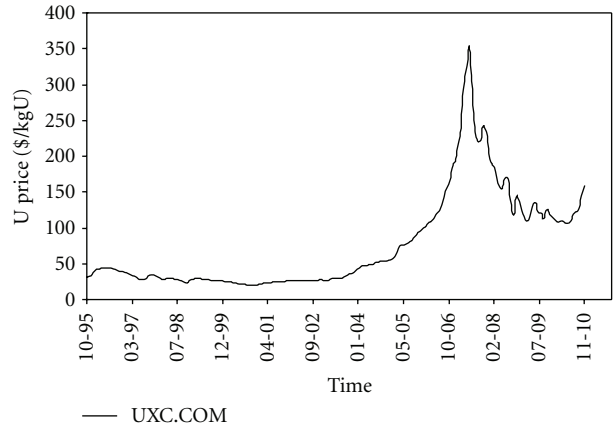

Figure 2: Uranium spot prices.

3.3. Pyrotechnique Cost. As no commercial experience exists, the unit costs concerning the pyrotechnique for fuel reprocessing are theoretical and estimated using engineering judgments with high uncertainty. Because of the difference of the fuels treated and a big gap between the material flows evolved, there are two pyrotechnique-related components in the Pyro-SFR recycling scenario. One pyrotechnique treats the PWR SF (named as Pyro-UO_2), which includes an

Table 2: Lead and lag time of fuel cycle steps.

	Fuel cycle process	Lead/lag time (month)
Lead time (month)	Purchase	21
	Conversion	18
	Enrichment	12
	Fabrication	6
Lag time (month)	Interim storage	18
	Reprocessing	78
	Final disposal	480

additional electroreduction procedure to reduce the oxide fuels into the metallic fuels, and the other is used for SFR metallic SFs (named as Pyro-Metal-Fab.), which requires a fuel fabrication facility along with it. The unit costs reported in AFCCB 2008 [15] were applied to give a nominal cost of 5000$/kgHM for Pyro-Metal-Fab., and the unit cost of 1500$/kgHM is defined for Pyro-UO_2 with regard to the study at the Korea Atomic Energy Research Institute [6, 18]. As the R&D proceeds, more economical cost data might be expected.

3.4. Storage Cost. It is assumed that the interim storage cost consists of two parts: a fixed cost and a variable cost depending on the storage time, which was set for 5 years in this paper [1, 5]. The decay storage of Cs and Sr which are main heat emitters separated by pyroprocessing, employs a shallow disposal as a low-interim level waste for around 200–300 years [18].

4. Fuel Cycle Cost Calculation

4.1. Lead and Lag Time. The costs depend on the amount of material or service consumed and the unit price of each component. The payments for the various components of the nuclear fuel cycle are usually made at different moments in time. Each step-cost should be calculated with consideration of its implementation time, starting from the fuel purchase costs and ending to the final disposal costs. It is therefore reasonable to consider the discount rate to compare all the payments at the same time according to the refueling interval plus or minus a lead or lag time as listed in Table 3.

4.2. Electricity Generation.

(1) the amount of fuel required by one reactor is estimated based on the reactor parameters, fuel loading per core (MTHM):

$$\text{Fuel loading per core} = \frac{P \times 100}{\varepsilon \times SH}, \tag{1}$$

where P, SH, and ε are the electric power (MWe) of a reactor, the specific heat (MWt/MTHM), and efficiency (%), respectively;

(2) the annual requirement of fuel (MTHM) is calculated based on fuel burnup and other parameters:

$$\text{Annual requirement} = \frac{P \times 365 \times C}{\varepsilon \times BU}, \tag{2}$$

where C and BU are the capacity factor (%) and burnup (MWD/MTHM), respectively;

(3) the electric power generation (MWh) per fuel loading (MTHM) is calculated as follows:

$$\text{Power generation per fuel loading} = 24 \times \text{loading(MTHM)} \times BU \times \varepsilon. \tag{3}$$

The number of PWRs is determined from the equilibrium core ratio mentioned above.

4.3. Fuel Cycle Cost. The amount of fuel passing through a certain step multiplied with the unit cost of the specific material offers the fuel cost of a single step and combined with the additional cost associated with the operation, the overall cost of an operation, namely, the component cost, can be obtained. By summarizing the costs of all the operations involved in an NFC, the overall costs of the NFC can be obtained as listed in Table 3. The method employed for the calculation of FCC is the constant money (levelized life-time cost) method. The levelized unit cost is based on the cash flow of all component costs discounted to the base year. A 5% discount rate was applied to all unit costs in this paper. To get the total fuel cycle cost, the net present value (NPV) was used, which can be expressed as follows:

$$\text{NPV} = \sum_i F_i. \tag{4}$$

4.4. Levelized Fuel Cycle Cost. The LFCC is derived in terms of mills/kWh (1 mill equals to 10^{-3} \$) by dividing the NPV of the entire fuel cycle cost by the NPV of the total electricity output over the plant life-time as follows:

$$\text{LFCC} = \frac{\sum_i F_i}{E} = \frac{\text{NPV}}{E}, \tag{5}$$

where E is the electric power generated.

4.5. Uncertainty Analysis. The unit costs for each of the components in the fuel cycle were applied using an uncertainty analysis by Monte Carlo simulation using Latin Hypercube extraction mode [19]. It was assumed that the costs of the components would be simulated by triangular distribution. The triangular distribution is a representative nonparametric distribution, which is effective in cases when there is not much data, and the distributions are unknown. The triangular distribution may appear symmetric, right-skewed, or left-skewed according to the expert opinions. The triangular distribution has a very obvious appeal because it is easy to think about the three defining parameters in a fuel cycle economic analysis and to envisage the effect of any changes.

Table 3: Equations used in levelized fuel cycle cost calculation.

Cost of each fuel cycle component	Cost calculation methods	
Uranium	$F_U = M_f \cdot f_U \cdot P_U \cdot (1+r)^{t_U}$,	(4)
	$M_f = M_p \cdot [(e_p - e_t)/(e_f - e_t)]$,	(5)
	where $f_U = (1+l_C)(1+l_E)(1+l_F)$	(6)
Conversion	$F_C = M_f \cdot f_C \cdot P_C \cdot (1+r)^{t_C}$,	(7)
	where $f_C = (1+l_C)(1+l_E)(1+l_F)$	(8)
Enrichment	$F_E = \mathrm{SWU} \cdot f_E \cdot P_E \cdot (1+r)^{t_E}$,	(9)
	where $\mathrm{SWU} = M_p \cdot V_p + M_t \cdot V_t - M_f \cdot V_f$	(10)
	$M_t = M_f - M_p$	(11)
	$V_x = (2e_x - 1)\ln[e_x/(1-e_x)]$ and x is subscript for $f, p,$ *or* t	(12)
	$f_E = (1+l_E)(1+l_F)$	(13)
Fabrication	$F_F = M_p \cdot f_F \cdot P_F \cdot (1+r)^{t_F}$,	(14)
	where $f_F = (1+l_F)$	(15)
Transport and storage	$F_{TS} = M_{TS} \cdot f_{TS} \cdot P_{TS} \cdot (1+r)^{t_{TS}}$,	(16)
	where $f_{TS} = (1+l_{TS})$	(17)
Disposal	$F_D = M_D \cdot f_D \cdot P_D \cdot (1+r)^{t_D}$,	(18)
	where $f_D = (1+l_D)$	(19)

F_x: Cost of fuel cycle component (\$), M_x: Mass of materials (kg), f_x: Loss factor (%), P_x: Unit cost (\$/unit), l_x: Material loss (%), e_x: Fraction of U-235 (%). Subscript x: *U: Natural uranium, C: Conversion, E: Enrichment, F: Fabrication, TS: Transportation & storage, D: Disposal, f: Feed natural uranium (0.71%), p: Product of uranium fuel, t: Tail.*

4.6. Sensitivity Analysis. This study conducted a sensitivity analysis of some unit costs in which the variability is considered large, such as the uranium price, Pyro-UO_2 reprocessing, and Pyro-Metal-Fab. The break-even prices necessary for the Pyro-SFR fuel recycle to be economic compared to the OT option were also obtained by changing the input of the uranium price, Pyro-UO, and Pyro-Metal-Fab., respectively.

5. Results and Discussion

5.1. Levelized Cost of Electricity. The calculation results of the LFCC concerning these four fuel cycle scenarios show the following: OT 7.35 mills/kWh, DUPIC 9.06 mills/kWh, PUREX-MOX 8.94 mills/kWh, and Pyro-SFR 7.70 mills/kWh. The relative total costs of the fuel cycle options are presented by the bar chart in Figure 3. It shows that DUPIC, PWR-MOX, and Pyro-SFR are 23%, 22%, and 5% higher than the OT option, respectively.

Figure 3 shows that the uranium price is the key cost component of the LFCC in all of these four nuclear fuel cycles. With the current uranium price, the OT is the most economical option and the Pyro-SFR is the second due to the low uranium consumption. In the Pyro-SFR scenario, the uranium consumption decreases because of the utilization of the metal fuel made from the reprocessed TRU. Pyro-Metal-Fab., however, makes up for the difference in uranium costs between the Pyro-SFR and OT scenarios. In the PWR-MOX scenario, the uranium consumption is still high, while meanwhile the reprocessing is costly. The relative high cost of the DUPIC scenario is because of the low uranium utilization efficiency due to the low burnup and high fabrication cost required to make the PWR SF into CANDU fuel.

Generally, two decisions, that is, which kind of reactor to employ and whether or not to deploy a spent fuel treatment technology, mainly determine the direction of the nuclear fuel cycle. In this study, we focused on the impact of the introduction of spent fuel treatment technologies, that is, PUREX, DUPIC, and pyroprocessing. The introduction of reprocessing techniques in PWR-MOX and Pyro-SFR scenario do affect the back-end cost due to the recycling of Pu or TRU. For the DUPIC case, the treatment of spent PWR fuel for CANDU fuel plays a similar role to take advantages of residual fissile in the spent fuel. Due to the introduction of techniques to treat the PWR spent fuel, the mass flows of nuclear fuel cycles were changed accordingly. Therefore, it is informative to present the cost share of the spent fuel treatment technique in the LFCC as shown in Figure 4.

5.2. Uncertainty Analysis. The results from the Monte Carlo simulation are shown in Table 4 and Figure 5. With the assumption that each unit cost has a triangular distribution, a total of 50,000 extractions of Latin Hypercube were performed. The standard deviation (SD) for the LFCC ranges between 1.16–1.69 mills/kWh, as shown in Table 4. The difference between the LFCC of the Pyro-SFR and OT is 0.04 mills/kWh concerning the mean data, which is much smaller than the SD for the OT option, 1.69 mills/kWh. This means that the cost of the Pyro-SFR fuel recycling lies within the error bound of the direct disposal option. The costs of DUPIC and PWR-MOX also have the possibility to fall within the error bound of the OT, respectively, but their possibilities are relatively smaller.

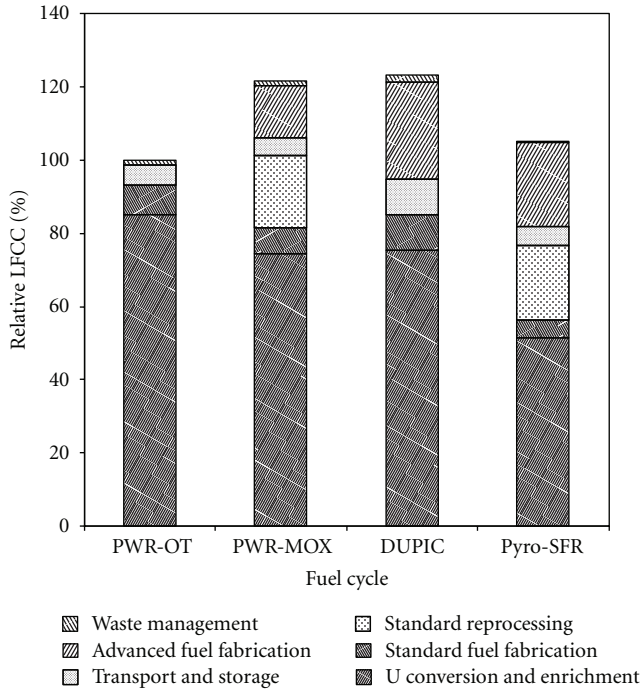

Figure 3: Relative LFCC of four fuel cycles.

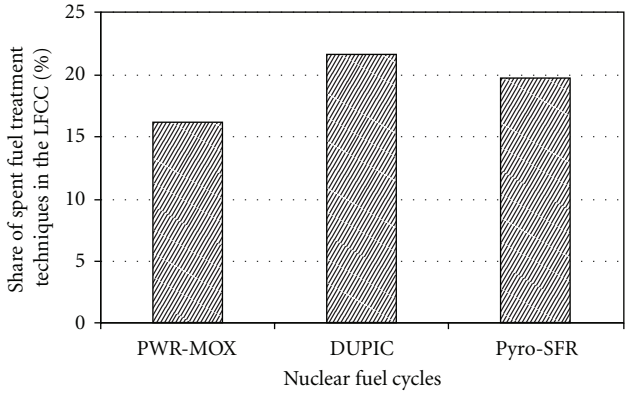

Figure 4: Share of spent fuel treatment techniques in the LFCC.

Table 4: Results of a Monte Carlo simulation for the uncertainty analysis of LFCCs.

	OT	DUPIC	PWR-MOX	Pyro-SFR
Min.	3.99	5.68	5.74	4.51
Max.	13.79	15.30	14.77	12.64
Mean	8.35	10.06	9.83	8.31
SD	1.69	1.57	1.55	1.16

5.3. Sensitivity Analysis. A sensitivity analysis was conducted on the key cost components, such as the uranium price, Pyro-UO_2, and Pyro-Metal-Fab. Figure 6 shows the results of regression sensitivity analysis, for which a multivariate stepwise regression was applied as an analytical method for the sensitivity of multiple inputs and for deriving the regression coefficient to assess the degree of sensitivity. A value of 1 of the regression sensitivity means that a variation of 1 SD for the input variable brings a variation of 1 SD in the results. On the contrary, a regression sensitivity of 0 means that there is no influence from the input to the output.

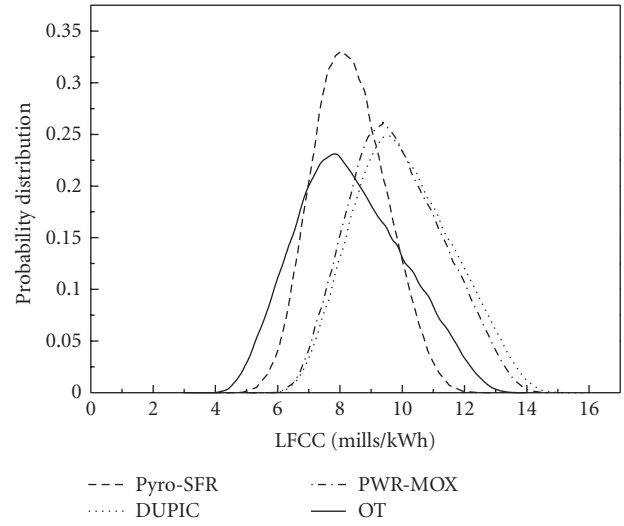

Figure 5: Comparison of the probabilistic density function of LFCCs using a triangular distribution.

As can be noted from Figure 6, the uranium price indicates the highest sensitivity value. It was determined that the regression coefficient of the uranium ranges from 0.95 to 0.96 for the OT, DUPIC, and PWR-MOX options. However, the coefficient of the Pyro-SFR fuel recycle, 0.85, shows a lower sensitivity of the uranium price compared to other fuel cycle options. While another high sensitivity factor is shown to be the uranium enrichment in the OT and PWR-MOX scenarios. In the Pyro-SFR option, Pyro-UO_2 and Pyro-Metal-Fab. show higher sensitivities.

5.4. Break-even Uranium Price. Since uranium is the main driver of the LFCC, a fluctuation of uranium price influences the total cost considerably. The historical data of uranium price, however, changed dramatically, and it is challenging to predict the future uranium price. A large range of uranium prices is therefore adopted to find out at which price level the recycled fuel cycle options will be more economical than the OT option, or at which level they will break even.

The sensitivity analysis on the uranium price shows that the OT option depends more on the cost of uranium than on any other fuel cycle options (Figure 6 and Figure 7), which could be explained by the largest amount of uranium consumed for producing a given quantity of energy. Pyro-SFR, however, is much less sensitive to the uranium price indicated by a smaller slope in Figure 7. By increasing the uranium price, the LFCC of the OT option finally reaches and surpasses those of Pyro-SFR and PWR-MOX, respectively, due to the different weight of uranium cost in each cycle scheme.

A break-even price is defined to specify the price at which the LFCC of the OT equals the LFCC of another fuel cycle

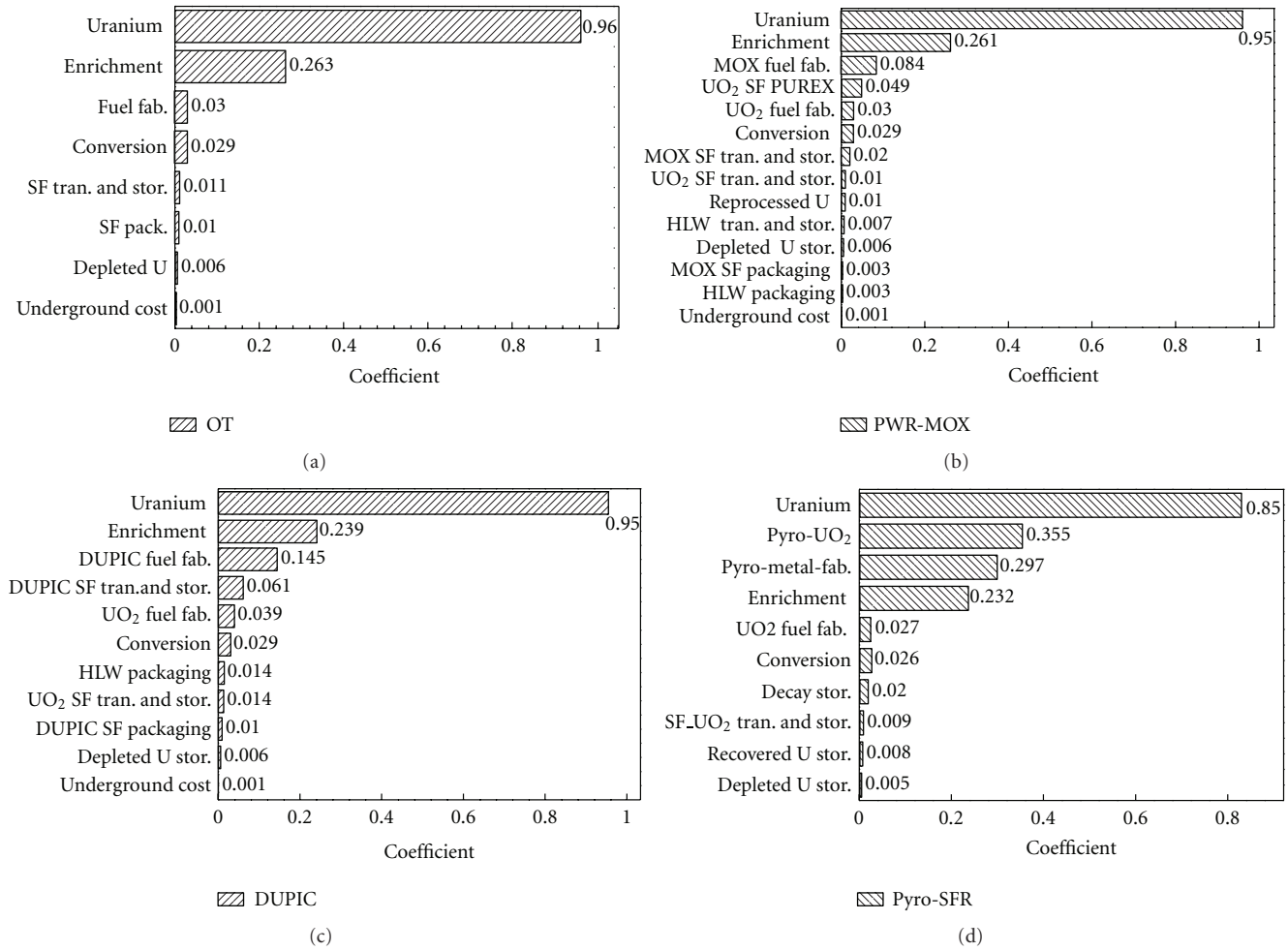

Figure 6: Sensitivity coefficient of fuel cycle components.

option. The calculation of uranium break-even price is a kind of sensitive analysis. By setting the input unit costs fixed and only changing the uranium unit price, a unit price of uranium can be derived at which the LFCC cost of a specific nuclear fuel cycle equals to the LFCC of OT. However, it should be noted that the calculation was based on the reference unit cost listed in Table 2. Even the nominal data have unavoidably uncertainty and that is why a cost scale is associated with each unit cost. However, the nominal data is currently highly reliable, and the purpose of calculating the break-even price is to indicate a potential trend not to offer a precise and exact data, so the use of the nominal data for discount rate sensitive analysis is reasonable.

The break-even price of uranium was calculated to be 800$/kgU for PWR-MOX fuel cycle and 215$/kgU for Pyro-SFR fuel cycle with reference to the OT option. The actual price of uranium in July 2007 recorded 350$/kgU, which is 13 times higher than that of 2001. If Pyro-SFR was available as of 2007 peak in uranium price, its nongeneration fuel cycle costs would have been competitive with those of the OT. The gap of LFCCs between the Pyro-SFR and OT still exists at the current uranium price. The amount of uranium with an acceptable price, however, is definitely decreasing, and the nuclear power capacity in East Asia is increasing dramatically at the same time. According to this trend, the higher uranium consumption efficiency a nuclear fuel cycle pursues the better competitiveness it may obtain.

5.5. Break-even Uranium Price Dependent on Pyrotechniques. With regard to a potential cost decrease of certain components, it is of great interest to analyze the influence of the changes of fuel cycle components on the LFCCs, especially focusing on the cost of Pyro-UO_2 and Pyro-metal-Fab., respectively.

Pyro-UO_2 and Pyro-Metal-Fab. are currently under development, and there is no industrial experience worldwide yet. The cost data concerning those unavoidably maintain a high uncertainty. Pyro-UO_2 and Pyro-Metal-Fab. contribute heavily to the LFCC of Pyro-SFR recycling by changing the cost of each pyrotechnique, and it is therefore possible to estimate the sensitivity of the break-even uranium price of the Pyro-$UO_2$and Pyro-metal-Fab. compared with OT, as shown in Figure 8. When the cost of Pyro-UO_2 equals to the cost of PUREX, or around 50% of the nominal unit cost, the break-even price of uranium is around 125$/kgU. This means when the cost of Pyro-UO_2 becomes equal to

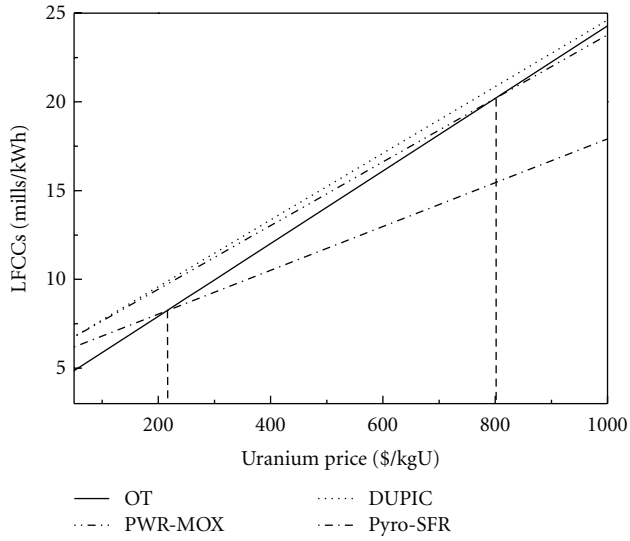

Figure 7: LFCCs dependent on the uranium price.

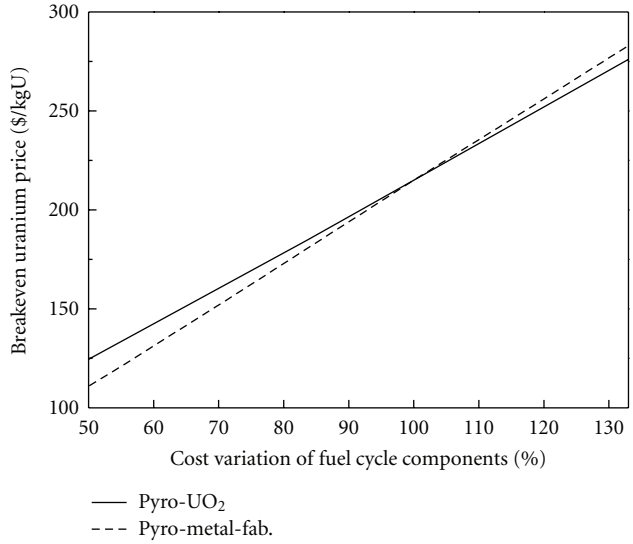

Figure 8: Break-even uranium price dependent on pyrotechniques.

the cost of PUREX, the LFCC of Pyro-SFR cycle can become the same as the LFCC of the OT with a uranium price of 125$/kgU. If the unit cost of Pyro-Metal-Fab. decreases by 50% of the current nominal unit cost, the break-even price of uranium is around 110$/kgU by reaching which the LFCC of Pyro-SFR and LFCC of OT become the same value. The research and development of pyrotechniques may offer a promising economic advantage to Pyro-SFR over the others.

5.6. Sensitivity Analysis of Pyro-UO_2 and Pyro-Metal-Fab. The sensitivity analysis was also performed on the key components of Pyro-SFR with comparatively high uncertainty at the current price. For instance, the reference unit cost of 1500$/kgHM for Pyro-$UO_2$ and 5000$/kgHM for Pyro-Metal-Fab., as quoted from the AFCCI report, was deemed

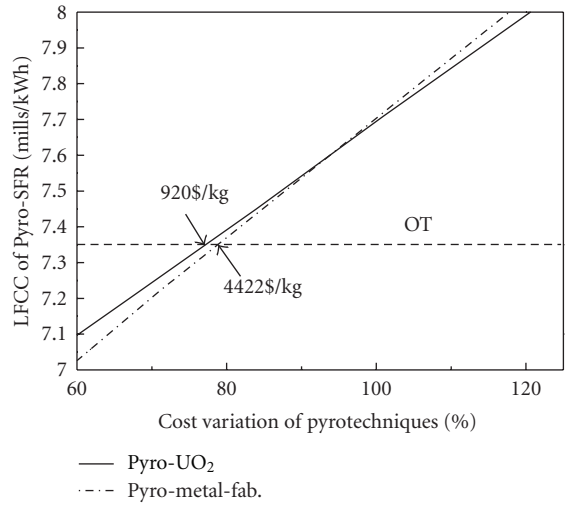

Figure 9: LFCC of Pyro-SFR dependent on the cost of pyrotechniques.

to be a bit too high by some commentators, in view of the possible decrease by research and development.

The break-even price of Pyro-UO_2 with reference to the OT option was evaluated to be 920$/kgHM, which is around 61% of the nominal cost, as shown in Figure 9. This calculation was performed by varying the Pyro-UO_2 costs, while all other costs were fixed to their reference values until the equalization with that of the OT cost was achieved.

The break-even price of Pyro-Metal-Fab. was calculated to be 4422$/kgHM, which is around 88% of the nominal cost, as shown in Figure 9. This break-even price is 18 times higher than the nominal cost of uranium fuel fabrication, which indicates that a promising price decrease may be realized by research and development.

6. Conclusion

The economics of OT, DUPIC, PWR-MOX, and Pyro-SFR fuel cycle scenarios have been calculated and compared by employing an equilibrium model. LFCCs were obtained for a fair comparison: OT 7.35 mills/kWh, DUPIC 9.06 mills/kWh, PUREX-MOX 8.94 mills/kWh, and Pyro-SFR 7.70 mills/kWh. The uranium price in the four scenarios generally acts as the dominant driver of LFCCs. Pyrotechniques also weigh considerably in the Pyro-SFR scenario. In consideration of the current unavoidable uncertainties introduced by certain cost data, a cost range and the triangle techniques were used to perform an uncertainty study, which indicates that the gap between the Pyro-SFR and OT fuel cycle scenarios is relatively smaller than the other options.

Also, the sensitivities of uranium, Pyro-UO_2, and Pyro-Metal-Fab. were carried out to determine the potential advantages of the Pyro-SFR scenario. The break-even price of uranium for a Pyro-SFR was obtained by an increase in the uranium price within a large range, and the break-even price was 215$/kg for Pyro-SFR and 800$/kg for PWR-MOX. With regard to the uranium historical peak price in

2007, it may be worth deploying Pyro-SFR in the foreseeable future. The influences of pyrotechniques on the LFCC of the Pyro-SFR were carried out to clarify the targets for current immature technologies. If the current uranium price remains stable, the break-even price for Pyro-UO_2 is 920$/kgHM and 4422$/kgHM for Pyro-metal-Fab., respectively, which are actually close to the nominal costs employed.

In conclusion, the difference in the fuel cycle costs between the Pyro-SFR and OT fuel cycle is negligible, considering the uncertainty associated with the unit cost of the fuel cycle components. Therefore, other factors such as technological and political risks, environmental effects, public acceptability, and nonsproliferation, could play important roles in determining the future nuclear fuel cycle options.

Acknowledgments

This project has been carried out under the Nuclear R&D Program funded by the Ministry of Education, Science, and Technology of Korea.

References

[1] OECD/NEA, *The Economics of the Nuclear Fuel Cycle*, OECD, Paris, France, 1994.

[2] B. Dixon, W. Halsey, S. Kim, G. Matthern, S. Piet, and D. Shropshire, Dynamic Systems Analysis Report for Nuclear Fuel Recycle, INL/EXT-08-15201 Rev.1, 2008.

[3] Economic Analysis Working Group. AFCI Economic Tools, Algorithms, and Methodology, INL/EXT-07-13293, 2009.

[4] J. M. Deutch and J. P. Holdren, *The Future of Nuclear Power: An Interdisciplinary MIT Study*, Massachusetts Institute of Technology, Cambridge, Mass, USA, 2003.

[5] OECD/NEA, *Advanced Nuclear Fuel Cycles and Radioactive Waste Management, NEA No. 5990*, OECD, Paris, France, 2006.

[6] W. I. Ko, J. W. Choi, J. S. Lee, H. S. Park, and K. J. Lee, "Uncertainty analysis in DUPIC fuel-cycle cost using a probabilistic simulation method," *Nuclear Technology*, vol. 127, no. 1, pp. 123–140, 1999.

[7] S. G. Hong et al., "600 MWe sodium cooled fast reactor core designs for efficient TRU transmutation," The Korean Nuclear Society Spring Meeting, Chuncheon, Korea, May 2006.

[8] T. Inoue, "Actinide recycling by pyro-process with metal fuel FBR for future nuclear fuel cycle system," *Progress in Nuclear Energy*, vol. 40, no. 3-4, pp. 547–554, 2002.

[9] B. H. Park, F. Gao, E. H. Kwon, and W. I. Ko, "Comparative study of different nuclear fuel cycle options: quantitative analysis on material flow," *Energy Policy*, vol. 39, no. 11, pp. 6916–6924, 2011.

[10] M. Bunn, J. P. Holdren, S. Fetter, and B. Van Der Zwaan, "The economics of reprocessing versus direct disposal of spent nuclear fuel," *Nuclear Technology*, vol. 150, no. 3, pp. 209–230, 2005.

[11] OECD/NEA, *Accelerator-Driven Systems (ADS) and Fast Reactors (FR) in Advanced Nuclear Fuel Cycles*, OECD, Paris, France, 2002.

[12] OECD, *Cost Estimating Guidelines for Generation IV Nuclear Energy Systems*, OECD, Paris, France, 2006.

[13] OECD, *Trends in the Nuclear Fuel Cycle: Economic, Environment and Social Aspects*, OECD, Paris, France, 2000.

[14] D. Shropshire et al., Advanced Fuel Cycle Cost Basis, INL/EXT-07-12107, 2007.

[15] D. Shropshire et al., Advanced Fuel Cycle Cost Basis, INL/EXT-07-12107 Rev.1, 2008.

[16] D. Shropshire et al., Advanced Fuel Cycle Cost Basis, INL/EXT-07-12107 Rev.2, 2009.

[17] The Ux Consulting Company, Weekly spot Ux U_3O_8 price, 2010, http://www.uxc.com/review/uxc_Prices.aspx.

[18] W. I. Ko, H. Choi, and M. S. Yang, "Economic analysis on direct use of spent pressurized water reactor fuel in candu reactors-IV: DUPIC fuel cycle cost," *Nuclear Technology*, vol. 134, no. 2, pp. 167–186, 2001.

[19] W. I. Ko, J. W. Choi, C. H. Kang, J. S. Lee, and K. J. Lee, "Nuclear fuel cycle cost analysis using a probabilistic simulation technique," *Annals of Nuclear Energy*, vol. 25, no. 10, pp. 771–789, 1998.

Hindawi Publishing Corporation
Science and Technology of Nuclear Installations
Volume 2012, Article ID 390758, 10 pages
doi:10.1155/2012/390758

Research Article

Dynamic Analysis of a Pyroprocessing Coupled SFR Fuel Recycling

Fanxing Gao and Won Il Ko

Division of Nuclear Fuel Cycle Systems Analysis, Korea Atomic Energy Research Institute, Yuseong, Daejeon 305-353, Republic of Korea

Correspondence should be addressed to Won Il Ko, nwiko@kaeri.re.kr

Received 2 February 2012; Revised 4 April 2012; Accepted 5 April 2012

Academic Editor: Massimo Salvatores

Numerous studies have attempted to solve the problems constraining the sustainable utilization of nuclear power, for example, the already accumulated HLWs, the worsening environment due to greenhouse emissions, the questionable reliability of natural uranium resources, and the argument over nuclear safety, which are certainly top issues to be addressed. A well-organized nuclear fuel cycle system is the basis for nuclear power sustainability. Therefore, which type of reactor to be employed and whether or not to adopt a reprocessing technique for spent fuel are two key issues to be addressed. A Sodium Fast Reactor (SFR), a Generation IV reactor, has gained considerable attention worldwide. SFR recycling coupled to pyroprocessing, a so-called Pyro-SFR Recycling, shows promising advantages, and therefore, this paper focuses on exploring a strategy of how to realize it, which can offer informative procedures for a better use of nuclear power. A dynamic model has been developed to quantitatively analyze a country-specific case employing two scenarios, a once-through and Pyro-SFR, for a comprehensive comparison, especially focusing on the uranium utilization, the HLW reduction, and the electricity generation cost.

1. Introduction

There are generally two methods used to perform a nuclear fuel cycle system analysis, namely, an equilibrium model and a dynamic model. An equilibrium (or steady-state) model focuses on a batch study built with certain assumptions: the referred reactors and fuel cycle facilities already exist and are in perfect operation regardless of the technological, political, and economic constraints on the reactor and back-end process implementation; the derived nuclear fuel cycles are well balanced and organized by different types of reactors with ideal ratios, and the associated infrastructures are already built. However, inevitably these simplified and ideal-condition assumptions appear optimistic in that they omit several important preconditions, including technological maturity, the time needed to reach equilibrium states, social and political concerns constraining the deployment of fuel-cycle technologies, and the economic competitiveness of the different fuel cycles considered [1–5].

It should be noted that the technology readiness level of each potential option is quite different, for example, the once-through cycling (OT) is currently available, but the components in the sodium fast-reactor-involved recycling require several decades to be fully applicable [1, 2, 6]. When to start building a certain component of the optimal option can be answered using a dynamic model.

In our previous studies, a leading alternative, Pyro-SFR recycling, has been derived with regard to several key criteria by employing an overall evaluation based on an equilibrium model [1, 2]. However, the outcome is for a general case, or a theoretical study, which may not be suitable for a specific country due to its own particular situation. Therefore, the goal of the equilibrium model study is to explore a generally optimistic fuel cycle alternative, which may be helpful in understanding the fuel cycle systematically and comprehensively and offer guidance to the promising development. Moreover, the equilibrium model is somewhat too ideal without consideration of several important factors, for example, the timing, technology readiness, and unit cost changes. For a country with specific interests in an objective situation, a variant may be more suitable, and therefore, a country-specific dynamic model has been used

to explore a relative realistic case following the guidelines of the equilibrium model [2, 3, 5].

Based on the equilibrium model study, the SFR involved closed fuel cycle options showing explicit advantages, and therefore, a dynamic model was used to analyze Pyro-SFR fuel cycles with consideration of the timing as a means to answer the following questions. (1) When and how to deploy a reactor fleet to meet the future electricity demand? (2) How much uranium will be consumed by 2100? (3) How large is the spent fuel inventory? (4) What is the state of the proliferation-sensitive actinides inventory by the end of 21st century? (5) Which one is more economically competitive, OT or Pyro-SFR? (6) What is the promising strategy of deploying breakeven reactors (BEs), such as an SFR with a CR of 1.0, and burner reactors (BNs), such as an SFR with a CR of 0.70 [7, 8]? (7) How do the discount rates affect the generation cost of an OT and Pyro-SFR? A once-through option was selected for a comparison with Pyro-SFR for a comprehensive evaluation.

The dynamic model offers a better way to simulate the deployment process of a fuel cycle, which may take several decades. Based on the direction and final target set by the equilibrium model, it is the role of dynamic model to indicate when and how to realize this.

2. Calculation Basis and Methodology

2.1. Reactors and Reprocessing Technology. Generally, two decisions, that is, which kind of reactor to employ and whether or not to deploy a reprocessing technology, mainly determine the direction of the nuclear fuel cycle. The PWR is currently the most popular reactor commercially employed worldwide. Therefore, the parameters of the PWR can refer to the industry facilities. The parameters of SFR, however, mainly come from the conceptual design study with an emphasis on the conversion ratio.

With regard to the specific characteristic of SFR spent fuel, that is, high-burnup and high-plutonium-concentration, the pyroprocessing employing electro-metallurgical techniques in a molten salt medium has the potential to replace the conventional wet reprocessing technology for the treatment of short-cooled SFR spent fuel. The pyroprocessing has been developed to treat the spent oxide fuel discharged from PWRs and recycle the metallic components containing TRUs for SFRs [9, 10]. The metal-fueled SFR using alloys of Actinides-Zirconium (AcZr) has a high potential of recycling actinides by integrating with the pyroprocessing. Accordingly, the pyroprocessing has been assumed to treat metallic SFR spent fuels. However, it should be noted that in this study there are two kinds of spent fuels treated, that is, the spent PWR fuels and the spent fuels of fast reactor. The treatment of PWR spent oxide fuel is for feeding fast reactor with TRU fuels, and the treatment of the spent fuels of fast reactor is for sustaining the Pyro-SFR cycles. According to the different spent fuels to be treated, the locations or organizations of these two pyroprocessing facilities are different. Typically, SFR spent fuel reprocessing is colocated with the fast reactor, and however, LWR spent fuel reprocessing is centralized due to the capacity difference.

In this study, for a country-specific case study, an assumed country that has mastered certain nuclear power operations experience with a PWR spent fuel inventory of 5 ktHM has been adopted. A high population with a small territory and intense dependence of imported uranium are the special characteristics of the assumed country, which makes resource utilization and waste management important. In this study, uranium resource utilization and the amount of waste generation with regard to the fuel cycle options are evaluated in particular, which are indispensable considerations for directing the assumed country toward energy sustainability, as the scarce amount of natural uranium resources and the difficulty of deploying an underground repository for HLW disposal require a longer time, especially due to its high population and small territory.

With regard to the limited domestic uranium resources and issues of HLW disposal, this country plans to transfer the current reactor fleet consisting of PWRs into a combination of advanced PWR and GEN-IV reactors by introducing SFRs and pyroprocessing to close the fuel cycle. Upon consideration of proliferation resistance, two SFR reactors were employed with a conversion ratio no more than 1, or 0.70 and 1.00. The specifications of the PWR and SFRs are listed in Table 1.

The purpose of this study is to simulate and analyze the assumed country with some nuclear power experience and has an intense interest in developing nuclear power. Therefore, at the beginning it was assumed that the specific country has 5 newly built PWR reactors and a certain amount of accumulated spent fuel inventory for a promising introduction of SFR. Actually, such a case study has a wide scale of application, especially for the nuclear power new comers.

2.2. Nuclear Cycle Specification. In the OT Cycle presented in Figure 1(a). SFs from PWRs would be directly sent to a permanent disposal site without further processing. Therefore, the cycle considers only one type of nuclear reactor, and there is no reprocessing associated with the SF under the OT Cycle concept.

Spent UO_2 fuel from a PWR is treated by the pyroprocessing to separate TRU. The recovered TRUs through the process would be recycled into the fast reactors to close the fuel cycle as described in Figure 1(b). The fuel cycle will be referred to as the Pyro-SFR cycle throughout this paper. The same conversion ratios have also been applied to this cycle. Pyroprocessing is suitable for a country that has not been developing a relatively proliferation-risky PUREX but wants to realize a closed fuel cycle, as the pyroprocessing is deemed capable of depositing TRU all together on a liquid Cd cathode without producing pure Pu consequently with a high proliferation resistance. The impact of CR on the SFR to PWR core ratio was determined by the consumption of TRU, because with a higher CR less TRU was burned, and thus fewer PWRs were required for TRU production to support SFRs. The electricity produced would be compatibly distributed between the PWR and SFR. The spent fuel compositions and fuel cycle parameters are listed in Table 2.

Table 1: Characteristics of the reference PWR and SFR.

Reactor Parameters	PWR	SFR (CR = 0.71)	SFR (CR = 1.0)
Electric power (MWe)	1000	600	600
Thermal efficiency (%)	34.23	39.4	39.4
Thermal power (MWt)	2921.40	1,522.8	1,522.8
Load factor	0.85	0.85	0.85
Cycle length (full power day)	290	304	550
No. of batches	3	5	3

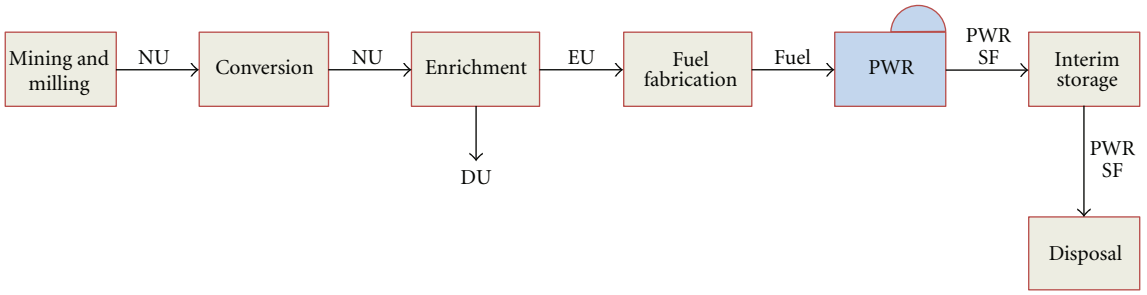

(a) OT

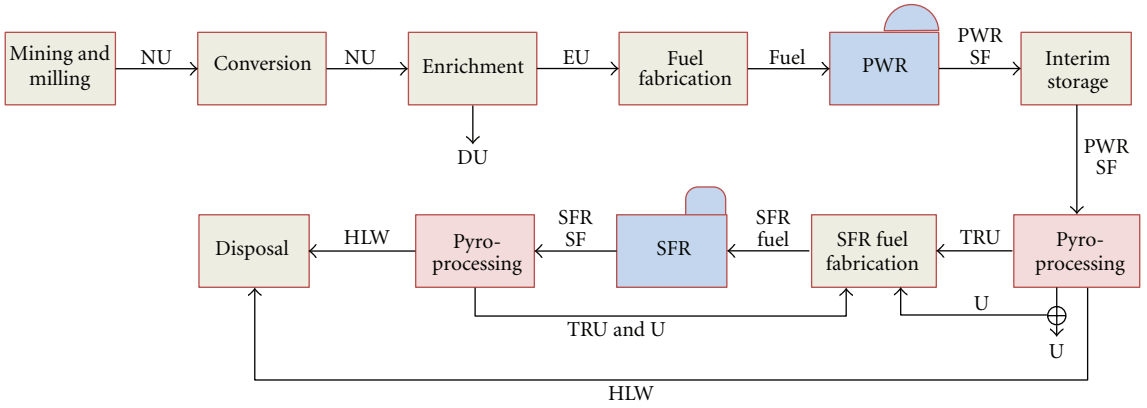

NU: natural uranium
DU: depleted uranium
EU: enriched uranium
SF: spent fuel
TRU: trans uranium

(b) Pyro-SFR

Figure 1: Schematic description of Pyro-SFR fuel cycle option. *NU: natural uranium; DU: depleted uranium; EU: enriched uranium; SF: spent fuel; TRU: trans uranium.

Table 2: Parameters of fuel cycle options.

Fuel Cycle	OT	Pyro-SFR
Enrichment	NU: 0.71% ^{235}U DU: 0.25% ^{235}U EU: 4.5% ^{235}U	NU: 0.71% ^{235}U DU: 0.25% ^{235}U EU: 4.5% ^{235}U
PWR fuel Burnup (UO_2)	55 GWd/tHM	55 GWd/tHM
Back-end for PWR SF	—	Pyroprocessing loss: 0.1% major waste: FP
Metallic TRU SFR fuel (CR = 0.71)	—	Burnup: 131 GWd/tHM TRU: 30%
Metallic TRU SFR fuel (CR = 1.00)	—	Burnup: 100 GWd/tHM TRU: 17%
Back end for SFR SF	—	Pyroprocessing loss: 0.1% major waste: FP

Table 3: Unit costs for nuclear fuel cycle steps.

				Unit	Unit cost
Overnight cost	PWR			\$/kWe	4244
	SFR			\$/kWe	5092
O&M cost charge rate					4.00%
Nuclear fuel cycle		Uranium		\$/kgU	172
		Conversion		\$/kgU	12
		Enrichment		\$/SWU	155
	Fabrication		UO_2 fuel	\$/kgHM	269
	Reprocessing		PWR SF pyro.	\$/kgHM	1194
	Pyro. and fab.		Pyro. and SFR metal fuel fab.	\$/kgHM	5599
	Long-term stro.		Depleted U	\$/kgHM	5
			Reprocessed U	\$/kgHM	3
	Tran. and sto.		SF_UO_2	\$/kgHM	156
			Decay storage	\$/kgIHM	17473
			HLW	\$/m^3	114698
	Packaging		SF_UO_2	\$/kgHM	35
			HLW from pyro.	\$/m^3	35485
	Underground cost			\$/m^3	213
Decommissioning charge rate					15.00%

* SWU stands for separative work unit.

2.3. Unit Cost Specification. The main sources of the unit cost data used in this study were mainly from the OECD/NEA study [11–13] and Advanced Fuel Cycle Cost Basis (short for AFCCB) [14–16], and engineering judgments were used when certain data were not available. The input cost data are listed in Table 3. All the data are presented in 2010 dollars. For the data not in 2010 values, an escalation rate of 3% was used to realize the conversion of the base year. Some specifications of the key components are described as follows.

The cost uncertainties concerning pyroprocessing and capital cost of SFR are unavoidable according to the R&D status. There are numerous studies in the capital costs and pyroporcessing cost, but it is difficult to determine an exact or accurate data and the uncertainties are obvious. In this study, we focus on the impacts of inflation ratio and uranium price prediction model (escalation ratio), and therefore, the somewhat reliable unit costs from OECD studies and AFCCB have been adopted.

In this paper, the pyroprocessing cost was calculated by multiplying the material flow and the corresponding unit costs. The unit cost was obtained by literature survey and reviewed by expert term of Korea Atomic Energy Research and discounted accordingly to the initial year. Therefore, there is no information concerning the capacities of several facilities. However, the authors do admit the importance of facility capacity in the deployment of a nuclear fuel cycle system.

2.4. Calculations. An excel code was composed to finish the material flow study. The equations used to calculate the fuels and services needed to meet the energy demand are the same with those used in the equilibrium model [17, 18]. In the cost analysis, the levelized fuel cycle costs (LFCCs) and levelized generation cost (LGC) have been derived in terms of mills/kWh, respectively, for a fair comparison among the different FCCs. the LFCC and LGC (consisting of all reactors and the supporting fuel cycle services) calculation methods can be referred from the following papers: [3, 17, 18].

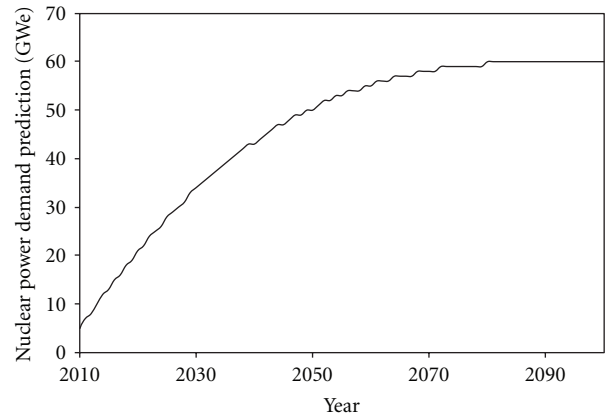

Figure 2: Electricity demand prediction.

2.5. Electricity Demand Prediction. The energy demand determines the reactor employed and finally affects the material flow. The material flow is the basis for the dynamic model analysis. In this study, the evaluated country has been assumed to pursue a nuclear development plan as follows: the nuclear capacity may reach 35 GWe in 2030, 50 GWe in 2050, and finally 60 GWe, and the nuclear power demand prediction is shown in Figure 2 which applies to all the scenarios considered in this study.

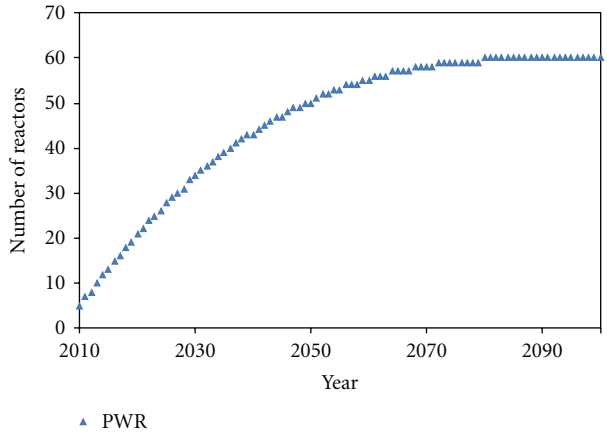

Figure 3: The reactor fleet of OT.

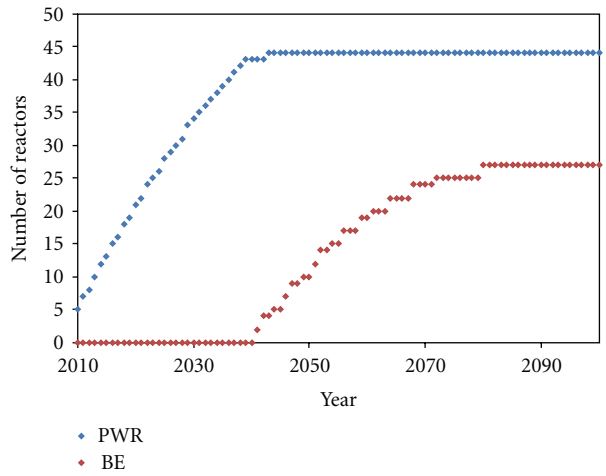

Figure 4: The reactor fleet of BN-only case.

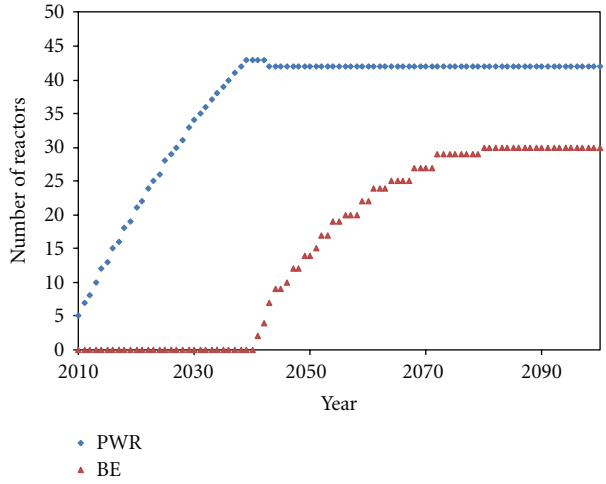

Figure 5: The reactor fleet of BE-only case.

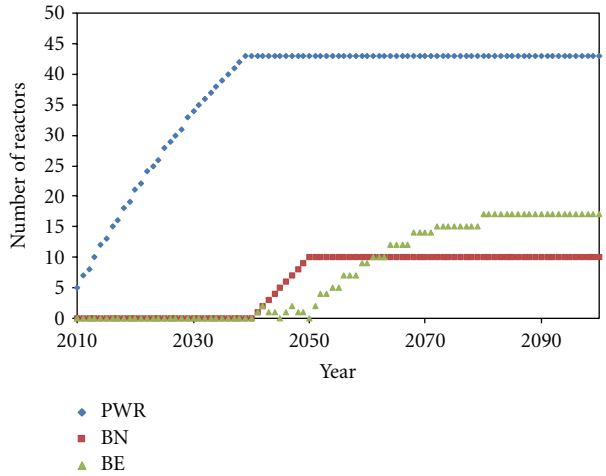

Figure 6: The reactor fleet of BN & BE case.

2.6. Reactor Fleet Deployment Specification. For the OT option, there is only one type of reactor, or PWR, and thus the capacity of PWRs employed equals the nuclear power demand, as shown in Figure 3. For the Pyro-SFR option, there are three types of reactors considered, that is, PWR, BN, and BE, and thus the reactor fleet deployment strategies are different. Assuming that SFRs will be in operation until 2041, three cases of reactor deployment, that is, BN only, BE only, and BN & BE, are specified in Figures 4 and 5, respectively.

A burner (BN) just consumes TRU and a break-even reactor (BE) burns the same amount of TRU as it generates. The reason to employ a BN mixed with BE scenario (BN & BE case) is for a comprehensive comparison to explore the difference performances between the BN & BE mixed case and a sole BN or BE case. The principle or the rule of managing the ratio of BN to BE in the BN & BE mixed case is shown in Figure 6, which was derived on consideration of several factors, for example, the TRU inventory fueling the fast reactors, the pyroprocessing capacity, the technical readiness, and the experts evaluation. It may not be a fully proved plan. However, it serves well as a useful reference. In this study, it should be noted that because the reactor deployment, the schedule of which depends on several factors, plays an important role in controlling the fuel consumption, the waste generation, and the cost, in our future study a more detailed study on the strategy of deployment of new reactors will be carried out.

Some contingency can cause major changes in outcomes, for example, the reactor fleet deployment with consideration of time consumed for the delay of construction or licensing. In this paper, a dynamic model was used to perform a case study with a specific assumption, that is, the deployment of the reactor fleet set in advance will follow the schedule and any disturbs which may probably delay the deployment can be avoided properly. The seemingly easy deployment of a new reactor is based on the assumption that all the constraints during the deployment can be solved timely. In other words, no matter what kind of difficulties may constrain the deployment of a reactor, it can be closed and the deployment will not be affected. This assumption will not affect the dynamic characteristics of the study especially concerning the materials flows, however, which may cause the reduction of some contingency costs.

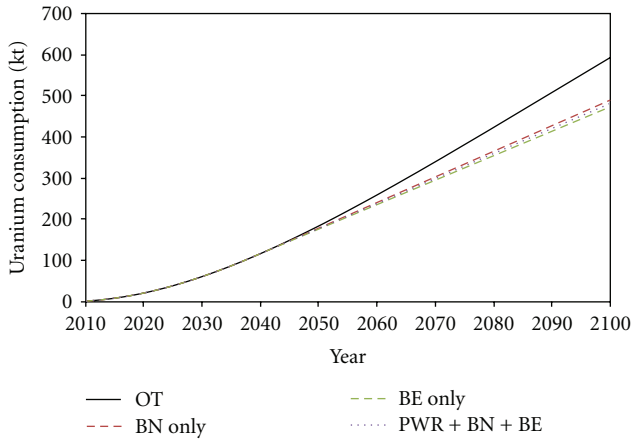

Figure 7: Uranium consumption.

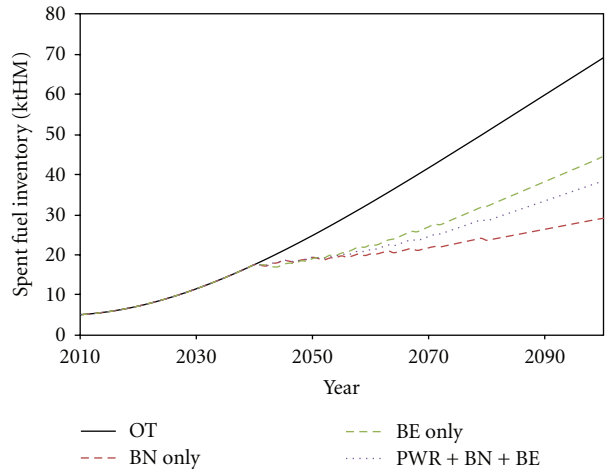

Figure 8: Spent fuel inventory.

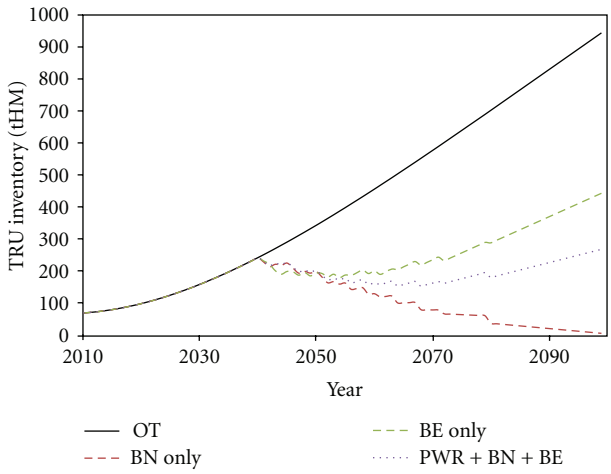

Figure 9: TRU inventory.

2.7. Pyroprocessing Capacity Specification . The reprocessing is the core issue of the back end of a fuel cycle. The impact of pyroprocessing on the fleet of BN/BE and the inventory of spent PWR fuel are essential. Generally, there are two strategies concerning the capacity of pyroprocessing facilities, that is, (1) the annual capacity of the facility is determined by a predetermined pattern, which should be verified by the spent fuel inventory and the experts evaluation; (2) the annual capacity is determined by the practical need of the BN and BE. In this study, the strategy of the capacity pyroprocessing facility follows the TRU needed for refueling the fast reactors, which may be not realistically correct from industrial operation point of view but it is somewhat a clear strategy.

2.8. Consumptions Specification. Dynamic system analysis of nuclear fuel cycle serves as a useful tool for recommending a promising nuclear fuel cycle. Integrated with the outcome of an equilibrium model, it is informative to simulate practical scenario employing a dynamic model. As stated in Section 1, a dynamic mode is deemed to be capable of answering several essential questions concerning the future deployment of nuclear fuel cycle. However, it should be noted that each conclusion derived was based on several assumptions, or the background of the scenario. A slight change to the assumptions can lead to different outcomes. In this study, we mainly focus on a country with an intense interest in nuclear power and an ambitions nuclear power plan. This scenario maybe somewhat too specific, however, which does not affect it to be an informative and useful reference for decision makers.

3. Results and Discussion

3.1. Material Flow Study

3.1.1. Uranium Consumption. With the reactor fleet pattern deployed as shown in Figure 7, Pyro-SFR options saved around 20% of uranium due to the bigger burnup derived by the SFRs making use of TRU recovered from PWR spent fuel. Because natural uranium is mainly consumed by PWRs, there is almost no uranium consumption difference between BN-only, BE-only, and PWR + BN + BE scenarios.

3.1.2. SF Inventory. Figure 8 shows the spent fuel inventory of these four scenarios. The OT generates the most spent fuel without deploying any spent fuel treatment. Accordingly, with reprocessing, SFR-involved fuel cycles considerably decrease the spent fuel inventory.

3.1.3. Actinide Inventory. Pu once disposed of in a geological repository may become "plutonium mines" and cause a nonproliferation burden. Therefore, out-pile Pu, TRU, and MA inventories were obtained as shown in Figures 9, 10, and 11, respectively. A BN can consume 18.8% of the TRU loaded into the reactor, and a BE can consume 1.5% of the loaded TRU, which explains why the BN-only case generates the smallest amount of Pu. The OT option without reprocessing of PWR spent fuel leaves all spent fuel and therefore generates the largest plutonium mines. In the

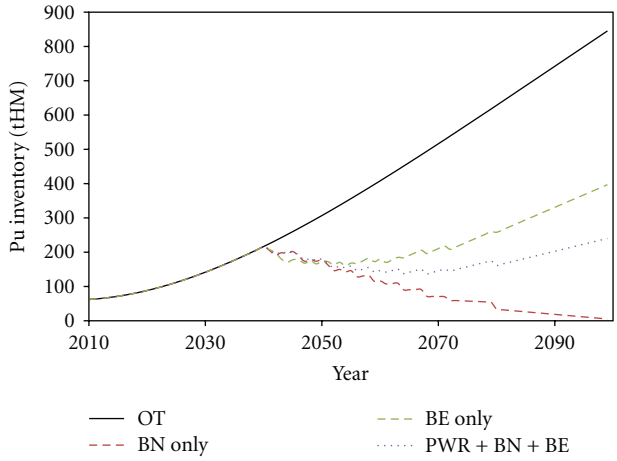

Figure 10: Pu inventory.

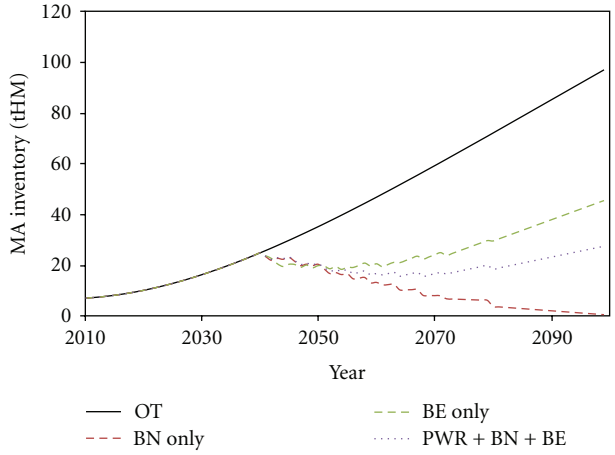

Figure 11: MA inventory.

BN-only case, almost all of the spent fuel from the PWR was reprocessed with the assumption that there is 5 ktHM of accumulated spent fuel in 2010. However, it should be considered that the deployment of BN might be constrained due to a lack of TRU to feed the BN, which can be solved by postponing the BN or reducing the BN percentage in a reactor fleet.

3.2. Cost Analysis

3.2.1. LFCC and LGC. For a fair comparison, the LFCC and LGC of OT and Pyro-SFR (BN & BE) were calculated, and the detailed cost components are listed in Table 4, based on the same unit costs input into the equilibrium model. In the LFCC costs, for both options, the uranium cost plays a dominant role, 73.4% for OT and 68.08% for Pyro-SFR.

For Pyro-SFR case the HLW waste-related costs consists of three parts, that is, the transport and storage cost, the packaging cost, and the disposal underground cost. As listed in Table 4, Pyro-SFR shows obvious advantages over OT concerning the costs of HLW treatments. The disposal of HLW is a burden for nuclear power industry not only because of the troublesome procedures but also because of the high cost, and therefore, it is of great importance to focus on the reduction of HLW. SFR-involved cycle shows clear advantage in reducing the HLW generation, which definitely will contribute to the cost reduction.

On consideration of the relatively smaller share of LFCC in LGC, however, the uranium cost is negligible. In the LGC costs, investment cost and O&M costs take a considerable share. Therefore, due to the bigger capital cost and O&M of a SFR, the fewer the SFRs introduced into a reactor fleet, the less expensive the LGC becomes. However, with consideration of the advantage of SFR in reducing the environmental burden and high costs caused by HLW treatments and its contribution in strengthening the uranium resource reliability, it is worth pondering the cost value.

3.2.2. Sensitivity Analysis

(1) Escalation Rate. Natural uranium spot price is mainly determined by a balance of supply and demand, which is hard to predict with regard to the considerable amount of the world's nuclear power development and the somewhat unclear uranium resource exploration. In this paper, a simplified uranium price model, an escalation model, which is capable of covering a large promising trend, was used [14–16]. The following equation was employed to obtain the uranium price (net present value) prediction shown in Figure 12:

$$\mathrm{U}(t) = \frac{\mathrm{U}(0) \times (1+e)^{(t-t_0)}}{(1+r)^{(t-t_0)}}, \quad (1)$$

where $\mathrm{U}(t)$ is the uranium price at time t (\$/kgU), $\mathrm{U}(0)$ is the uranium price at the reference date (\$/kgU), e stands for the escalation rate, r is the discount rate (e.g., 5%), and t_0 is the reference time.

By changing the escalation rate applied to the uranium price model, the LGC dependent on the escalation rate was obtained and is shown in Figure 13. There is a cross point when the escalation rate surpasses 4.6%, which indicates that when the future uranium price shows the trend indicated by the plot in Figure 13, Pyro-SFR is more competitive than OT by a discount rate of 5%. This indicates that if the uranium price remains as high as 171 \$/kg, with a discount rate of 5% and an escalation rate of 4.6%, the OT is costly.

(2) Discount Rate. With regard to the lead and lad time of the money distribution pattern, a discount rate (DC) plays a considerable role in affecting the LGC. There are mainly two kinds of discount rates, that is, nominal discount rate and real discount rate. The nominal discount rate covers compensation for money purchase power reduction caused by inflation; a real return; compensation for the extent of risk undertaken by committing capital to this investment. The real discount rate does not consider the inflation. Discount rates have a close relationship with risks involved

Table 4: Levelized cost components (unit: mills/kWh).

Component		OT		Pyro-SFR	
		Cost	Share	Cost	Share
Capital cost		35.05	49.49%	36.60	50.13%
O&M		22.80	32.19%	24.31	33.30%
LFCC	Uranium	9.32	73.40%	8.06	68.08%
	Conversion	0.23	1.80%	0.21	1.80%
	Enrichment	2.19	17.28%	2.05	17.29%
	PWR fuel fabrication	0.55	4.36%	0.52	4.36%
	SFR fuel fabrication	—	—	0.33	2.79%
	Subtotal for front-end	12.29	96.84%	11.17	94.32%
	Transport and dry storage	0.32	2.53%	0.13	1.14%
	Pyroprocessing	—	—	0.50	4.21%
	Decay storage (Cs/Sr)	—	—	0.04	0.33%
	Packaging cost	0.07	0.57%	0.00	0.00%
	Disposal underground cost	0.01	0.07%	0.00	0.00%
	Subtotal for back end	0.40	3.16%	0.67	5.68%
	LFCC total	12.69	100.00%	11.84	100.00%
D&D		0.28	0.40%	0.26	0.36%
LGC total		70.82	100.00%	73.02	100.00%

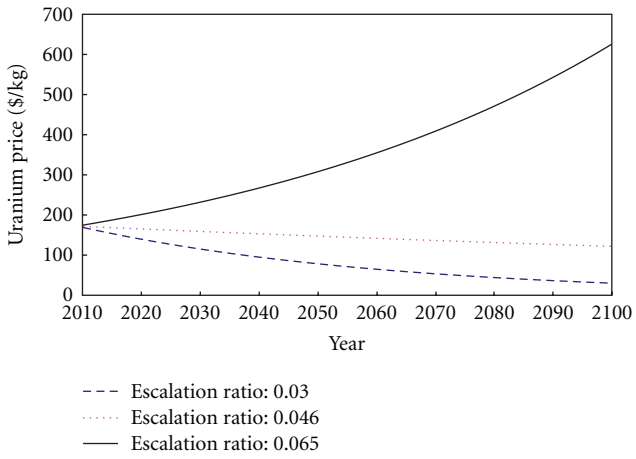

Figure 12: Uranium price model with a discount rate of 5% applied.

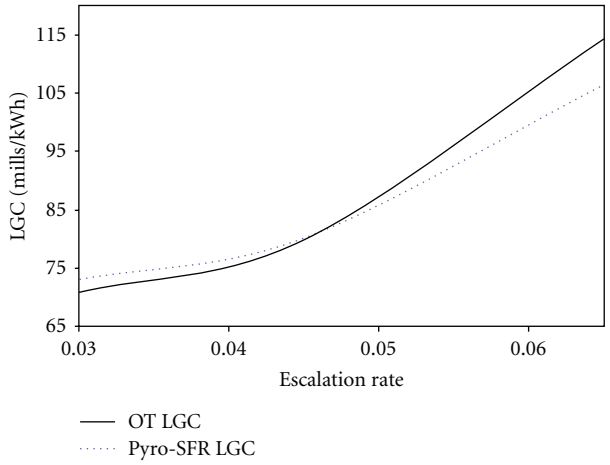

Figure 13: LGC dependent on escalation rate.

in each technique. In the fuel cycle system analysis, various technologies are employed, so case-dependent discount rates should be adopted correspondingly, which leads to different discount rate for each new technology. For projects employing risky technologies, the appropriate discount rate should be somewhat higher than that for a project with less risky technologies. For a fair comparison, it is worth considering the varieties of discount rate. The risks of investing in different components of an NFC and among various NFCs are quite different, it is reasonable not to adopt the same discount rate for all fuel cycle alternatives, and therefrom, a range of real discount rate was applied to each nuclear fuel cycle.

Consequently, in order to resemble the uncertainty of discount rate, attention was always paid to cover a range of discount rate usually from 0 to 15% for each fuel cycle option, respectively. Actually, in the same nuclear fuel cycle, however, the big effects due to employing different discount rates for each component should be also taken into account, especially for D&D cost due to its expenditure pattern. Fundamentally, the longer time considered the more important role the discount rate plays. The cost of D&D is therefore transformed into a neglected value with somewhat 5% discount rate, however, which might not be the case actually [19]. The contribution of D&D cost to the LGC will be reconsidered by employing a specified discounting pattern with consideration of the social responsibility.

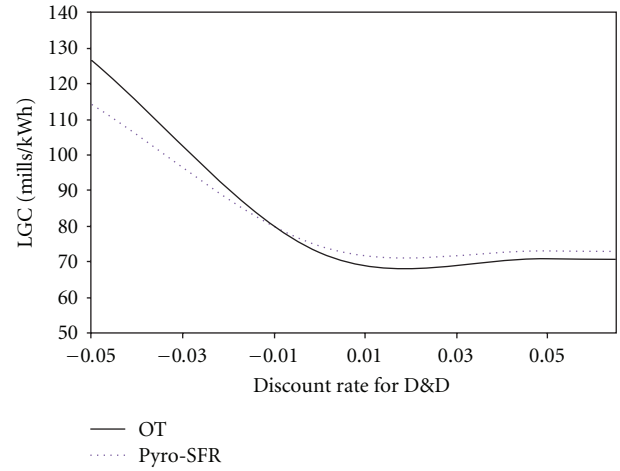

Figure 14: LGC dependent on discount rate for D&D.

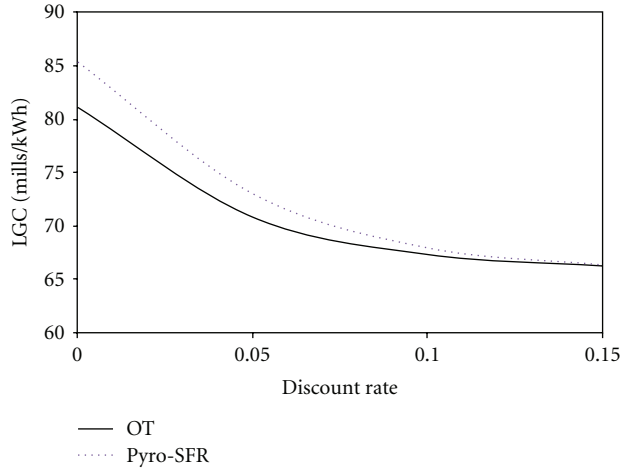

Figure 15: LGC dependent on discount rate.

(a) Discount Rate for D&D. Concerning the social pressure and future uncertainty, it was suggested that a specific discount rate should be applied to the decommissioning. To clarify the important impacts of discount rates on LGC, a sensitivity analysis of the discount rate for D&D was carried out, as shown in Figure 14. There is a cross point when the specific discount rate for D&D reaches −1%. This indicates that, if the social pressure or future uncertainty increases the D&D cost, the electricity generated by the Pyro-SFR may become cheaper than the OT.

(b) Discount Rate for Fuel Cycles. A sensitivity analysis was also performed for a discount rate applied to all components in the OT and Pyro-SFR. It is explicit that, by increasing the discount rate used, the LGCs of both OT and Pyro-SFR decrease dramatically, as shown in Figure 15. Therefore, attention should be paid to discount selection, which may affect the outcome considerably, however, without changing the rankings.

It should be noted that the specific discount rate or price escalation rate that represent a value point at which the SFR is as economic as the LWR has been obtained employing a set of unit costs. However, there are unavoidably high uncertainties associated with certain component unit costs, and therefore, by changing the inputted unit costs, the obtained discount rate or escalation rate can be considerably different. In this study, the input unit cost data are from somewhat reliable OECD series studies and AFCCI reports; nevertheless, the unavoidable uncertainties still exist.

4. Conclusion

Following the guidance of an equilibrium model study, Pyro-SFR Recycling was selected to perform a country-specific dynamic analysis by a comparison with OT Cycling to explore a realistic strategy for nuclear fuel cycle deployment in the long term by 2100.

The reactor fleet deployment in the long term is generally constrained by several factors, that is, a national energy demand, resource sustainability, technology availability, social acceptance, and so forth. Assuming a country has committed an explicit nuclear power development plan with its specific situations concerning resource, technology, and social acceptance, this dynamic study performed a comparison between OT and Pyro-SFR options focusing on the material flow and cost analysis.

Total uranium consumption by the year 2100 can be reduced by burning TRU recovered from spent fuel in SFR, BN, or BE, and therefore, Pyro-SFR options show predominant advantages over the OT option in terms of fuel efficiency. The spent fuel inventory of Pyro-SFR by employing reprocessing is also much smaller than that of OT without any spent fuel treatment. In a Pyro-SFR option, two SFRs with different CRs were employed (i.e., BN, BE). The TRU metallic fuel for SFR is from the reprocessing of PWR spent fuel, and thus accumulated PWR spent fuel constrains the beginning year of SFR operation and the number of SFRs available. With regard to inventories of a proliferation-sensitive material, that is, Pu, TRU, and MA, Pyro-SFR also indicates an advantage over the OT option.

The cost analysis of OT and Pyro-SFR was performed for a comprehensive comparison. LFCC and LGC of an OT and Pyro-SFR were obtained, that is, 12.69 mills/kWh for LFCC of the OT, 11.84 mills/kWh for LFCC of the Pyro-SFR, 70.82 mills/kWh for LGC of the OT, and 73.02 mills/kWh. With consideration of the uncertainties of three key parameters which play a considerable role in the cost analysis (i.e., escalation rate applied to the uranium price model, specific discount rate for decommissioning, and discount rate for the whole nuclear fuel cycle), a sensitivity analysis was carried out to compare the LGCs of the two options. If the escalation rate is more than 4.6%, the Pyro-SFR is more economically competitive than the OT. If the future burden of D&D increases considerably, with a specific discount rate of −1% applied to D&D, the OT is more costly than the Pyro-SFR. The outcome of a sensitivity analysis of the discount rate applied to the whole fuel cycle indicates that the impact of the discount rate was explicit, and thus more attention should be

paid to the appropriate selection of a discount rate for the long-term strategy study.

It should be noted that, although this is a country-specific case study concerning an assumed country with some nuclear experience and an ambitious nuclear plan, both the methods and outcomes of this paper can provide guidance for other future studies.

Acknowledgment

This work has been carried out under the Nuclear Research and Development Program of Korea Ministry of Education, Science and Technology.

References

[1] B. H. Park, F. Gao, E. H. Kwon, and W. I. Ko, "Comparative study of different nuclear fuel cycle options: quantitative analysis on material flow," *Energy Policy*, vol. 39, no. 11, pp. 6916–6924, 2011.

[2] G. Fanxing, *Modeling and system analysis of different fuel cycles for nuclear power sustainability*, Ph.D. thesis, Department of Quantum Energy and Chemical Engineering, Korea Atomic Energy Research Institute Campus, Korea University of Science & Technology, Seoul, Republic of Korea, 2012.

[3] DANESS v1.0 Users Manual, Argonne National Laboratory Nuclear Engineering Division, 2004.

[4] B. Dixon, S. Kim, D. Shropshire, S. Piet, G. Matthern, and B. Halsey, "Dynamic systems analysis report for nuclear fuel recycle," Tech. Rep. INL/EXT-08-15201 Rev.1, 2008.

[5] W. I. Ko, *Model development for quantitative evaluation of nuclear fuel cycle alternatives and its application*, Ph.D. thesis, Department of Nuclear Engineering, KAIST, Daejeon, Republic of Korea, 2000.

[6] W. I. Ko, H. D. Kim, and M. S. Yang, "Advantages of irradiated DUPIC fuels from the perspective of environmental impact," *Nuclear Technology*, vol. 138, no. 2, pp. 123–139, 2002.

[7] Y. Ishiwatari, Y. Oka, and S. Koshizuka, "Breeding ratio analysis of a fast reactor cooled by supercritical light water," *Journal of Nuclear Science and Technology*, vol. 38, no. 9, pp. 703–710, 2001.

[8] S. G. Hong, Y. Kim, and F. Venneri, "600 MWe sodium cooled fast reactor core designs for efficient TRU transmutation," in *Proceedings of the The Korean Nuclear Society Spring Meeting*, Chuncheon, Republic of Korea, May 2006.

[9] M. Cometto, P. Wydler, and R. Chawla, "A comparative physics study of alternative long-term strategies for closure of the nuclear fuel cycle," *Annals of Nuclear Energy*, vol. 31, no. 4, pp. 413–429, 2004.

[10] T. Inoue, "Actinide recycling by pyro-process with metal fuel FBR for future nuclear fuel cycle system," *Progress in Nuclear Energy*, vol. 40, no. 3-4, pp. 547–554, 2002.

[11] OECD/NEA, *Uranium 2009: Resources, Production and Demand*, OECD Nuclear Energy Agency, Paris, France, 2009.

[12] OECD/NEA, *The Economics of the Nuclear Fuel Cycle*, OECD Nuclear Energy Agency, Paris, France, 1994.

[13] OECD/NEA, "Advanced nuclear fuel cycles and radioactive waste management," Tech. Rep. 5990.OECD, Nuclear Energy Agency (NEA), Paris, France, 2006.

[14] D. Shropshire, K. A. Williams, W. B. Boore et al., "Advanced fuel cycle cost basis," Tech. Rep. INL/EXT-07-12107, 2007.

[15] D. Shropshire, K. A. Williams, W. B. Boore et al., "Advanced fuel cycle cost basis," Tech. Rep. INL/EXT-07-12107 Rev.1, 2008.

[16] D. Shropshire, K. A. Williams, W. B. Boore et al., "Advanced fuel cycle cost basis," Tech. Rep. INL/EXT-07-12107 Rev.2, 2009.

[17] J. Deutch and E. Moniz, *The Future of Nuclear Power: An Interdisciplinary MIT Study*, Massachusetts Institute of Technology, Cambridge, Mass, USA, 2003.

[18] M. Bunn, B. van der Zwaan, J. P. Holdren, and S. Fetter, "The economics of reprocessing vs. direct disposal of spent nuclear fuel," Tech. Rep. DE-FG-26-99FT4028, 2003.

[19] H. Khatib, "Review of OECD study into 'Projected costs of generating electricity-2010 Edition'," *Energy Policy*, vol. 38, no. 10, pp. 5403–5408, 2010.

Hindawi Publishing Corporation
Science and Technology of Nuclear Installations
Volume 2012, Article ID 718034, 19 pages
doi:10.1155/2012/718034

Research Article

Development of Tools, Instrumentation and Codes for Improving Periodic Examination and Repair of SFRs

François Baqué,[1] Frédéric Reverdy,[2] Jean-Michel Augem,[3] and Julien Sibilo[4]

[1] *Nuclear Technology Department, CEA, 13108 Saint Paul lez Durance Cedex, France*
[2] *Imaging and Simulation for Control Department, CEA, 91191 Gif-sur-Yvette Cedex, France*
[3] *EDF, SEPTEN, 12-14 Avenue Dutrievoz, 69628 Villeurbanne Cedex, France*
[4] *Nuclear Power Division, AREVA, 10 rue Juliette Récamier, 69456 Lyon Cedex 06, France*

Correspondence should be addressed to François Baqué, francois.baque@cea.fr

Received 21 December 2011; Accepted 1 March 2012

Academic Editor: Toshikazu Takeda

In the frame of the CEA, EDF, and AREVA coordinated research program launched in 2007 for the development of Generation IV sodium-cooled fast reactors (SFRs), the improvement of in-service inspection and repair (ISI&R) capabilities was identified as a major issue. Within the French-associated multiannual SFR research program, the periodic examination and repair are looked at through the following main R&D axes: (i) improvement of the primary system conceptual design in order to ease periodic examination and repair, (ii) development of inspection techniques (periodic inspection tools and associated simulation), (iii) accessibility and associated robotics, and (iv) development and validation of repair processes. Associated needs are being defined through an iterative method between designers and inspection specialists: adaptation of the SFR design to ISI&R requirements, validation of the ultrasonic transducers, of associated ultrasonic nondestructive examination techniques, of laser repair processes, of associated robotic equipment. International collaboration is also running for some specific items such as ultrasonic visualization under liquid sodium.

1. Introduction

From within the framework of the French Act, dated June 28, 2006, which requests an assessment of the industrial perspectives of transmutation by 2012, the Generation IV systems, especially the sodium-cooled fast reactors seem to be the most mature technology to be developed among the systems proposed for sustainable energy. Thus, since 2007, the CEA, EDF, and AREVA French partners launched a coordinated research program on sodium cooled fast reactors (SFR), which is now being used for the next ASTRID (advanced sodium technological reactor for industrial demonstration) prototype [1]. These program main axes were classified into four R&D items:

(1) design of a core with enhanced safety;

(2) better resistance of SFRs to severe accidents and external hazards;

(3) research on an optimized energy conversion system to reduce the sodium risk;

(4) review of reactor and component design options in order to:

   (i) improve inspection, maintenance, availability, and decommissioning;

   (ii) reduce the environmental impact while reinforcing resistance to proliferation;

   (iii) improve the reactor performance and overall economic aspect.

Among these items, improvement of in-service inspection and repair (ISI&R) is a major transverse issue [2]. ISI&R is strongly linked to safety analysis (the three defense lines: checking the state of material and equipment during the reactor's life span, detection of premature failures, and in

operation detection of significant failures), economic reliability (implementation delays), and investment protection (repair).

One of the major difficulties for SFR ISI&R deployment is the sodium environment. Indeed, the sodium has several characteristics which tend to make in-service inspection and repair complex, especially by comparing with Light Water Reactor ISI&R.

Firstly, the sodium is very reactive with air and water: this leads to monitor carefully the confinement and steam generators leakage and to control the tightness during the interventions.

Secondly, due to the risk of under stress caustic corrosion appearance (when a small quantity of sodium, recovering the stainless steel internal structures is in the presence of moisture), the reactor sodium draining is only planned for exceptional interventions, and the current inspections and operations have then to be realized under sodium.

Thirdly, linked to the sodium physical characteristics, the temperature corresponding to plant cold shutdown condition is about 200°C (the in-operation temperatures being comprised between 400°C and 550°C). Thus, ISI&R devices have to work at these high temperature levels.

Last but not least, the sodium being opaque, each intervention (inspection/repair) below the free sodium level cannot be performed/followed by optical devices, so, up to now the mostly used techniques are the ultrasonic ones.

Considering the ISI&R importance for SFR, but also the sodium environment complexity, the multiannual R&D program launched in 2007 takes into account feedback experiences from former French sodium reactors (Rapsodie, Phenix and Superphenix [3]).

This specific R&D program, whose global objective is to increase ISI&R capabilities, can be divided into four sections [4]:

(i) conceptual design improvement of the primary and secondary systems in order to reduce the number of structures and components to be surveyed, to locate sensitive zones in accessible areas from either inside or outside, and to reduce the number and length of welds;

(ii) development of measurement techniques and surveillance devices for continuous monitoring during reactor operation and for periodic examinations during reactor shutdown;

(iii) improvement of accessibility and development of remote-controlled devices (robotics) with suitable carriers;

(iv) identification, development, and validation of repair processes (core discharge and sodium draining), as well as techniques for repair operations in sodium environment.

Based on existing ISI&R feedback experience from sodium-cooled systems, the general ISI&R objectives were defined, with respect to the preliminary specifications issued by the French utilities (EDF) for the future SFRs.

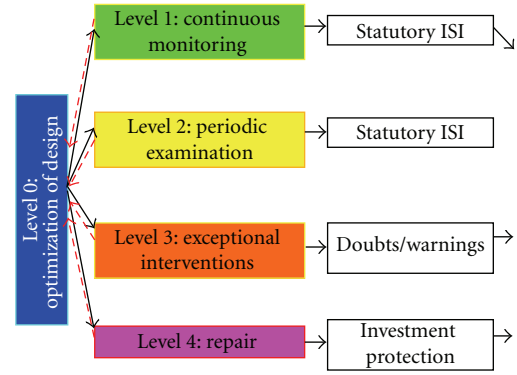

Figure 1: ISI&R approach for future French SFRs.

For ASTRID first criticality, it will be necessary to get a sufficient, available, efficient, and qualified instrumentation. Moreover, it is planned to test in ASTRID during its operation, the instrumentation which has to be qualified for the future nuclear plants (Generation IV).

The running program of research and development implies, on the one hand, usual and available devices to be improved, and, on the other hand, innovative ones to be developed, tested, and qualified.

This paper focuses on the French developments undertaken for periodic examination and repair of reactor core vessel and associated internals. ISI&R of other components (such as heat exchangers like steam generator units) are also looked at in the running program but are not described here.

2. Specifications for ISI&R Future SFRs

In service inspection for SFR must take part in the reactor integrity demonstration, by checking the structures insuring the three main safety functions (reactivity monitoring, decay heat removal, and containment of hazardous products).

The surveillance graduation applied to each structure is defined thanks to the "risk-informed method," which takes into account the damage probability all along plant life and the associated consequences.

Repair ability is also an important specification for SFR, as it can save the overall investment.

ISI&R approach is now parted in five levels for SFR design (Figure 1): a new Level 0 allows both to reduce ISI&R needs by design optimization and to take into account ISI&R requirements for design.

2.1. L1-Continuous Monitoring. ISI&R level 1 deals with continuous monitoring during reactor operation (including power operation with sodium temperature reaching 550°C). It is mainly based on the operating parameters checking (neutronics, temperatures, flow rates, and pressure) with some global measurements reflecting the structure and component states (leaks, mechanical deformation, and vibratory or acoustic characteristics). continuous monitoring of the inner structures within the reactor block (Figure 2) is mainly performed by the book keeping of reactor phases

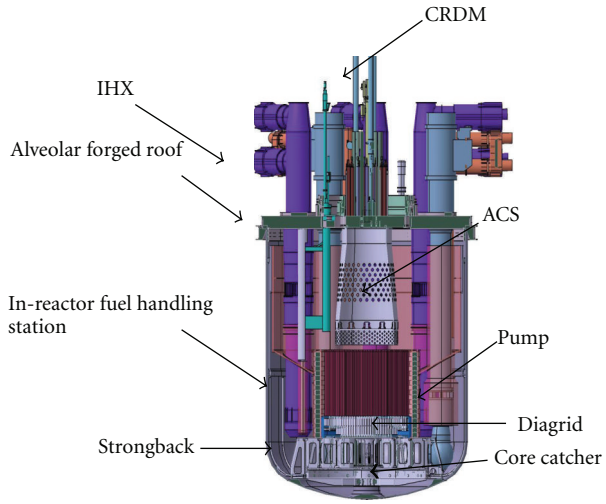

Figure 2: Preconceptual design for SFR reactor block.

(countdown of allowed transients). Level 1 monitoring has to early detect any parameter drifts, or irregularities with regard to the operating range. This item is out of the scope of the present paper.

2.2. L2-Tests and Periodic Examinations. During reactor cold shutdowns (sodium at about 200°C), ISI&R level 2 brings together tests and examinations in a statutory program (NDE purpose: nondestructive examinations).

In addition to the confirmation of the status observed by continuous monitoring, the periodic inspection program must provide the validation of the hypothesis and project values about the damaging mechanisms considered during the design studies. Moreover, ISI&R level 2 must look for the unforeseen damaging mechanisms, in order to check the material mechanical property degradation process, and the absence of corrosion-type mechanism. Mainly focused on safety-related structures (core support structure (see Figure 3), above core structure (ACS), and reactor vessel), these checks may be also carried out on minor structures (inner vessel, and various baffles).

Even if some components can be inspected after their removal from the reactor (primary pump (PP), control rod drive mechanisms) for maintenance, other parts of the reactor block need specific means for in situ inspection.

Because they are easier and quicker, other inspections are preferentially performed from outside the main vessel, even for example, using immersed structures as ultrasonic waveguides.

Nevertheless, other inspections have to be performed within the reactor block: the checks mainly consist in visual observation in the gas upper volume, but also in sodium telemetric positioning control, and volumetric non-destructive examinations of welded junctions.

Even if up to now ultrasonic techniques are mainly used, other means are of course to be investigated.

Although the SFR inspected zone rate has to be highest as possible; nevertheless, the periodic inspection program

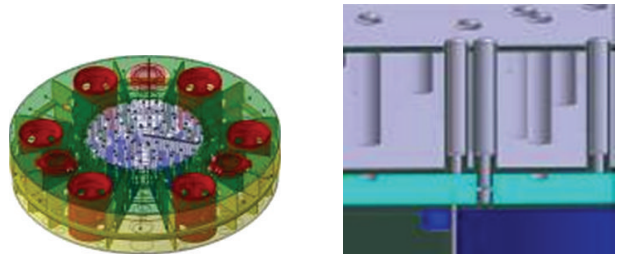

Figure 3: Integrated diagrid-strongback option (general view and strongback access detail).

duration must be suitable for a high-target plant availability rate.

2.3. L3-Inspection Exceptional Extension for Analysis. ISI&R level 3 is the answer to abnormal situations, which may be consecutive to in-operation warning or to an operation mistake. This ISI level purpose is to allow exceptional intervention for control. From reactor shutdown, due to unforeseen event, to the localization and characterization of the fault, the level 3 insures the entire range of associated operations.

According to the possible hazardous situations, this level must enable to reach and inspect most of the reactor zones. For that purpose, it is necessary to provide the most extensive access to the internal structures. First, the design studies have to take this requirement into account. Then, the sodium-immersed devices, including sensors and carriers (like for L2), have to be available. Furthermore, if the needed operation requires a more accurate examination, or if it is sodium incompatible, core unloading and sodium draining have to be performed. These provisions, considered only in exceptional cases, are studied since the preliminary R&D phase. Main issues deal with draining without caustic stress corrosion risk and performing the entire operation (core unloading, draining, examination, and reverse operations) within the duration target of one year maximum.

In addition, the primary components withdrawal (intermediate heat exchangers IHX, PP) may be necessary to get an improved access. The target duration for the associated removal and replacement is about one month per component (within the one-year maximum duration for exceptional intervention).

In this frame, only few technical solutions are available, then this justifies undertaking a significant effort for innovation, especially for under-sodium applications.

2.4. L4-Repair and Replacement. For SFRs, it is necessary to be able to guaranty the investment protection during the whole life span, even in case of unforeseen damage. That is why ISI&R specifications incorporate the repair ability for all the structures, and the replacement possibility for the primary components. These provisions are now insured by ISI&R level 4.

The level 4 operations are considered, when the defect origin has been identified (after levels 2 or 3 examination).

Repair or replacement operations are performed in sodium environment: in the argon cover gas standard volume, under sodium with tight cavity, or in argon gas after sodium draining. The choice between the repair and the replacement is made by taking into account the damaged structure type (replacement possibility), the failure extent, and the implementation costs and durations.

To favor this ISI&R level implementation, the reactor structures have to be simple and accessible. As far as possible, the high thermomechanically loaded structures have to be designed as replaceable. Then, the ISI&R level 4 operations require repair tools to perform preliminary sodium local removing, machining, and welding. The robotic carriers, which carry the tools, have to be suitable for sodium environment, but they have also to absorb machining forces, and to recover the produced wastes.

Of course, repair has to be avoided; nevertheless, associated operations have to be foreseen. Consequently, both reactor block and repair tools have to be designed in adequacy in order to allow any exceptional intervention.

Even if the main challenge deals with the reactor block system, the same approach is also applied to all other sodium devices and loops.

In this frame, other useful existing industrial or R&D feedback experience is looked at, whatever the original field.

3. Design Studies for ISI&R Improving

3.1. Global Design. Being a welded stainless steel manufacturing, operating at high temperatures (400–550°C), with significant thermal gradients, under neutron and gamma fluxes, during 60-year lifetime, future SFRs will undergo some significant loadings. These loadings may lead to failure modes such as:

(i) excessive deformation;

(ii) ratcheting;

(iii) fatigue for the cold pool zones;

(iv) creep-fatigue for the hot pool zones;

(v) buckling for thin structures in compression;

(vi) thermal striping for zones subjected to high thermal gradient mixtures;

(vii) irradiation damage for the structures near the core;

(viii) corrosion;

(ix) wear.

The risk reduction of the potential damage, which is an important issue for design studies, also allows minimizing surveillance, examination, and repair needs. Thus, the reactor global design has to be selected, taking into account this requirement, and by collaborating with ISI&R specialists. The work mainly consists in proposing a robust design with no thermomechanical weak areas. Therefore, the welds number has to be reduced, and the remaining ones are to be located in low-loaded areas. Moreover, geometrical singularities which may induce some stress concentrations or unusual operating ranges (cavitation wear, erosion, excessive, and vibrations) are to be avoided. Finally, this previous design work, which reduces ISI&R provision range, is being made for SFR design architecture (1500 MWth pool type) shown in Figure 2.

A related work is undertaken by the French partners for improving existing design rules: thus, RCC-MRx new code will include, in 2012 edition, NDE "good practice" information in order to ease/make them possible, through specific NDE recommendations for designers. This is part of Level 0 item (see Figure 1).

3.2. Access and Examination Ability Improvements. The reactor design has to favor ISI implementation with the help of sufficient accessibility and a suitable positioning of areas to be inspected. Therefore, an advanced design of the pool type architecture has been proposed. Additional design studies have to be made to fully increase the reactor design ability for ISI&R deployment and performing.

3.3. Repair and Replacement Ability. The design has also to deal with repair operations by simplifying the structures and with replacement operations enabled by the removable component proposals.

The structure simplification has been evoked in the previous paragraphs, and the design proposed options contribute to make the repair operations easier, especially the ISI&R dedicated pool type reactor with few and simple internal structures.

The replacement operations have also to be foreseen since the design phase, taking into account the components and structures which may require it. Being the case for the PP and the IHX, some optimizations of the interfaces between the components and the roof have been proposed in order to make the removal easier and to reduce the associated durations. Above core structure (ACS) is a highly thermomechanically loaded structure, and so its replacement during reactor lifetime has to be considered too.

4. Technological Developments

4.1. Multiannual R&D Program. In parallel to increasing ISI&R performances, the feedback experience taken into account, and the design improvements, the new SFR ISI&R objectives require also some technology progresses, and more particularly for under sodium devices: non destructive examination (NDE), tools for basic repairs, robotic for carriers.

Thus, a multiannual R&D program, implying the CEA, EDF, and AREVA, started in 2007 for SFRs, the following paragraphs focusing on the main significant developed technologies up to now in this frame.

Since 2010, the program purpose is not only to develop and to master the ASTRID ISI&R requested technologies but also more innovative ones.

4.2. Inspection Simulation: CIVA Software for Ultrasonic Applications. Ultrasonic inspection deals with:

(i) telemetry measurement within primary sodium of the main vessel, for the periodical checking of internal structure location;

(ii) nondestructive Examination of internal structures and vessels.

Two approaches are being followed: inside inspection where transducers are directly immersed in sodium coolant (see Figure 8 and Section 4.3) and inspection from outside with transducers positioned along the wall of the main vessel (see Figure 4 and Section 4.4). For both cases, acoustic bulk waves and guided/surface waves (see Figure 12 and Section 4.5) are looked at. Probe design and inspection performances can be predicted by using comprehensive models that can take into account the various variables of the problem: attenuation and deflection, transmission and reflection of ultrasounds, which depend on liquid sodium characteristics (mainly temperature and micro bubble fields), of immersed structures characteristics (mainly wetting at liquid/solid interface, thickness, and shape).

4.2.1. Simulation of Ultrasonic Inspection Through Screens. Telemetry based on ultrasonic waves can be used to monitor the position of internals and equipment introduced inside the vessel. Ultrasonic probes positioned outside the reactor along the main vessel wall can be used to perform telemetry measurement without requiring previous sodium conditioning (Figure 4). However, inspection from outside requires to go through one or several metal plates (main vessel wall, baffle) leading to losses of energy at each interface. It is important to determine the level of these losses in order to estimate the possibility to measure the position of the various internals and propose other configurations of inspection in case the signal-to-noise ratio (SNR) becomes too low. One way to perform this estimation is to use modeling.

Ultrasonic simulation tools have been developed and implemented in CIVA [5, 6]. A method based on a pencil approach allows the calculation of ultrasonic beam fields in heterogeneous media taking into account material attenuation and energy losses at interfaces between media of different acoustic properties. Kirchhoff models have been developed to calculate the interaction of these beams with surfaces and/or defects of various shapes. In order to validate these models for telemetric applications, experiments were carried out in water with two 40 mm thick stainless steel plates supposed to represent the main vessel wall, and an internal structure was used. Transducers were positioned along one of the plates in a pulse/echo normal configuration and in a pitch and catch nonnormal incidence configuration.

For normal incidence application, CIVA predicts well the exponential decay of the ultrasonic energy reflecting back and forth in the plate supposed to represent the main vessel wall (Figure 5). Multiple reflections still have significant energy by the time the echo off the front surface of plate 2 is detected, meaning that it can be difficult to interpret echoes coming from objects located close to the main vessel wall. Simulation can thus be used as a tool to predict the arrival times of the various echoes reflected off the internals. CIVA predicts correctly the amplitude of all the echoes,

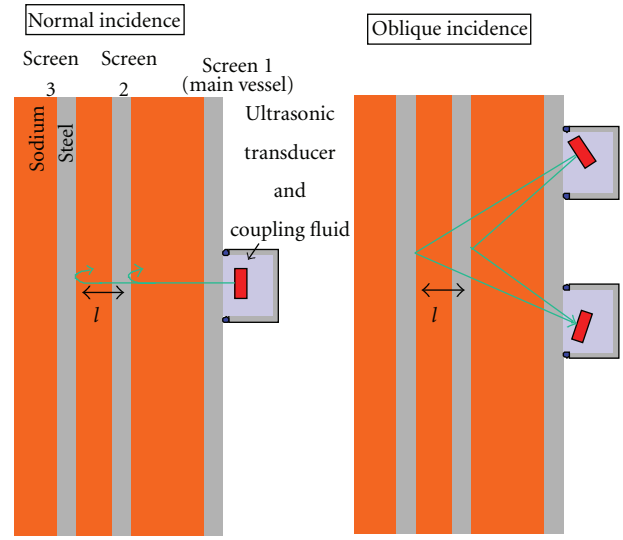

Figure 4: Inspection through screens, for a normal incidence with a transducer working in pulse/echo mode (left) and nonnormal incidence with a pitch-catch configuration (right).

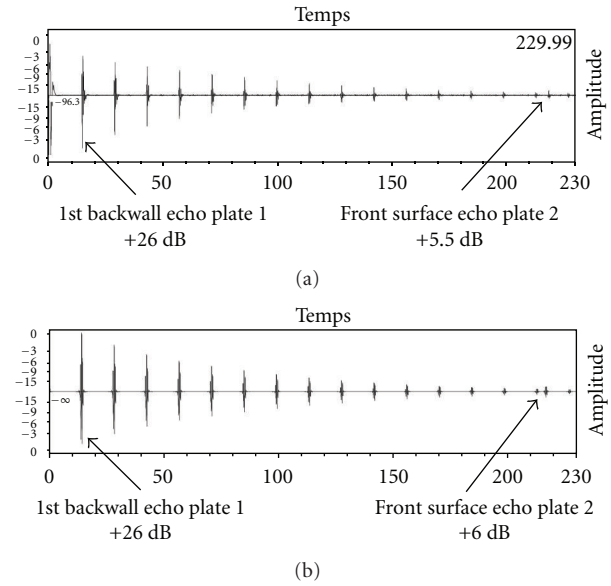

Figure 5: Inspection through screens for a normal incidence configuration at 2.25 MHz, experimental (a) and simulation (b).

particularly the echo coming from the front of the surface of the second plate supposed to represent the surface of an internal structure.

For non-normal incidence application (pitch and catch configuration with ultrasonic waves propagating at 45° in the main vessel wall), the distance between the emitter and the receiver is adjusted to obtain an intersection of the emission and reception focal paths along the surface of plate 2. Non-normal configurations can be used to inspect internals that are not parallel to the main vessel wall and/or to decrease the duration of the multiple echoes inside the main vessel wall observed at normal incidence. When comparing

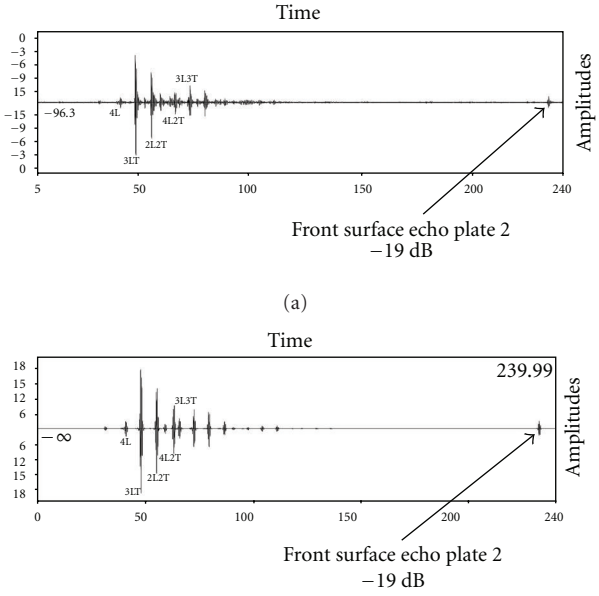

Figure 6: Inspection through screens for a 45° configuration at 2.25 MHz, experimental (a) and simulation (b).

experimental results and simulation calculated with CIVA (Figure 6), we observe multiple echoes early in the signals. They are coming from modes converted inside the main vessel wall; their time of flight allows analyzing each of them. The amplitude of the front surface echo off plate 2 is measured; reference is the mode conversion echo noted 3 LT.

We see that CIVA predicts correctly the mode conversions obtained in the first plate representative of the main vessel wall. We confirm that the duration of these echoes is shorter than the multiple echoes observed for the normal incidence configuration, allowing the detection of objects closer to the main vessel wall. We verify as well that the amplitude and the time of flight of the echo obtained off the surface of the second plate are well predicted.

Validations performed for various frequencies and various angles of incidence confirm that CIVA can be used as a tool to predict telemetric applications for a quasistatic fluid. Further validations will be conducted for configurations with a third plate representative of a baffle and with defects inside the plate supposed to represent the internal. This will help determining which internal can be inspected from outside the main vessel wall.

4.2.2. Simulation of Ultrasonic Inspection in Turbulent Fluid. Models presented in the previous section are valid for homogenous fluids meaning quasi-static and isothermal fluids: sodium is likely to be in that state during shutdowns for periodic inspections. For measurements associated to reactor operation, the flow of sodium creates zones of turbulence, which induce local variations of temperature. These variations translate into velocity inhomogeneities, which can impact greatly the precision of telemetry measurements. It is thus important to have the capability to predict the influence of the turbulence on the precision of the telemetry measurements.

Telemetry inside the reactor can be performed to monitor core compaction for example. A probe positioned at the core exit would see effects of sodium flow, which can create local variations in temperature of approximately 50°C that translate into velocity variations of 1% (see next formula). We have followed two approaches to model the propagation of ultrasonic waves in a inhomogeneous fluid: a determinist model that propagates rays inside a predetermined cartography representative of the temperature distribution and a statistical model that modifies times of flight according to a distribution representative of the inhomogeneities inside the fluid.

We first generate cartography of temperature, which is going to be used as the medium of propagation. The generation of the cartography is based on a Gaussian model of thermal turbulence [7]. The parameters of the model are the maximum temperature variation and the characteristic length L, which represents the scale of the inhomogeneities. This technique allows generating spatial temperature cartographies from which we generate spatial velocity cartographies using the following basic relationship:

$$c\ (\mathrm{m/s}) = 2577.2 - 0.5234\ T\ (^{\circ}\mathrm{C}), \tag{1}$$

where in sodium sound velocity c depends only on sodium temperature T.

After building the medium of propagation, we apply the ray theory to model the acoustic field. The process is done in two steps: the first one calculates the time of flight between a point source and a point of observation solving a system of differential equations known as the kinematic ray tracing system. The second step allows the calculation of the amplitudes associated to the rays determined in the first step. Calculation at one point is based on the energy conservation criterion in a tube of rays.

We used the model to calculate the acoustic rays radiated by a punctual source for different values of the characteristic length L supposed to represent the inhomogeneities met in a sodium-cooled reactor in operation. The L value depends on the specific case to be treated: for example, at core outlet, L should corresponds to subassembly spacing. The results are shown in Figure 7; the rays appear in black and are superimposed to the velocity cartographies calculated with each characteristic length.

We see that rays are not affected in terms of direction except for the case $L = 50$ mm (small inhomogeneities). Variations of time of flight are smaller than 4%, and there is phase continuity between neighbour rays. It is necessary to take into account the variations of time of flight to consider the interferences between neighbour rays. We noticed as well small variations in amplitude (less than 0.1 dB) compared to the propagation in a homogeneous medium meaning that we do not need any amplitude correction.

The goal of the statistical aberration model is to estimate the spatial variations of the time of flight of an acoustic beam after propagation into a turbulent medium. Using

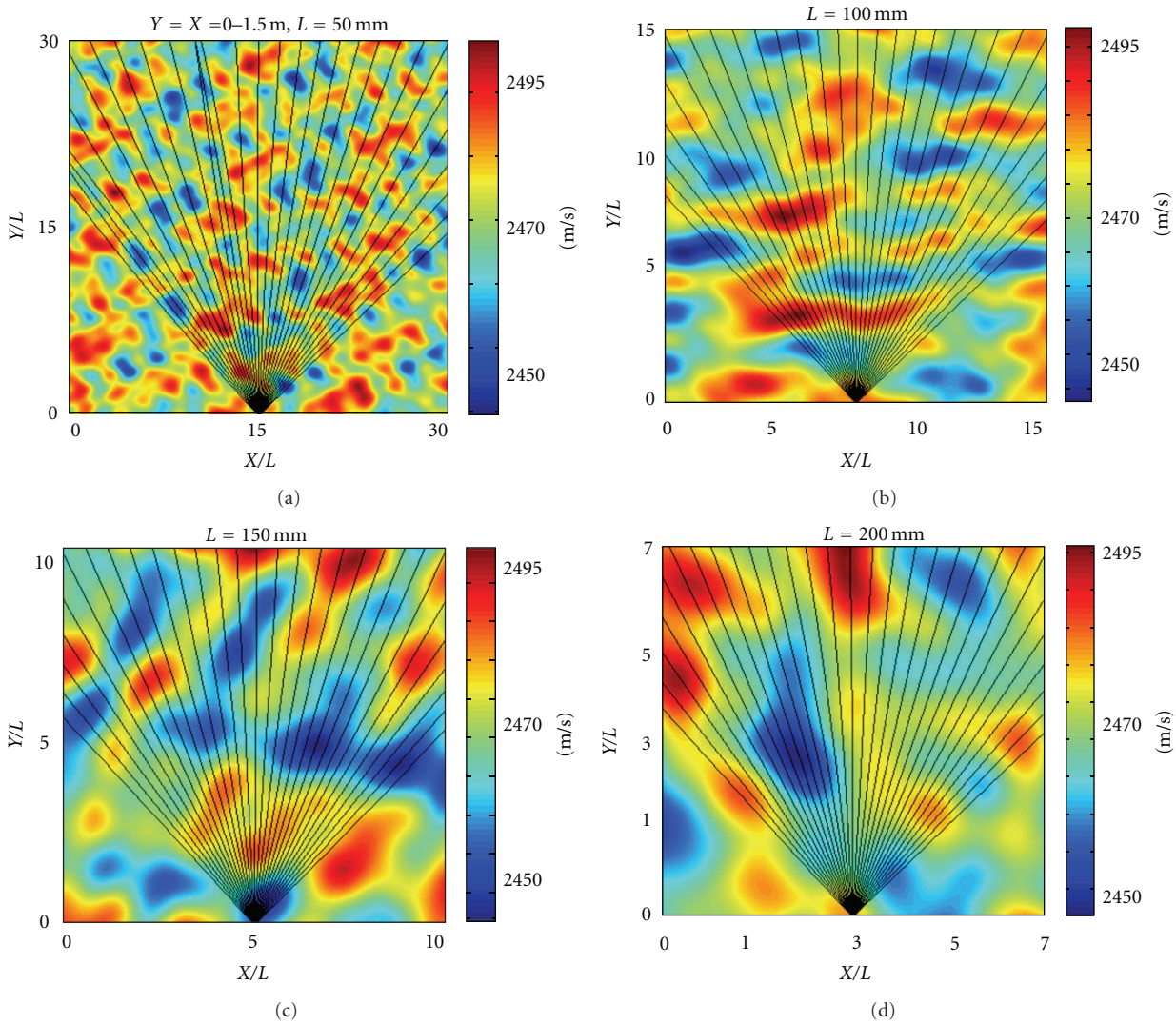

Figure 7: Ray tracing using the determinist model for four different values of the characteristic length.

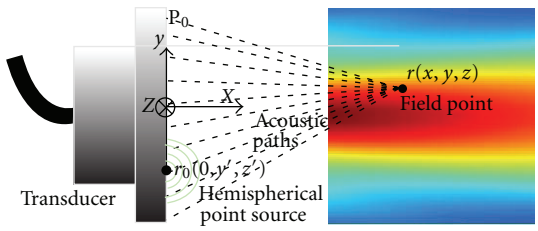

Figure 8: Ultrasonic transducer with radiating surface, in sodium acoustic beam predicting.

these variations, we introduce a time correction to the model used for homogenous media to represent the inhomogeneity of the medium. The statistical aberration model is based on a stochastic process: it generates a series of spatially continuous random values. We thus need statistical inputs such as the average time of flight, the time of flight variance, and a correlation function to insure spatial phase continuity. The average and variance values can be obtained from the determinist model by realizing a great number of velocity cartographies for the same characteristic length. The correlation function is as well extracted from the determinist model results obtained for a point source and observation points located at equal distance to the source.

We applied the two models to calculate the acoustic beam field radiated by a transducer into an inhomogeneous fluid. A transducer can be modelled by a distribution of particle velocity source over the radiating surface of the transducer. A Rayleigh integral describes the acoustic scalar potential at any observation points caused by a set of sources located on the radiating surface. This formulation considers that each elementary source (a hemispherical point source) on the radiating surface contributes to the field at an observation point with amplitude inversely proportional to the acoustic path between the two points. Then the field is computed by a simple integral over the whole radiating surface of these contributions (Figure 8).

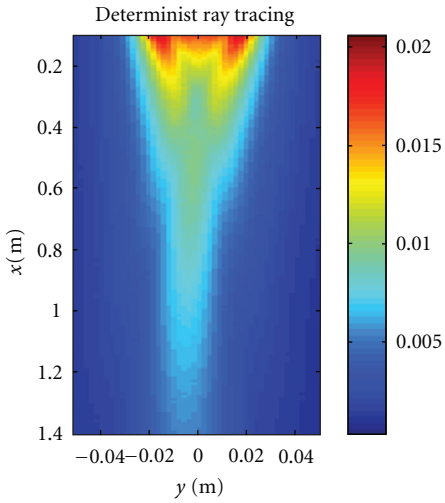

Figure 9: Acoustic beam propagation in inhomogeneous medium calculated by determinist ray tracing model (acoustic source position is at $[x = 0; -0.02 < y < 0.02]$ coordinates).

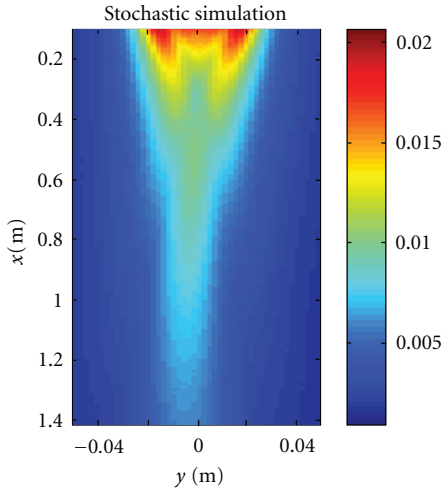

Figure 10: Acoustic beam propagation in inhomogeneous medium calculated by stochastic simulation mode (acoustic source position is at $[x = 0; -0.02 < y < 0.02]$ coordinates).

Figure 8 shows the acoustic field calculated in a homogeneous medium. The integral is calculated over a circular radiating surface of 30 mm. The signal is a Gaussian-modulated sinusoidal pulse with a central frequency of 2 MHz and a 60% bandwidth. To calculate the acoustic beam in an inhomogeneous medium, we compute the acoustic paths using the determinist model for a given inhomogeneous velocity cartography. The impulse response for each point is the convolution of all contributions from the radiating surface. Figure 9 shows an example of the acoustic beam prediction in an inhomogeneous medium calculated by the determinist ray tracing. The parameters of the transducer are the same as the ones used for the homogeneous case. The random velocity is defined by the standard deviations $\sigma_\varepsilon = 0.0018$ and the characteristic length $L = 100$ mm.

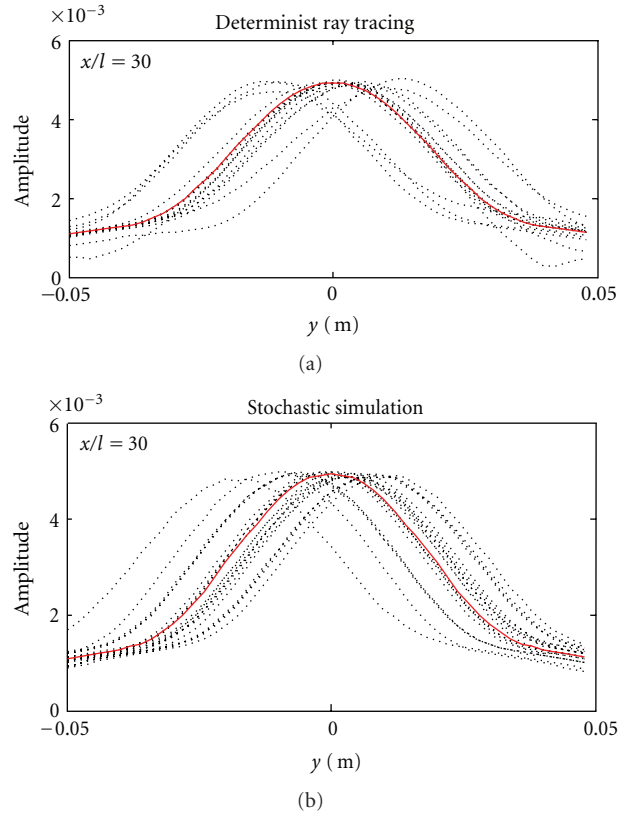

Figure 11: Acoustic beam deviations for the determinist and stochastic models; result for the homogeneous model is in red.

We find that the focal axis of the acoustic beam is no longer aligned with the normal to the surface of the transducer. The inhomogeneities lead to some slight deviations of the acoustic beam. At a distance of 1.4 m, we observe a deviation of 0.01 m, which means that the beam could totally miss the intended target and hit a different location. We then calculated the beam field using the statistical aberration model. The field is first calculated for a homogeneous medium by the Rayleigh integral, and the stochastic simulation model provides the variations of travel time for all acoustic paths. Result is displayed in Figure 10.

We can see that the acoustic beam predicted by the stochastic model also displays a deviation off the main focal axis similar to the one observed with the determinist model. To compare the two models, we ran several calculations for both models and compare the deviation to a calculation for a homogenous medium. Results are displayed in Figure 11; the red curve represents the result for the homogenous case and the dotted curves represent the result of each calculation for each model. Acoustic field is calculated for a single given random map of insodium sound velocity.

We see that the deviations obtained with both models are similar. However, the computation time of the determinist model is proportional to the number of rays, the number of observation points, and the discretization of each path. It is thus much more time consuming than the statistical model. In the future, we will use the stochastic approach to

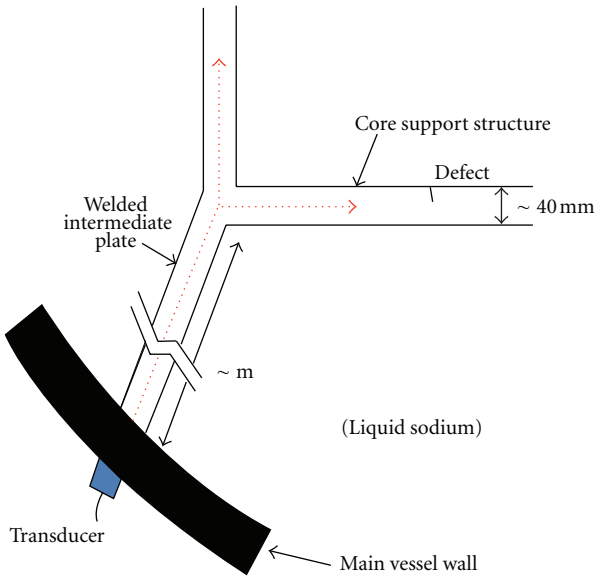

Figure 12: Inspection of structures used as wave guides.

predict the influence of the flow turbulence on the detection of internals during operation.

4.2.3. Simulation of Ultrasonic Inspection with Guided Waves. We expect to examine structures welded to the main vessel wall such as the core support, using guided waves. The goal is to generate guided waves from the main vessel external skin up to the inner vessel zone to control, by using intermediate plates as wave guides (Figure 12). The CEA has implemented in CIVA a model for the propagation of elastic guided waves using the semianalytical finite element method (SAFE) [8, 9]. This method allows predicting the elastic field under the form of a modal decomposition for guides of complex section. It decomposes the solution into an analytical part for the propagation of the waves along the guide axis and a numerical approach using finite elements for the section of the guide. This method is, however, limited to guides that have a constant section along one extrusion plane and to defects that are contained along the section of the guide.

To model the propagation of guided waves along the core support, we need to be able to deal with discontinuities such as the junctions between the various parts of the core support and defects of arbitrary shapes. One way to handle these problems is to use a finite element method around the areas presenting these discontinuities. Diffraction by a discontinuity or a defect is calculated using the finite element (FE) method to which we add transparent boundary conditions allowing to minimize the volume meshed (Figure 13).

4.3. Ultrasonic Control with Sodium-Immersed Sensors. For future SFRs, ultrasonic transducers working under sodium at about 200°C are required [10]. They are planned to be used for the telemetric and volumetric examinations of the internal structures, during periodic inspection phase. If needed, they also could be exceptionally used for the core support structure. These transducers must be able to measure distance of some meters with 100 μm accuracy and to detect cracks of about 200 mm × 10 mm.

On the one hand, with regard to the high-temperature transducers, these volumetric examination transducers are operated at a lower temperature and during a shorter duration. It implies a constraint reduction for the electroacoustic element choice. On the other hand, this kind of transducer use demands a better damping and efficiencies than high-temperature transducers and easier focusing capacities. Furthermore, the low temperatures (below 300°C) may cause some acoustic coupling deficiency, hence, requiring a special treatment of the transducer active face.

4.3.1. Ultrasonic Transducers for Control in Liquid Sodium. Available Standard high temperature ultraSonic transducer (TUSHT) has been qualified by CEA in sodium and used in Phenix plant during 15 years: it is a multipurpose transducer, that was initially designed in order to be usable in a wide range of frequency (up to 5 MHz) and of applications, in the main vessel of sodium-cooled fast breeder reactors (and also PWR reactors), for all reactor conditions (shutdown, full power, and transients).

It uses a piezoelectric lithium niobate single crystal, $LiNbO_3$ or LN, with a Curie temperature of approximately 1150°C.

The casing is made of AISI 304L stainless steel. The transmission of ultrasonic signals through the front face of the casing is ensured through an efficient acoustic bonding between the casing and the crystal, *via* a hard-soldering technique, developed by CEA. This bonding allows stable high-frequency transmission (up to 5 MHz at least), at high-temperatures (more than 550°C).

Two models have been qualified: TUSHT 4540 (LN diameter: 40 mm; overall diameter 55 mm) and TUSHT 4515 (LN diameter: 15 mm; overall diameter: 32 mm). Front faces are flat, or concave (spherical or cylindrical) to focus the ultrasonic waves. Figures 14 and 15 show a drawing of the TUSHT architecture and examples of TUSHT 4540 realizations.

The standard TUSHT (Figure 15(a)) is built with a front face thickness which must be compatible with very long service time (30 years) at full-power conditions. The frequency response contains several resonance frequencies (ranging from 0.7 MHz to 4.5 MHz, approx.). Ultrasonic pulses rise times (5–15 μs, approx., according to frequency) and durations are compatible with telemetry purposes (overall accuracy of 0.1 mm can be achieved, with use of suitable detection processing), but may be too long with regards to NDE usual specifications (e.g., flaw detection).

The immersed TUSHT are, at the present time, reference transducers for use in the main vessel of sodium fast reactors, in all the possible operating conditions. The major current improvement studies aim at reducing the oxygen-loss causes and effects (it is why one can see in Figure 14 two so-called "breathing tubes" which allow continuous air supply within the casing), for use at full-power conditions (550°C, long time operation), and to improve the bandwidth in pulse-echo applications, at least for use in inspection conditions

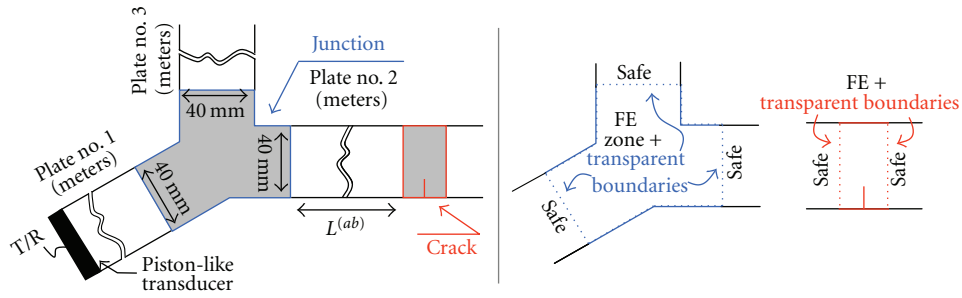

Figure 13: Left: configuration of testing of plate number 2 through a triple junction. Right: the two phenomena of scattering (junction, crack) are computed independently by FE; guided propagations are computed by SAFE.

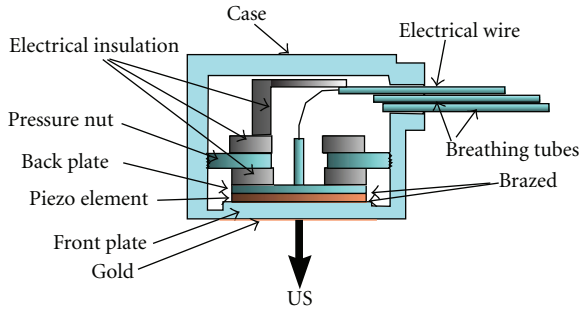

Figure 14: TUSHT general architecture.

(200°C, short time operation), with better damping and time resolution.

Figure 15(b) shows the first AREVA prototype which has been manufactured and tested under sodium. It integrates a piezo electric ceramic. The associated results are quite satisfying. AREVA-NDE solutions were contracted to design and fabricate a transducer capable of performing NDE under liquid sodium. They developed an ultrasonic transducer called TUCSS, which is an acronym in French for "ultrasonic transducers for NDE under liquid sodium." This transducer employs a piezoelectric material for the generation of the ultrasonic pulse.

As shown in Figure 15, the outside packaging of this transducer is entirely metallic to prevent any risk of innerpart chemical degradation. Moreover, the front of the transducer is made of nickel, and the emissive surface has been subject to a mirror-polished surface treatment. This solution allowed to obtain an immediate acoustic coupling into liquid sodium at temperature as low as 110°C.

For some applications, electro magnetic acoustic transducer (EMAT) is an interesting alternative to conventional piezoelectric transducers. The principle of an EMAT is to generate ultrasonic waves using the Lorentz force [11]. Eddy currents J are induced into the inspected part thanks to a coil, while magnets generate the required magnetic field B. The interaction between these two fields creates the Lorentz force F, which produces ultrasonic waves, as shown in Figure 16. Reciprocally, the interaction of ultrasonic waves with a magnetic field induces currents in the receiving EMAT coil.

A monoelement EMAT probe has been developed for liquid sodium inspection at 200°C. First experimental results are promising (see the first sampling in Figures 15(c) and 16). A full-phased array EMAT system is under development for sodium testing in 2012.

Further developments aim at using phased array transducers in order to get ultrasonic beam easy focusing and geometrical flexibility: this will be of a great importance when performing under sodium scanning for visualization purpose.

4.3.2. Ultrasonic Transmission at 200° C Liquid Sodium/Transducer Interface. Good acoustic coupling between sodium and the active surface must be achieved when using an ultrasonic sensor immersed in sodium. During periodic examinations of the reactor at shutdown, the sodium temperature is about 180°C. However, when a high-temperature ultrasonic transducer is immersed in sodium for the first time at this temperature, its acoustic coupling is not achieved [12].

The inprogress studies set out to assess the possibility of achieving good acoustic coupling of high-temperature ultrasonic transducers as soon as they are immersed in liquid sodium at reactor shutdown temperatures, without subjecting their active surface to vacuum gold plating. Gold plating the active surface of the sensor under vacuum makes it possible to achieve the acoustic coupling of the high-temperature ultrasonic transducer at the lowest temperatures at which liquid sodium can be used, that is, just above its melting point which is 98°C under atmosphere.

The attenuation generated by the gas present at the interface can be explained by considering:

(i) the relative amplitude of the acoustic impedances of steel, sodium, and of a gas (argon in the case of SFRs);

(ii) the expression of the energy transmission coefficient of acoustic waves between two elastic media.

In order to study the transmission of ultrasonic waves at a solid material-liquid sodium interface, we use the Liquidus sodium device which main components are a tight 400-liter containment (glove box under argon atmosphere) fitted with an airlock, and a 3-liter sodium pot whose temperature can be increased up to 450°C. Two cylindrical metal bars made of

(a) TUSHT available CEA transducer (AISI 304L casing)

(b) TUCSS AREVA transducer (Nickel front face)

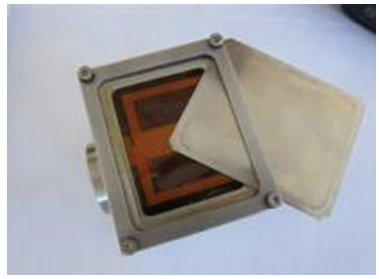

(c) EMAT CEA transducer (thin AISI 316L front face: here partially removed)

Figure 15: Available undersodium transducers.

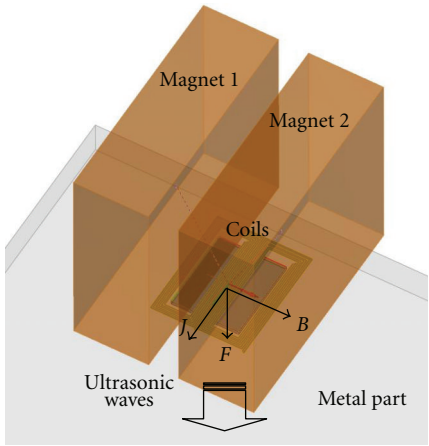

(a)

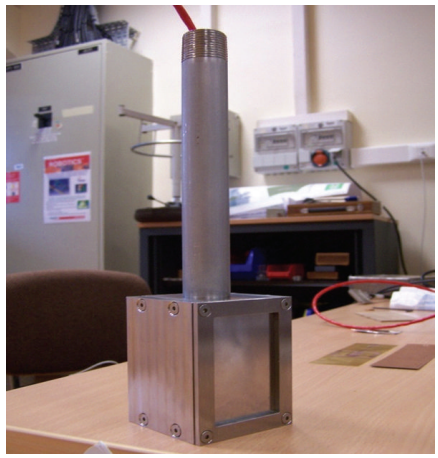

(b)

Figure 16: Principle of an EMAT and first insodium sampling.

316L steel, referred to as waveguides, are used for conveying the ultrasonic waves.

An ultrasonic transducer, employed as an emitter, is positioned at the free end of the left waveguide (Figure 17). An identical ultrasonic transducer, employed as a receiver, is positioned at the free end of the right waveguide.

The emitter transducer is excited by identical recurrent electrical pulses. The emitted wave propagates inside the left waveguide, passes through the left waveguide,sodium interface and then through the sodium/right waveguide, propagates inside the right waveguide and finally excites the receiver transducer.

During the tests, the variations of the electrical signal generated by the receiver transducer are recorded. Based on the assumption that transducer-waveguide couplings remain identical over time, the electrical signal generated by the receiver transducer provides information on the transmission of ultrasounds at sodium-waveguide interfaces.

The interpretation of these results is based on the assumption that acoustic coupling is improved due to a decrease in the gas surface fraction at the interface. Inert gases, and particularly argon, are used as cover gases for liquid sodium in fast reactors. Their solubility in sodium increases exponentially with temperature. If the temperature of sodium is increased, part of the gas present in the crevices of the rough surface dissolves and diffuses to the sodium [13].

Furthermore, in addition to increasing solubility, a temperature rise also increases the diffusion coefficient (or diffusivity) of argon in sodium [13]. This phenomenon accelerates the dissolution of the gas contained inside the crevices and as a result accelerates the decrease of the gas surface fraction at the interface.

Lastly, another temperature-related effect is observed. This effect has the most significant impact on the gas surface fraction and consists in the variation of the contact angle according to temperature.

The combination of these three effects leads to an interpretation based on two main observations. The first observation is that a good acoustic coupling is achieved at the same temperature at which the wetting process is observed. The second observation is that the increase rate of transmitted energy increases with temperature. In this interpretation, wetting consists in the dissolution of gas pockets.

4.3.3. Liquid Sodium Ultrasonic Telemetry Experimental Tests. In order to qualify CIVA software (see Section 4.2), an

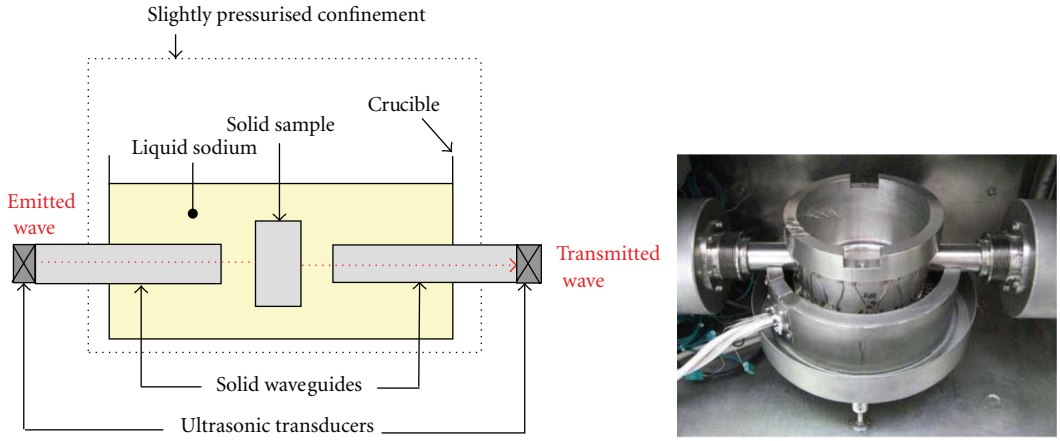

Figure 17: Schematic view of the acoustic path of Liquidus device and view of the facility (with 210 mm diameter sodium pot).

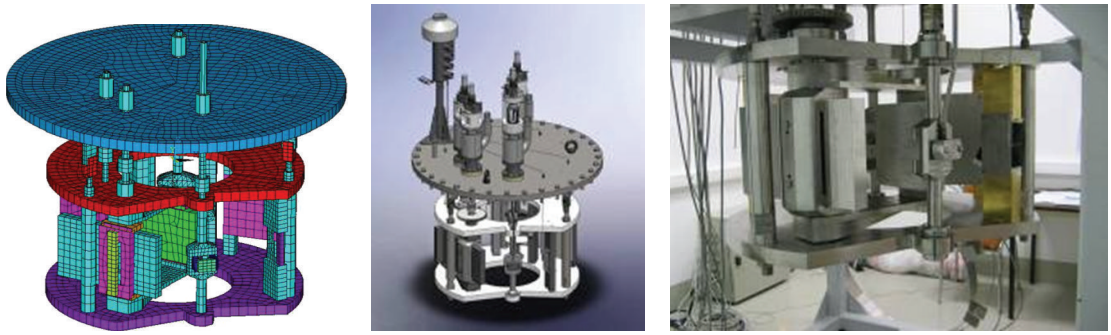

(a) (b) (c)

Figure 18: multireflector mockup (1 m diameter) devoted to in sodium ultrasonic telemetry study.

experimental mockup "multireflector" was specified for the study of ultrasonic diffractions and reflections in liquid sodium and was successfully tested in 2010 [14]. It included a rotating high-temperature ultrasonic transducer TUSHT, a fixed target, rotating targets, and thermocouples (Figure 18). In order to reach the metrological objective, in air initial calibration at room temperature of all components was performed and led to a global uncertainty equal to ±0,02 mm (20 μm) for their location and to ±0,02° for their angular position.

After under-water commissioning tests, the mockup was used in a 1 m diameter pot inisothermal 200°C static sodium conditions: test parameters were TUSHT frequency and 6 target positions. Then, global uncertainty on ultrasonic distance measurement could be checked and is better than 100 μm.

4.3.4. Liquid Sodium Ultrasonic Visualization. Extending telemetric measurement leads to the possibility of ultrasonic under sodium "vision," also called, "visualization" able to deal with different applications:

(i) surface mapping (imaging) of submerged structures/components;

(ii) integrity inspection of structure/component surfaces (including the detection and sizing of opened cracks);

(iii) determination/confirmation of robotic system positioning;

(iv) fuel assembly identification;

(v) detection, localization and sizing of immersed objects (including migrating bodies).

R&D program is beginning in 2012 and intends to compare all the identified ultrasonic technologies available for surface telemetry options: orthogonal antenna (former CEA IMASOD project: see Figure 19 [15]), conventional or innovative SAFT (synthetic aperture focusing technique), 2D matrix with Full Matrix Capture for example (Figure 19).

Depending on the visualization system chosen, in water tests will be performed in CEA VISIO facility (Figure 20). Surface examination under sodium conditions seems possible and could be used also for:

(i) surface metrology: measuring shape defects, detecting, and measuring through crack openings;

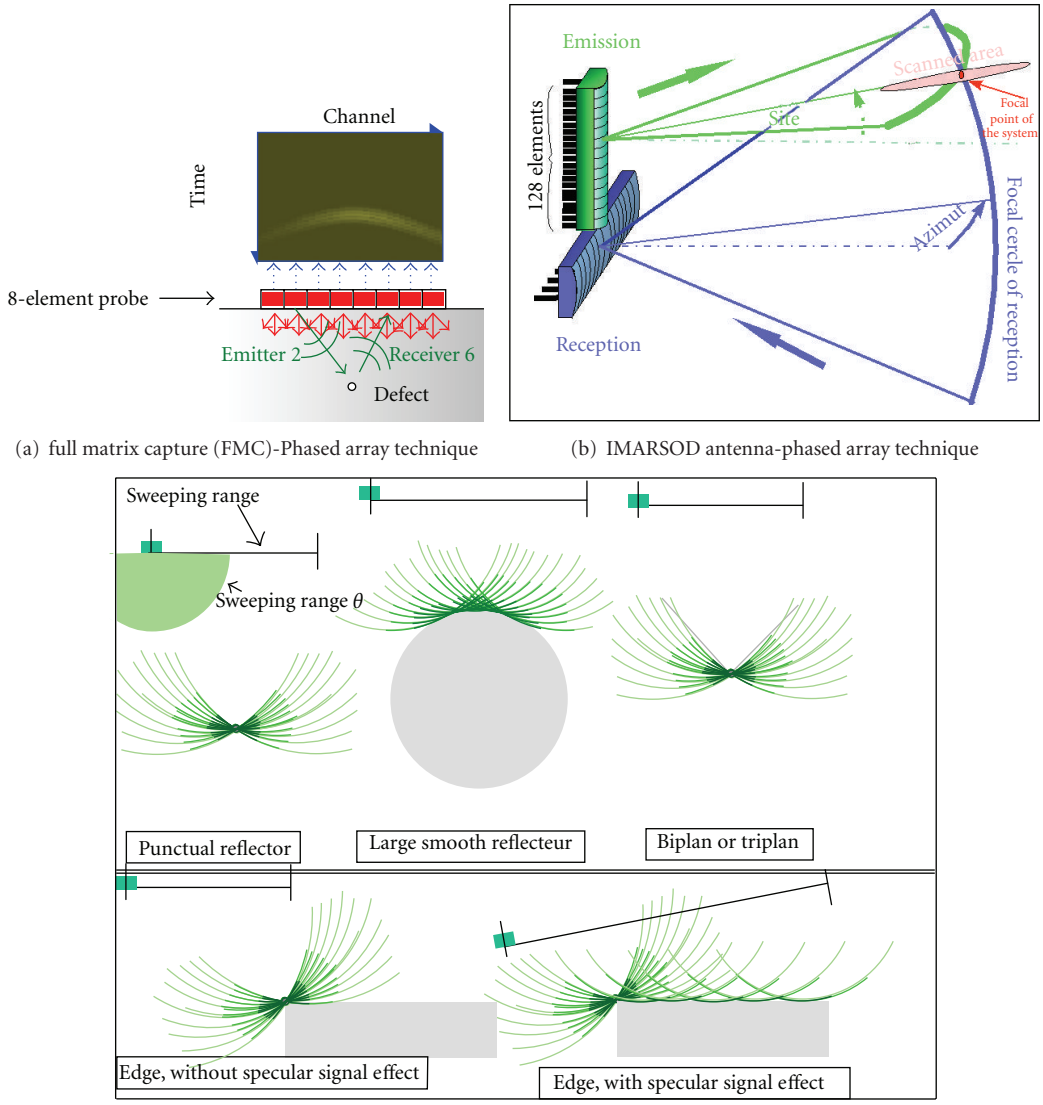

(a) full matrix capture (FMC)-Phased array technique

(b) IMARSOD antenna-phased array technique

(c) synthetic aperture focusing technique. (SAFT)

Figure 19: Ultrasonic visualization techniques (examples).

(ii) remote operations under sodium viewing: detecting and measuring positions and dimensions of migrating bodies, detecting the absence of mechanical parts, and helping to position a robot.

The different ultrasonic techniques are considered to be more or less adapted to specific cases where ultrasonic echoes can come from diffraction on edges, reflection on flat surfaces, and retrodiffusion due to surface roughness. Specification for vision performance can be extended from optical case (capability of detection, resolution, and accuracy): a first step can be considered to assume ASME rules which specify a 800 μm capability of detection. Ultrasonic techniques imply rotating and translating scanning which can be realized with mechanical or electronic phased array systems. Directivity of ultrasonic sensors will have a great importance, depending on acoustic technique to be used.

Underwater tests will first be performed and then sodium tests will be carried out when ultrasonic corresponding sensors will become available.

4.4. Ultrasonic Control without Sodium-Immersed Sensors. The harsh environmental constraints inside the main vessel require developing high-temperature transducers conditioned for sodium. But conditioning greatly affects the performances of the transducer such as the SNR ratio. It is why ultrasonic probes positioned outside the reactor along the main vessel wall can be used to perform telemetry measurement without requiring previous sodium conditioning.

Such examination seems to be possible for some internal peripheral structures: it could be facilitated by an external mean, displayed from the inter-vessel gap [16, 17].

As said before, such an ultrasonic method is being investigated for the two main purposes (see Figure 4):

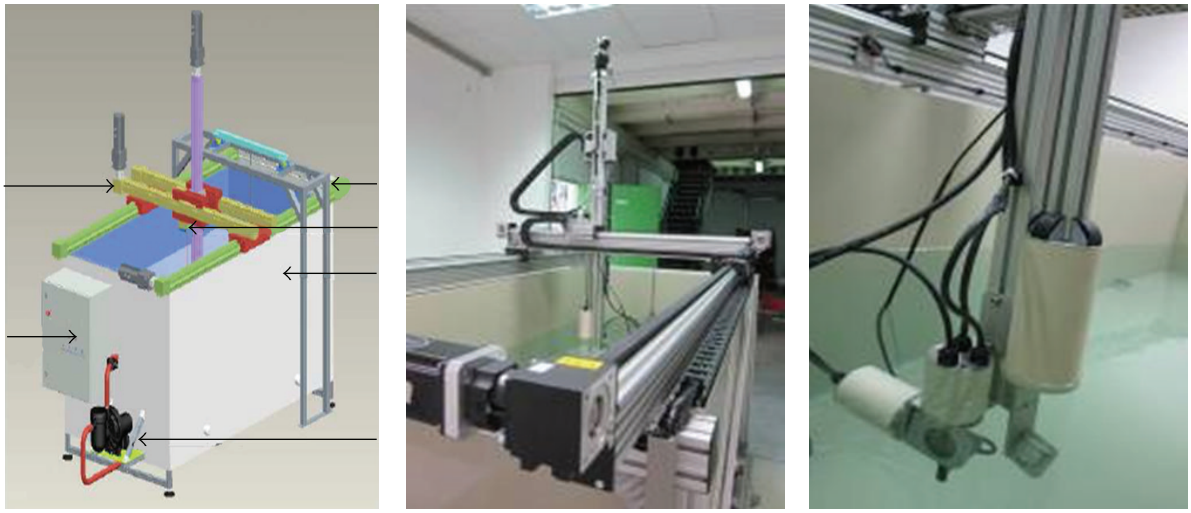

(a) (b) (c)

Figure 20: VISIO water facility (2 m long, 1 m large, and 1 m high) devoted to ultrasonic visualization study.

(i) telemetric measurements in order to check the immersed structure positioning and thickness;

(ii) volumetric NDE of the core support peripheral welded junctions in order to verify the absence of cracks.

Transfer matrix method is used in order to simulate the ultrasonic transmission through several immersed plates. The need to propagate the maximum energy possible through bounded media orientated the study towards Lamb waves. These waves are often employed for single plates or solid layers but are rarely used for liquid/solid pile. The set of alternating steel plates and layers of liquid sodium can be linked to a multilayer system. A common method for studying the propagation of waves in a theoretical layered medium is the method of transfer matrices. The idea is to build the propagation matrix for a stack of a known number of parallel layers by extending the solution from one layer to the next and satisfying the continuity conditions at interfaces. The principle is [18, 19]

(i) each layer of the system is associated with a transfer matrix, connecting the velocities and stresses at the "outer" interface (downstream) in terms of velocities and stresses at the "inner" interface (upstream);

(ii) the transfer matrix of the complete system is obtained by multiplying the transfer matrices of the constituent layers.

Therefore, the matrix can be used to determine the transmission and reflection coefficients of the system under the assumption of an incident plane wave. This calculation takes into account the interferences due to multiple reflections and possible resonances.

The transmission coefficients are calculated and represented by varying angle of incidence and frequency. The dynamic range varies between 0 (dark blue) and 1 (red), with large areas where the coefficient is about 0.1 (blue). It can be observed that the generated Lamb modes in a system with two plates (see maxima of Figure 21) are exactly the same as all Lamb modes generated in each individual plate. There is no mixed mode generated by the systems of n plates. Only the sum of elementary modes generated by each plate is present.

In order to qualify this method, tests in water have begun investigating various influential parameters (frequency, pulse mode or wave trains, sheet thickness, spacing, number of plates and parallelism), meanwhile simulation codes, that is, CIVA (see Section 4.2), must be developed and/or adapted to evaluate and compare the considered reactor designs from the method applicability point of view. Insodium testing will follow. Experimental tests will be conducted in water and then in sodium.

The experiments (Figure 22) are carried out in immersion using a broadband E/R transducer with a central frequency of 1 MHz. Two incidence angles (18° and 35°) are used to generate the Lamb modes A0 and S0 in the last plate. The signals are sent back by an artificial defect (notch) located in the last plate and recorded. The maximum amplitude of the signal is represented as a relative versus the distance from the notch.

The results (Figure 23) show that it is possible to generate a Lamb wave in a plate hidden behind two others, except in the case of different thicknesses and S0 mode. These screens can be of the same thickness or not. The amplitude of this wave consistently decreases with the distance from the reflector (notch).

It can be observed that the relative decrease in the case of three plates and A0 mode is lower than in the case of one and two plates.

It can be seen that an artificial defect can be detected in a plate located behind one or two screens by generating Lamb waves in the last plate. The measured attenuation on this scale is compatible with industrial NDE conditions. Thus, this inspection technique shows promising potential.

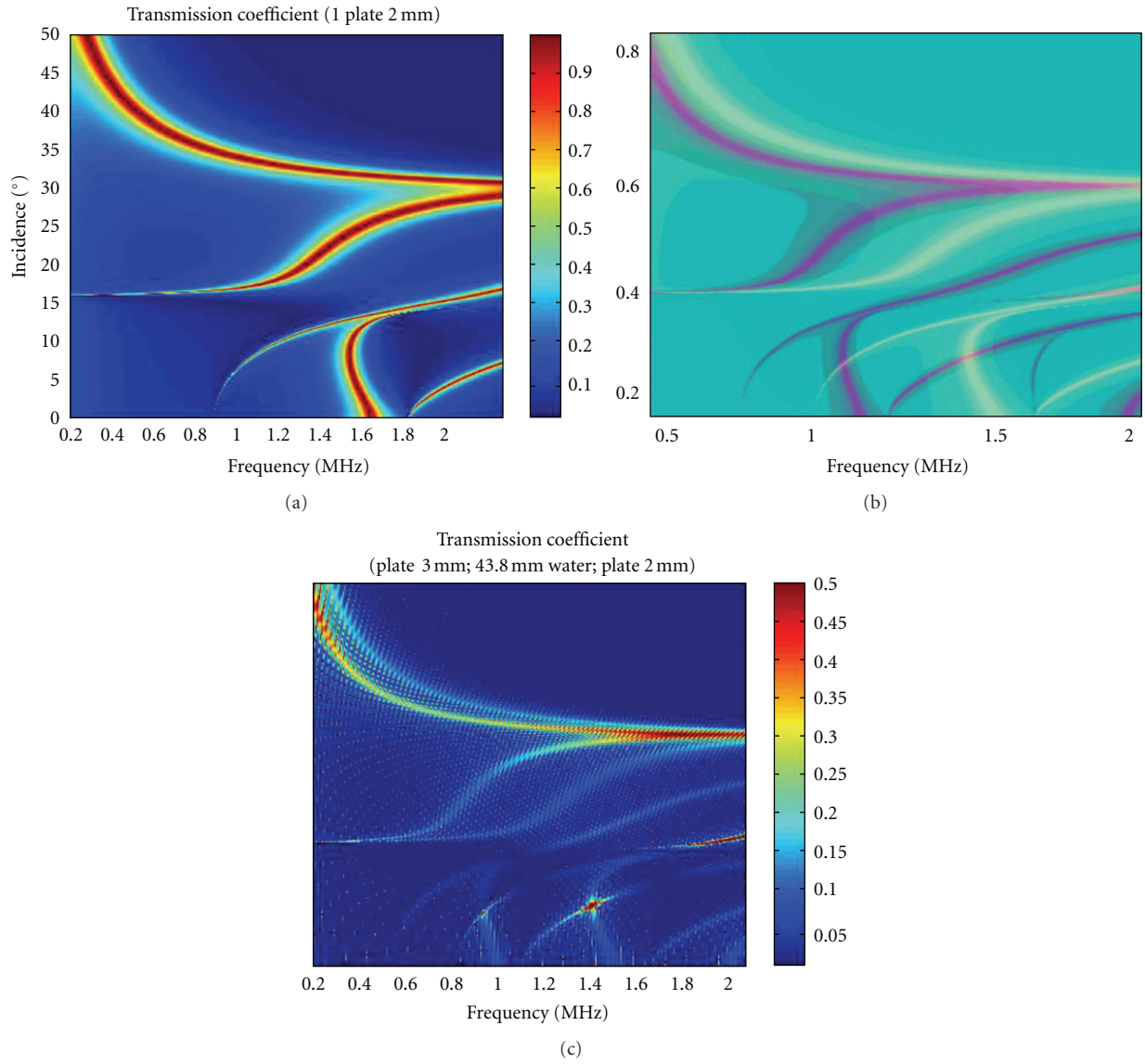

Figure 21: Transmission coefficients calculated for different systems: (a) a single 2 mm thick plate: Lamb wave modes appear very clearly, (b) graphical superposition for a single 2 mm thick plate and for a 3 mm thick plate: each plate has its own Lamb wave modes, (c) two plates (2 mm thick and 3 mm thick): there is a global Lamb wave mode filtering.

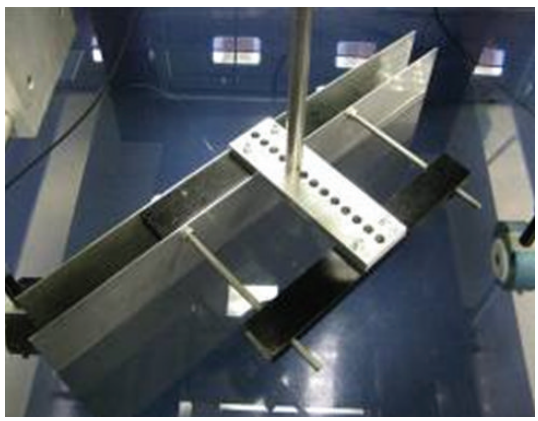

Figure 22: Inwater experimental mockup (300 mm square plates).

Further study will focus on identifying the plate containing the defect, and on the location of the crack.

Larger-scale experiments are being performed in water (Figure 24): 3 thick plates (20 and 30 mm) are immersed in water and submitted to 100 kHz acoustic waves in order to develop telemetry (distance between plates and plate thickness measurement) and volumetric NDE (detection and sizing of volumetric defects in the plates) applications. Some artificial defects have been machined in the plates: slits, holes, and grooves.

Then, qualification phase will be performed with tests in liquid sodium conditions.

4.5. Ultrasonic Surface Wave Performing. As evoked in the global design paragraph, several inner structures may

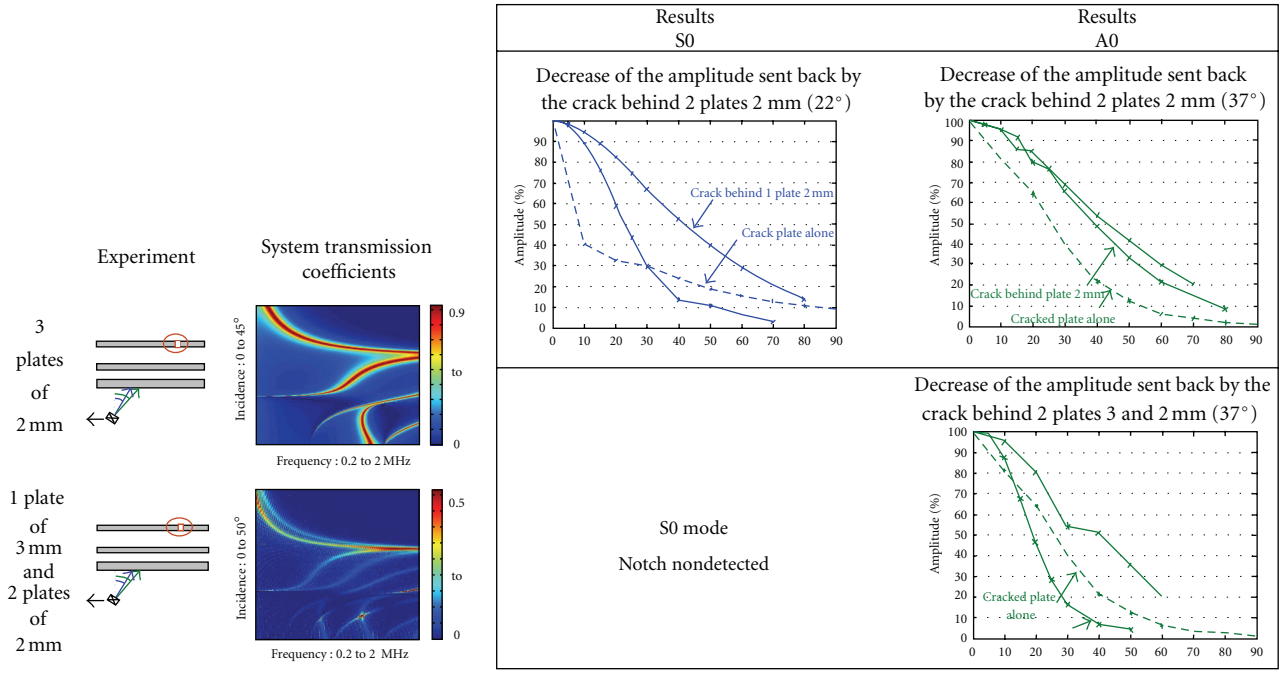

Figure 23: The results of three plates (solid lines) are compared in terms of the relative amplitude with the results of one and two plates (dashed lines).

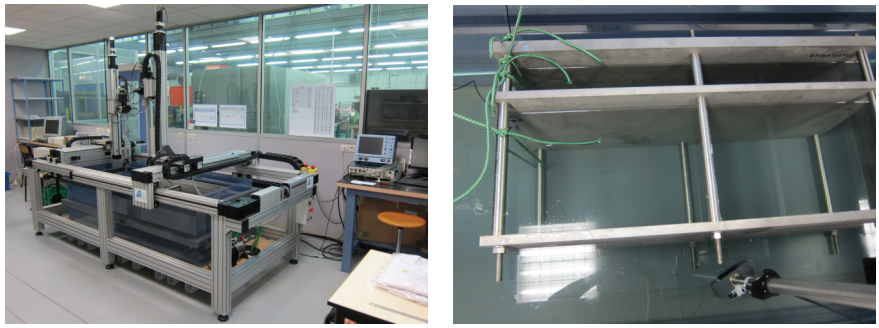

(a) (b)

Figure 24: Scale 1 in water tests with a 3-plate (1.5 m long and 1 m large) mockup.

undergo some thermal striping, especially the ACS lower zone. To be able to detect the resulting superficial cracks, a specific R&D program has been implemented.

The first tests on a representative mockup in air have shown that propagating US surface waves give some good results, detecting the artificial cracks positioned onto the mockup, as shown in Figure 25. The sensors used were monoelement with variable angle focus and phased array.

Next testing will analyze the method applicability for longer detection distance and immersed structure with a liquid free level.

4.6. Sodium Environment Repair. For the nonremovable components, repair operations will be performed in a gas environment: either in the upper dry zones of the reactor cover gas plenum, or in a gas-tight volume, if the faulty zone is located under the sodium free level. In that last case, the gas-tight system will have to contain the inspection and repair tools and protect them from the surrounding liquid sodium (Figure 26). Two concepts will be investigated: one in contact with the structures, having a seal formed by two flexible lips, and the other is a system that prevents liquid sodium penetration by using a gas-pulsed screen, supplemented by a scraper seal. Specific seal material is being tested in 200°C liquid sodium: conventional PWR silicone material is being tested for sodium qualification (Figure 26).

Concerning the repair tools, on the one hand, the laser method has been selected for future SFRs because it has the advantage of not generating any stress on the tool, and because it is suitable for the various applications: indeed, the repair scenario for insodium structures should be first removal of sodium (after bulk sodium draining), then machining and finally welding. On the other hand, the

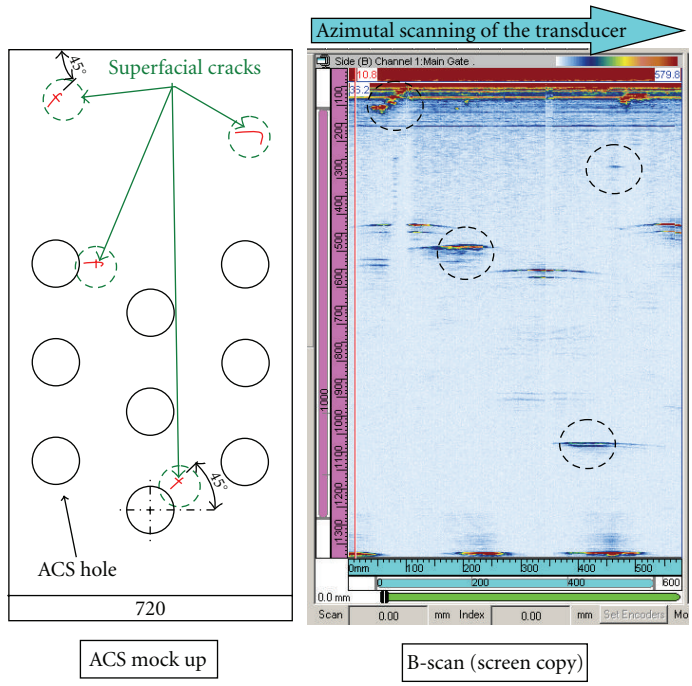

Figure 25: Surface ultrasonic controls of thermal striping cracks. Echoes are due to geometrical boundaries (holes) and to superficial cracks.

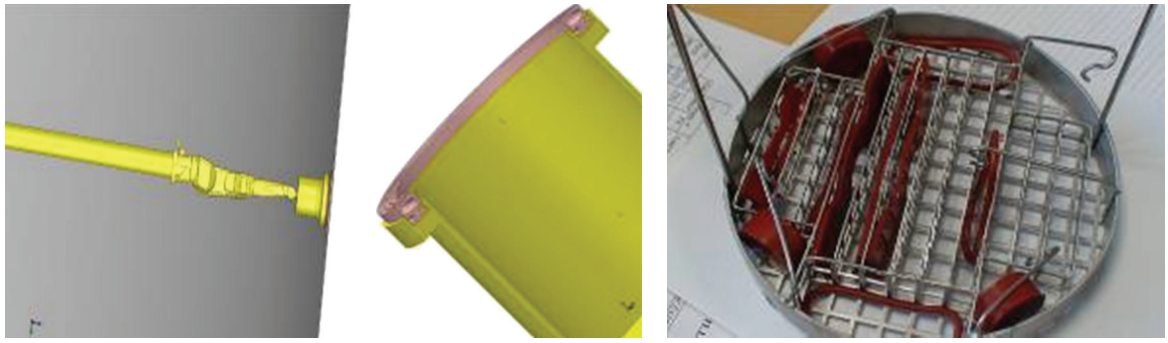

(a) insodium robot concept: articulated arm with a bell

(b) gas-tight bell design for Repair tools

(c) silicone samples before sodium testing

Figure 26: Tools for insodium intervention.

conventional tools (brush or gas blower for sodium removal, milling machine for machining, and TIG for welding, whose feasibility was demonstrated in the 1990s) are still considered as backup solution. Qualification tests have to be performed with the help of simulation of welding process (Figure 27).

In any case, the waste produced (smoke and aerosols; dust and chips) will have to be managed.

Sodium complete or partial draining induces a caustic corrosion risk which has to be considered carefully as it can produce fast cracking in stainless steel material of SFR structures: this is due to possible chemical reaction of sodium traces with oxygen or moisture in case of air ingress. If produced sodium hydroxide is wetted and if structure stress is high enough, stress corrosion cracking is likely to occur, depending on the temperature range [20]. That can happen when draining sodium but also during refilling it.

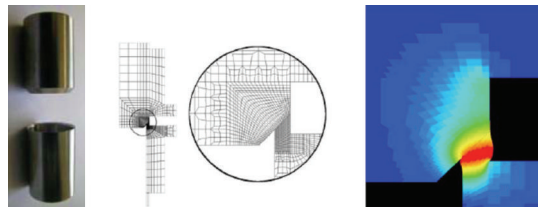

Figure 27: Simulation of electrothermic welding process for small samples (some mm thickness).

Even if associated intervention procedures are available, investment protection needs to study the case of complete draining of primary sodium (out of the main vessel), for both scenarios corresponding to shutdown 200°C and room

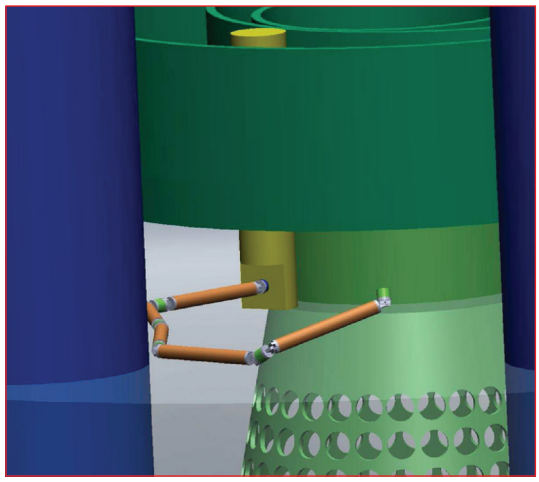

Figure 28: Insodium robotics for inspection/repair (CAD simulation example): articulated arm with NDE inspection too.

temperature conditions. Simulation of air ingress aerolics and chemical reaction with sodium traces will be performed.

4.7. Robotics for Insodium Examination and Repair. In pile deployments for examination or repair require some robotic carriers. These carriers have to be suitable for sodium environment: either in the cover gas plenum or in gas after sodium draining, or even under liquid sodium.

Few insodium carriers have been used in the past: it is why a specific R&D program has been initiated with the objective to have a prototype of robotic carrier for insodium testing by 2014.

This R&D program is parted in 10 axes:

(i) detailed definition for the SFR carrier needs (internal structure access, and possible defects to be detected/repaired);

(ii) carrier architecture definition and specifications (depending on inspection and repair scenarios);

(iii) carrier organ in sodium tightness;

(iv) carrier material compatibility with sodium;

(v) temperature resistance (200°C);

(vi) irradiation resistance (depending on location of main vessel);

(vii) intervention gas-tight bell for operation under liquid sodium;

(viii) carrier positioning control on liquid sodium;

(ix) development, validation and qualification of technological solutions, then of carrier fleet;

(x) worldwide benchmark regarding the previous axes.

The research work along these 10 axes must allow choosing between the adaptation of manufactured robots, in order to benefit from the reliability and the industrial experience, and the designing of specific robots compatible with the surrounding conditions (drive systems, coding, reduction, tightness, and data exchange).

In addition to this approach, the continuation of accessibility studies based on reactor design studies will help to optimize the accessible volume to a robot (Figure 28).

5. Conclusion

On the basis of available feedback and the new safety requirements, the ISI&R for next SFRs has been identified as a major task. The French R&D program launched in 2007 for periodic examination and repair improvement is based on several aspects: ensuring a strong connection between the reactor designers and inspection specialists, and developing tools and techniques applicable in a sodium environment (inspection at 200°C). The key milestones (and main available results) of this ambitious R&D program are:

(i) validation for ultrasonic simulation (achieved for isothermal sodium conditions);

(ii) validation of ultrasonic transducers (US telemetry and NDE sensors) under sodium conditions at 200°C (procedures for manufacturing of available CEA designed TUSHT have been validated);

(iii) definition of key components of the robotic equipment for operation in sodium at 200°C (in sodium seals and thermal isolation are being qualified);

(iv) validation of laser repair processes and techniques: sodium sweeping, structure machining, and welding (simulating zinc test are being performed).

In the frame of this R&D activity, feasibility and qualification tests are performed, simulation of techniques (ultrasonic inspection and laser repair) are developed, inspection and repair tools are designed, manufactured, and tested.

ASTRID prototype project orientates these actions and will get large benefits from them.

Acknowledgment

The authors would like to thank the colleagues who provided information or checked certain sections of this paper.

References

[1] F. Jadot, F. Baqué, G. de Dinechin, J. P. Jeannot, J. M. Augem, and J. Sibilo, "ASTRID Sodium cooled Prototype : program for improving in service inspection and repair," in *Proceedings of the 2nd International Conference on Advancements in Nuclear Instrumentation, Measurement Methods and their Applications (ANIMMA '11)*, Ghent, Belgium, June 2011, Paper 3–37.

[2] F. Baqué, G. Rodriguez, N. Jardin, J. M. Carpreau, J. M. Augem, and J. Sibilo, "Generation IV nuclear reactors—R&D program to improve sodium-cooled systems inspection," in *Proceedings of the 1st International Conference on Advancements in Nuclear Instrumentation Measurement Methods and their Applications (ANIMMA '09)*, Marseille, France, June 2009, Paper 77.

[3] J. F. Sauvage, *Phénix 30 Years of History: The Heart of a Reactor*, CEA, Paris, France, 2004.

[4] J. Sibilo, E. Breuil, F. Baqué, and J. M. Augem, "Generation IV nuclear reactors: strategy and challenges of R&D program for improving inspection and repair of sodium cooled systems," in *Proceedings of the International Congress on Advances in Nuclear Power Plants (ICAPP '10)*, San Diego, Calif, USA, June 2010, Paper 8096.

[5] F. Reverdy, F. Baqué, B. Lu, K. Jezzine, V. Dorval, and J. M. Augem, "Simulation of ultrasonic inspection for sodium cooled reactors using CIVA," in *Proceedings of the 2nd International Conference on Advancements in Nuclear Instrumentation, Measurement Methods and their Applications (ANIMMA '11)*, Ghent, Belgium, June 2011.

[6] M. Darmon, N. Leymarie, S. Chatillon, and S. Mahaut, "Modelling of scattering of ultrasounds by flaws for NDT," in *Ultrasonic Wave Propagation in Non Homogeneous Media*, vol. 128 of *Springer Proceedings in Physics*, pp. 61–71, Springer, Berlin, Germany, 2009.

[7] R. H. Kraichnan, "Diffusion by a random velocity field," *Physics of Fluids*, vol. 13, no. 1, pp. 22–31, 1970.

[8] K. Jezzine and A. Lhemery, "Simulation of guided wave inspection based on the reciprocity principle and the semi-analytical finite element method," in *Proceedings of the AIP Conference Proceedings*, D. O. Thompson and D. E. Chimenti, Eds., vol. 894 of *In Review of Progress in QNDE, 26A*, pp. 39–46, American Institute of Physics, Melville, NY, USA, 2007.

[9] A. Lhemery, V. Baronian, K. Jezzine, and A.-S. Bonnet-BenDhia, "Simulation of inspections of elastic waveguides of arbitrary section containing arbitrary local discontinuities or defects," in *Proceedings of the AIP Conference Proceedings*, D. O. Thompson and D. E. Chimenti, Eds., vol. 1211 of *In Review of Progress in QNDE, 29A*, pp. 145–152, American Institute of Physics, Melville, NY, USA, 2010.

[10] C. Lhuillier, O. Descombin, F. Baqué, B. Marchand, J. F. Saillant, and J.M. Augem, "In sodium tests of ultrasonic transducers," in *Proceedings of the International Conference on Advancements in Nuclear Instrumentation, Measurement Methods and Their Applications*, Ghent, Belgium, June 2011, Paper 3-06.

[11] H. M. Frost, "Electromagnetic-ultrasound transducers: principles, practice, and applications," *Physical Acoustics*, vol. 14, pp. 179–275, 1979.

[12] O. Descombin, K. Paumel, J. Moysan, G. Corneloup, and J.-M. Augem, "Acoustic coupling of ultrasonic transducers for in-service inspection of sodium fast reactors," in *Proceedings of the International Conference on Advancements in Nuclear Instrumentation, Measurement Methods and Their Applications (ANIMMA '09)*, Marseille, France, June 2009, Paper 78.

[13] P. K. Holland and R. H. S. Winterton, "Nucleation of sodium boiling from surface cavities containing gas," *International Journal of Heat and Mass Transfer*, vol. 16, no. 7, pp. 1453–1458, 1973.

[14] G. Gobillot, F. Baqué, C. Lhuillier et al., "Ultrasonic techniques for improving inspection of sodium-cooled systems," in *Proceedings of the International Conference on Advancements in Nuclear Instrumentation, Measurement Methods and Their Applications (ANIMMA '09)*, Marseille, France, June 2009, Paper 80.

[15] C. Imbert, J. L. Berton, and G. Gimenez, "Realization of ultrasonic images of immersed metallic structures using a digital beamforming system. Experimental study," in *Proceedings of the 5th International Conference on Nuclear Engineering (ICONE5 '97)*, p. 411, May 1997.

[16] G. Corneloup, M. A. Ploix, J. F. Chaix, I. Lillamand, and F. Baqué, "Potential of ultrasounds for NDT of a structure located behind parallel immersed plates," in *Proceedings of the AIP Conference Proceedings (QNDE '10)*, San Diego, Calif, USA, July 2010.

[17] F. Baqué, K. Paumel, G. Corneloup, M. A. Ploix, and J. M. Augem, "Non destructive examination of immersed structures within liquid sodium," in *Proceedings of the International Conference on Advancements in Nuclear Instrumentation, Measurement Methods and Their Applications (ANIMMA '11)*, Ghent, Belgium, June 2011, Paper 3-07.

[18] A. H. Nayfeh, "Elastic wave propagation in fluid-loaded multiaxial anisotropic media," *Journal of the Acoustical Society of America*, vol. 89, no. 2, pp. 542–549, 1991.

[19] B. Hosten and M. Castaings, "Transfer matrix of multilayered absorbing and anisotropic media. Measurements and simulations of ultrasonic wave propagation through composite materials," *Journal of the Acoustical Society of America*, vol. 94, no. 3, pp. 1488–1495, 1993.

[20] L. Champeix, P. Baqué, and C. Chairat, "Stress corrosion on austenitic stainless steels components after sodium draining," in *Proceedings of the 2nd International Conference on Liquid Metal Technology in Energy Production*, pp. 49–55, Richland, Washington, DC, USA, April 1980.

Hindawi Publishing Corporation
Science and Technology of Nuclear Installations
Volume 2012, Article ID 614973, 14 pages
doi:10.1155/2012/614973

Research Article

Safety Design and Evaluation in a Large-Scale Japan Sodium-Cooled Fast Reactor

H. Yamano,[1] S. Kubo,[2] Y. Shimakawa,[3] K. Fujita,[1] T. Suzuki,[1] and K. Kurisaka[1]

[1] *FBR Safety Unit, Advanced Nuclear System R&D Directorate, Japan Atomic Energy Agency, 4002 Narita-cho, O-arai, Ibaraki 311-1393, Japan*
[2] *Research and Development Department, Japan Atomic Power Company, 1-1 Kanda-Mitoshiro, Chiyoda-ku, Tokyo 101-0053, Japan*
[3] *Reactor Core and Safety Design Department, Mitsubishi FBR Systems, Inc., 2-34-17, Jingumae, Shibuya-ku, Tokyo 150-0001, Japan*

Correspondence should be addressed to H. Yamano, yamano.hidemasa@jaea.go.jp

Received 16 January 2012; Accepted 20 March 2012

Academic Editor: Sunil S. Chirayath

As a next-generation plant, a large-scale Japan sodium-cooled fast reactor (JSFR) adopts a number of innovative technologies in order to achieve economic competitiveness, enhanced reliability, and safety. This paper describes safety requirements for JSFR conformed to the defense-in-depth principle in IAEA. Specific design features of JSFR are a passive reactor shutdown system and a recriticality-free concept against anticipated transients without scram (ATWS) in design extension conditions (DECs). A fully passive decay heat removal system with natural circulation is also introduced for design-basis events (DBEs) and DECs. In this paper, the safety design accommodation in JSFR was validated by safety analyses for representative DBEs: primary pump seizure and long-term loss-of-offsite power accidents. The safety analysis also showed the effectiveness of the passive shutdown system against a typical ATWS. Severe accident analysis supported by safety experiments and phenomenological consideration led to the feasibility of in-vessel retention without energetic recriticality. Moreover, a probabilistic safety assessment indicated to satisfy the risk target.

1. Introduction

Since 2006, the Japan Atomic Energy Agency (JAEA) has conducted a fast reactor cycle technology development (FaCT) project in cooperation with the Japanese electric utilities [1]. In this project, a large-scale sodium-cooled fast reactor (SFR) is designed with oxide fuel cores towards its commercialization. This SFR was named the Japan sodium-cooled fast reactor (JSFR), characterized by an advanced loop type reactor with innovative technologies for economic competitiveness, enhanced safety, and improved reliability [2]. Key milestones were set in the project: the determination of innovative technologies to be adopted to JSFR in 2010 and the presentation of the conceptual design of JSFR in 2015. The JSFR demonstration reactor was planned to start its operation in 2025, and research and development (R&D) efforts are currently made regarding the JSFR design study and innovative technologies.

Several innovative technologies need to be developed in order to meet the safety requirements and reliability and economical targets. The key concept of this reactor is a two-loop primary heat transport system (PHTS) for a large power output (to 1500 MW electric) and adoption of high-chromium steel pipes to simplify arrangement of piping, thereby leading to reducing the volume of building with concentrated arrangement of major components. These technologies can greatly contribute to reducing the capital cost of the plant. An intermediate heat exchanger (IHX) was integrated with a primary pump in order to compact the layout of components. A newly designed upper internal structure (UIS) with a single rotational plug allows reduction in the diameter of the reactor vessel. The UIS has a slit of a certain width, where a fuel-handling machine can handle fuel assemblies beneath the UIS without completely removing the UIS itself from the original position. Such innovative technologies could significantly reduce the capital cost, which

was estimated approximately 0.18 Japanese yen per kW electric [3]. The JSFR design substantially mitigates adverse effects caused by sodium leakage or sodium-water reactions in steam generators (SGs). In particular, the leaked sodium can be accommodated by double boundary structures: guard pipes and guard vessels, which cover primary/secondary pipes and vessels, respectively. Besides, access routes for in-vessel structures are provided with the object of in-service inspection in the design [4].

JSFR is recognized as one of the Generation IV energy systems. Compared to current generation nuclear reactors, the Generation IV reactors are aimed to have superior features in terms of economics, safety, sustainability, and proliferation resistance. Therefore, the Generation IV SFRs require a number of innovative technologies, for which enormous R&D efforts are necessary. In contrast, evolutionary SFRs with conventional technologies are also being developed in some countries. Though there are two different approaches in the world, the development of SFRs is steadily moved ahead on.

The present paper describes conceptual safety designs and related evaluations for JSFR performed in Phase I of the FaCT project (i.e., Japanese fiscal years 2006–2010). Because fast breeder reactors are sure to contribute to future sustainable development, we assume that JSFRs with closed fuel cycle systems would be widely distributed through the global market. Safety design principles of JSFR and their implementation should be consistent with this assumption and also compatible with both economic targets and nuclear proliferation resistance/physical protection. Along this understanding, the safety design concept for JSFR will be developed in this study. Its validity will also be confirmed by safety evaluations for a wide accident range in this paper.

2. JSFR Safety Design Concept

2.1. Safety Design Requirements. In terms of safety, a development target and design requirements in the FaCT project are shown in Table 1 [3]. It can be said that these targets are basically consistent with the safety-related goals or user requirements in both the Generation IV project [5] and the International Project on Innovative Nuclear Reactors and Fuel Cycles (INPRO) [6].

Table 1: Safety-related development target and design requirements in the FaCT project.

Development target	
Safety level shall be equal to future light water reactors (LWRs) and related fuel cycle system.	
Design requirements	
SR-1.1	Fundamental safety principles shall be observed. Safety standards and guidelines for former SFRs shall be reflected while specific features of new reactors shall be considered
SR-1.2	Prevention and mitigation against severe accident initiators shall be considered so as to avoid execution of offsite emergency plans
SR-1.3	Total core damage frequency shall be less than 10^{-6}/reactor-year considering multiple units in a site, and total containment failure frequency in core damage conditions shall be less than 10^{-7}/reactor-year

2.2. Safety Design Principle

2.2.1. Deterministic Approach Based on Defense in Depth. In order to achieve the previously mentioned design requirements SR-1.1 and SR-1.2, we deterministically applied the defense-in-depth (DiD) philosophy, which was defined in the report of INSAG [7], to the same extent as it has been in LWRs. This is because we believe that the validity of DiD philosophy has been proven through the long experience of LWRs and that the DiD philosophy is an adequate strategy to achieve a high level of safety in advanced or innovative nuclear systems for which operational experience is rather limited. Essential to this philosophy are the establishment of a highly reliable system that rarely produces abnormal conditions and the design of measures for accident prevention and mitigation.

The deterministic approach was also adopted considering design-basis events (DBEs) to specify safety functions such as a reactor shutdown system (RSS) and a decay heat removal system (DHRS) for prevention of core damage. In this approach, it is necessary to have the following aims:

(i) selecting DBEs to cover the plant conditions that might lead to core damage;

(ii) selecting DBEs for JSFR with a similar sense to those for LWRs, taking into account their safety characteristics;

(iii) selecting conservative design conditions, as with those for LWRs, which include a single-failure criterion and conservative treatment of safety parameters in the evaluation.

In recent LWRs, such as ABWR-II, EPR, and AP1000, some design measures to support the containment function are explicitly provided against severe accidents, which are recognized as another level category of design condition in addition to the design-basis approach. Although this category was formerly described as a beyond DBE, it has recently been recognized that some extended function both for prevention and mitigation should be considered more explicitly in the design work. Such conditions for extended safety design are called design extension conditions (DECs) [8]. Therefore, we incorporated the DEC concept explicitly in our safety design policy. Passive safety features are also introduced into extended safety functions against DECs especially to enhance prevention capability. We believe that this safety design policy against DECs allows alleviating undue burden on offsite emergency plans.

2.2.2. Risk-Informed Approach. In addition to the DiD philosophy, we also adopted a risk-informed approach using a probabilistic safety assessment (PSA) technique that plays a role in considerations on the proportion or balance of different levels of DiD. At the beginning of the FaCT project, we determined that the reference value for large offsite release frequency should be less than 10^{-6}/site-year by referring to one one-thousandth of the risk encountered in our daily activities. We also paid attention to the specific sequences that could result in large early release so as to limit the frequency to be below that of the other sequences. For a reactor facility, our target for large offsite release frequency becomes the reference value with a further reduction by a factor of at least ten: judging from the fact that one site may already have several reactors, we assumed that about ten reactors would be located in a single site in the future. Therefore, the large offsite release frequency target was set less than 10^{-7}/reactor-year (ry). In terms of the safety design of containment function, containment failure frequency (CFF) is preferable target for designers. In the FaCT project, the CFF was set less than 10^{-7}/ry conservatively ignoring a reduction effect in the environment that can be considered in the large offsite release frequency. Since the containment function could suppress the offsite release of radioactive materials with a further reduction by a factor of ten, the risk target of core damage frequency (CDF) was determined less than 10^{-6}/ry.

2.3. Safety Design Concept for JSFR. Figure 1 shows the framework of safety assurance in JSFR. It also shows the structure of DiD, combined with three major safety functions, namely, reactivity control, heat removal, and containment. First of all, it is important to establish a reliable system by adequate design that stands on sound technologies. Furthermore, adequate operation and maintenance also have an important role in ensuring the first level of DiD. Then, the RSS and DHRS play key roles in the second and third levels of DiD, the objectives of which are the control of abnormal operation and accidents, respectively, as design measures against DBEs. Two independent RSSs (primary RSS and backup one) and a redundant/diverse DHRS with passive operation form sufficient defense lines so that fuel melting does not occur. Therefore, the containment function in these levels plays a role only for the confinement of radioactive materials which are not caused by fuel melting. The fourth level of DiD considers design measures against DECs. In this level including both of prevention and mitigation of severe accidents, the RSS and DHRS provide extended prevention functions (i.e., passive shutdown feature and accident management), and the containment system provides a mitigation function against radioactive material release. Moreover, attention is paid to the chemical activity of sodium so as to minimize and localize its influences.

Each of the safety functions is described in detail in Sections 2.3.1 to 2.3.4. It should be mentioned here that passive safety measures are preferable from the viewpoint of physical protection as well as enhancement of these functions [9]. JSFR has such systems for reactor protection and decay heat removal as described below.

2.3.1. Reactor Shutdown Function. The RSS has two independent subsystems, namely, primary and backup systems. Each of them, consisting of control rods and their drive and scram mechanisms, is designed to allow for rapid shutdown in order to prevent core damage against DBEs. RSSs are activated by the reactor protection system, which is composed of logic circuits for activation and an instrumentation system for detecting abnormal reactor conditions. In order to avoid common-cause failure and the propagation of failure, the diversity and independence of the two RSSs are promoted as much as possible. The primary RSS has mechanical delatch devices with acceleration by gas pressure for insertion of the control rods, while the backup RSS has electromagnets for the detachment devices. The control rods in the backup RSS are inserted by gravity. Various kinds of detectors are redundantly installed in the reactor protection system. Furthermore, different kinds of detectors are independently assigned to the primary and the backup RSSs against a single DBE.

In case of earthquakes, relative displacement between the core and the control rods might cause oscillatory reactivity insertion as well as hindering the control rod insertion. Both the stiff core barrel with its core-restraint function and the stiff support structure of the control rods are designed to suppress such displacement and oscillation so that the core fuel keeps its integrity against possible reactivity insertion during the postulated earthquake conditions. The seismic isolation of the reactor building has an important role in reducing the input acceleration for the reactor vessel.

When anticipated transients without scram (ATWS) are postulated, the reactor core becomes damaged in the order of minutes, during which period the operators may not be able to achieve any accident management measures to prevent core damage. Hence, a passive shutdown capability, especially against ATWS events, has been desired to bring the plant to the safe shutdown condition without the operator action as they become commercialized. In order to cope with ATWS, only for the backup RSS, JSFR introduced passive shutdown capability, in parallel with an active reactor protection system and instrumentation system.

A Curie-point electromagnet type self-actuated shutdown system (SASS) has been selected as the most promising provision for JSFR [10]. The SASS concept is schematically illustrated in Figure 2. One of its superior features is simple one-dimensional movement of the control rods with a large negative reactivity, which is triggered once the coolant temperature around a temperature sensing alloy rises high. This passive actuation principle does not require the activation of the reactor protection system, so that it is not necessary to consider a common-cause failure between the passive and active shutdown systems. This serves to enhance the reactor shutdown capability, resulting in the increase of reliability of the overall RSS. There is a favorable characteristic in that the uncertainty of the reactivity feedback mechanism could be small because of its one-dimensional movement in comparison with other passive safety characteristics, such as radial core expansion. The in-service testability in periodic inspections could also present an advantage in maintaining the reliability and safety levels of the plant. In addition, a

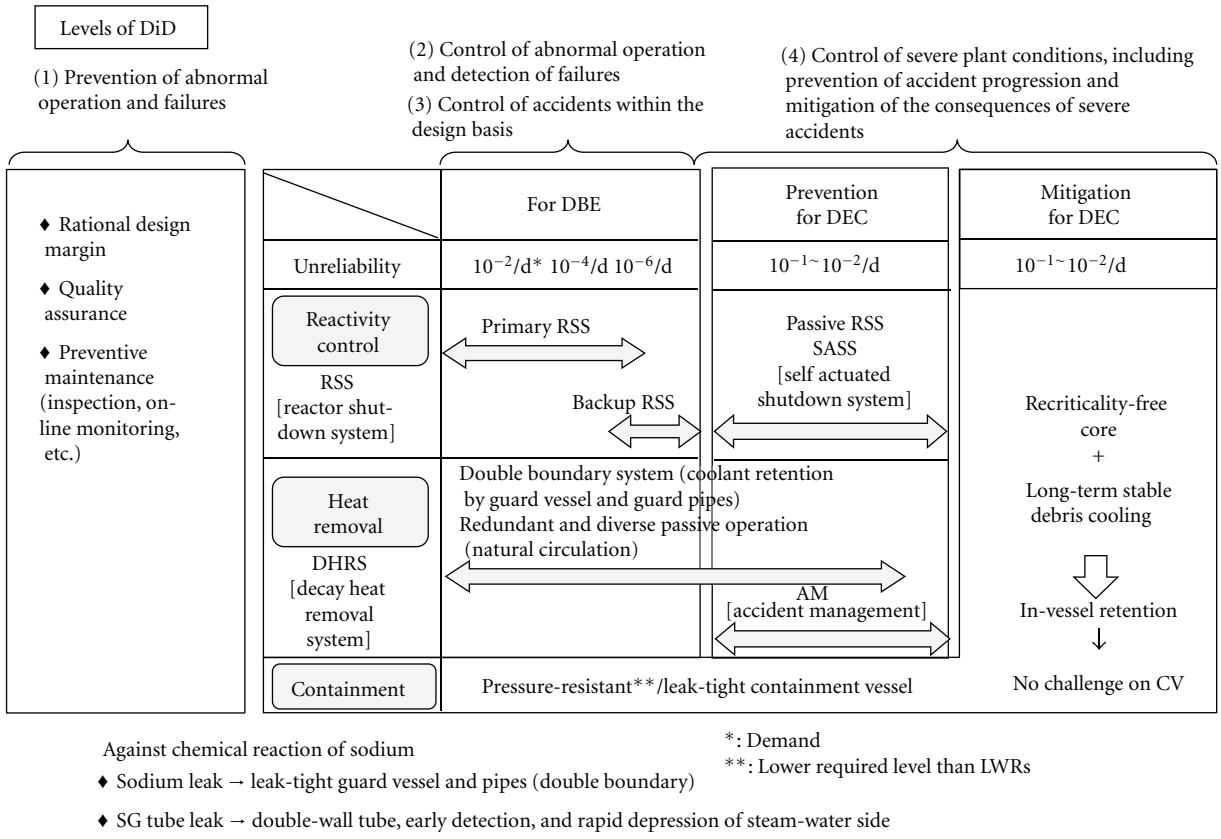

Figure 1: Basic framework of safety design in JSFR.

stable holding capability during normal reactor operation was demonstrated at the experimental fast reactor Joyo [11].

As previously mentioned, the core-restraint concept permits control rods to insert into the core in case of earthquake in the JSFR with the seismic isolation system. To assure the reactor shutdown capability in case of huge earthquake, flexible joints are adopted for the driveline of the backup RSS. Thanks to this, the control rods that stand by just above the active core can be inserted even if a large horizontal displacement unexpectedly occurs between the core structures and UIS.

2.3.2. Core Cooling Function. Since SFRs are generally operated at nearly atmospheric pressure, there is negligible risk of a loss-of-coolant accident, which is a critical issue in LWRs. In terms of maintaining the core cooling function after reactor shutdown, the JSFR necessitates the prevention of both loss of reactor sodium level (LORL) and protected loss of heat sink (PLOHS). In addition, the reduction of the core flow rate due to a PHTS pump failure has a large influence on the short-term core cooling because of its higher power density and because of some positive reactivity feedback of coolant density in the fast reactor core. Particulary, a PHTS pump seizure accident is a critical issue in the JSFR two-loop cooling system. To cope with the PHTS pump seizure accident, the JSFR required some minor but important design modifications, that is, prolonging the delay time to activate the PHTS pump trip sequence (e.g., 1.0 s) and the halving time of the primary flow rate within reasonable range (e.g., 5.5 s) [12].

In the loop-type SFR, unlike the pool-type one, the possibility of LORL due to PHTS piping failure is apprehended. In order to prevent the LORL with high reliability, the following systematic design measures were adopted.

(i) The reactor vessel and its guard vessel have no penetration at either the sides or bottom.

(ii) The primary coolant boundaries in the PHTS piping are located in the position above the liquid surface level in the reactor vessel in order to reduce a possible amount of leak.

(iii) The pressure of the secondary heat transport system (SHTS) is kept slightly higher than that of the PHTS so as to prevent the leaking of primary coolant at the interface breach.

(iv) The primary coolant boundaries are enclosed with a leak-tight backup structure (i.e., guard vessel and guard pipe) so as to restrict coolant leakage against the boundary failure.

(v) Decompressing operations (i.e., PHTS pump trip, isolation of the reactor cover gas from its supply system) are automatically actuated so as to prevent the LORL combined with the above item (ii) against

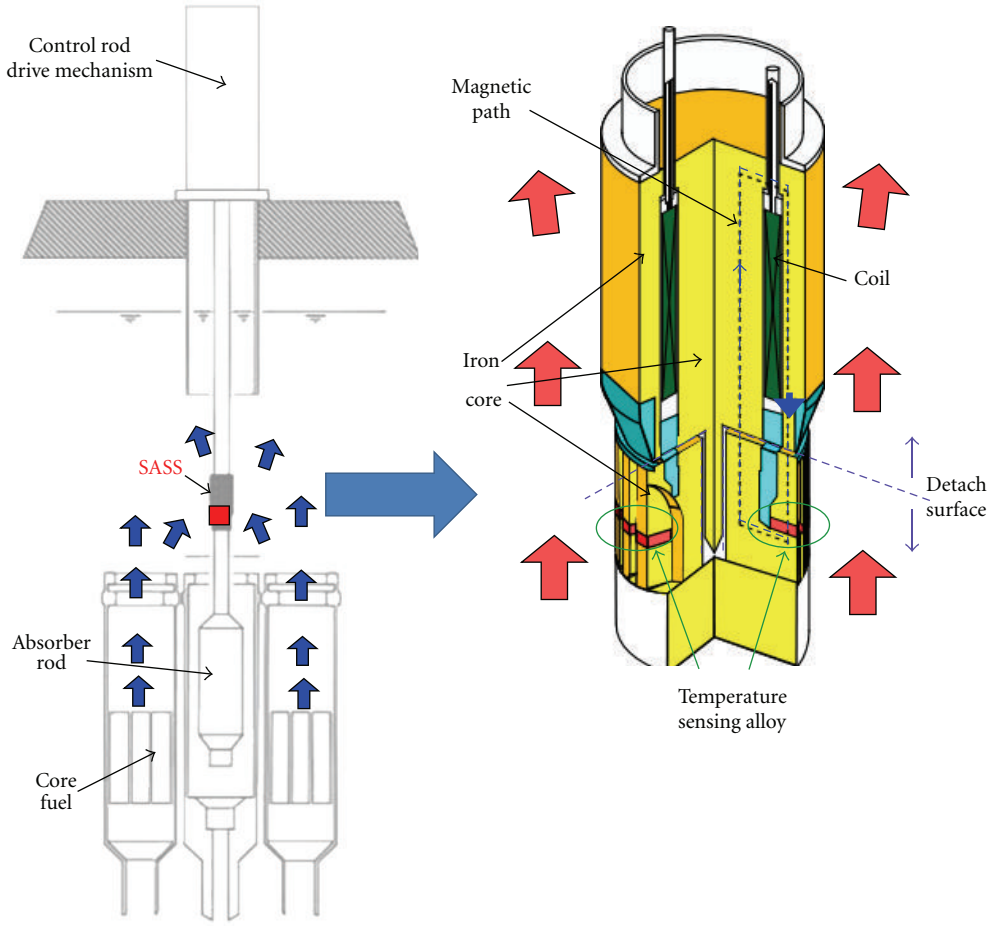

Figure 2: Schematic diagram of the SASS concept.

double failures in the PHTS boundary and its backup structure.

(vi) The open space between the primary pipe and its guard pipe is partitioned to limit the volume of the leak and prevent LORL.

Concerning the primary coolant leakage, the signal from the leaked sodium level meter inside the guard pipe for a large leak and sodium leak detector for a small leak can activate the reactor shutdown and cooling sequence so that core integrity is maintained.

As to prevention of the PLOHS, the decay heat removal is an important safety function, as in LWRs. In order to achieve sufficient reliability, certain redundancy and diversity are required. The DHRS should be designed so that the core is coolable under DBEs with a single-failure criterion as well as under DECs such that a long-term station blackout should be considered in the design. In addition, the DHRS should satisfy the reliability target value in order to achieve the reference CDF in the sense of the probability [12].

In general, a passive DHRS without any active components has higher reliability than an active system. The failure probability of a passive system is dominated by those of the vessel, pipes, and heat exchangers. Such probabilities are smaller than those of start-up or operation of active components (e.g., pumps, blowers). Thus, the passive DHRS is suitable for rational design from the viewpoints of minimizing redundancy and of suppressing subsystems such as the emergency power supply system. The current JSFR design adopts a combination of one loop of direct reactor auxiliary cooling system (DRACS) and two loops of primary reactor auxiliary cooling system (PRACS). These DHRSs can be operated under fully passive condition, which means that, without pumps and blowers, it is required only to activate the DC-power-operated dampers of the air coolers. The damper system has redundancy so that it does not lose its function even considering the single-failure criterion; that is, each air cooler has two dampers in parallel so that an opening failure of a single damper causes less than a 50% reduction in the air flow rate. In addition, diversity is taken into account in the mechanical design of the dampers between DRACS and PRACS. JSFR is suitable for natural circulation cooling due to its simple and short piping connection and due to the lower pressure loss of the core design, as well as the sufficient height

difference between the core and the heat exchangers. Both DRACS and PRACS have a sodium-sodium heat exchanger inside the PHTS. Therefore, they are not affected by the abnormal conditions initiated in the SHTS and the steam-water systems.

For DECs, accident management can be expected to prevent core damage because the grace period is long enough for operators to implement it. With PSA results, effective accident management measures are being proposed (e.g., additional damper system).

2.3.3. Containment Function. The reinforced reactor block of the JSFR reactor building is designed to form a leak-tight containment boundary, the leak rate of which is 1%/day. The containment is surrounded by a confinement area, where an emergency gas treatment system is installed. Function of the confinement area is to reduce the release rate of radioactive materials through the penetrations of piping at the containment boundary.

In the conventional safety design, the containment system has been designed to withstand a significant mechanical load resulting from core disruptive accidents (CDAs) [13]. Such an approach is not suitable for future reactors, which should meet the development target and at the same time should have the economic competitiveness. To significantly reduce the loads on the containment, the JSFR safety design pursues achieving in-vessel retention (IVR), which is defined as termination of CDAs within the reactor vessel, utilizing the advantageous features of SFR (i.e., the low-pressurized system and the superior cooling performance of liquid sodium). A special fuel assembly feature was suggested to eliminate a severe recriticality occurrence resulting in a mechanical load on the containment in CDAs as well as limiting the sodium void worth. For core debris retention within the reactor vessel, a multilayered structure was provided at the bottom of the reactor vessel.

In conventional SFRs, a sodium leak accident resulting in a little sodium combustion on the containment vessel was regarded as a representative DBE for the containment function. The double boundary system in the JSFR allows no significant impact on the containment due to sodium leak because of the accommodation of its consequence in the guard pipe. As an example of DBE, therefore, the break of cover-gas piping under the stop of air conditioning device operation due to the containment isolation is anticipated to confirm the containment function. Such an event is expected to give less significant impact on the containment vessel as the last barrier In the JSFR.

Although external events are out of the scope yet in the present conceptual design stage, several practical measures against external threats on the containment are being discussed.

2.3.4. Design Measures against Chemical Reaction of Sodium. The JSFR is a system concept suitable for the implementation of a complete double-wall structure (i.e., inner piping and guard piping) for both the PHTS and SHTS, combined with their short and simple pipe connection, as shown in Figure 3. The PHTS double-wall structure enables us to prevent or minimize the combustion of leaked sodium in addition to prevention against LORL. Even if a sodium leak resulting from a primary pipe failure occurs, the chemical interaction of the sodium can be prevented in the space between the primary pipe and its guard pipe, which is filled with nitrogen gas, as long as the external boundary is intact. The limitation of this space volume gives no impact on the reactor coolant level. According to safety analyses performed separately from this study, the core integrity can be ensured though the coolant leak rate through the flaw depends on the event sequence. A similar boundary structure is also applied to the SHTS, where a boundary failure does not lead to LORL, as a design measure against sodium leak caused by the inner pipe failure. In the JSFR, the SHTS guard pipe is called an enclosure. The adoption of the enclosure for the SHTS comes from the viewpoints not only of safety but also of plant availability, considering the fact that the influence of the social acceptance was fairly significant in a sodium leak accident in the SHTS of the prototype fast reactor Monju.

We expect introduction of a leak-before-break concept for high-chromium ferrite steel to contribute to minimizing the leak rate in coolant boundary failures and to eliminating the possibilities for an abrupt decrease in coolant flow in the reactor core. Although there are some R&D elements required for introduction of the leak-before-break concept, it would be feasible to accommodate sodium leak detection in the annular region between the inner and guard piping. With that in mind, a double-ended break of the inner piping should be taken into account in the DEC of the safety evaluation in order to verify the tolerance of the guard piping.

At the beginning of the FaCT project, a double-wall structure has been proposed for the heat transfer tubes in the SGs in order to suppress the probability of an SG tube leak event to an extremely unlikely level during the plant lifetime. This feature corresponds to the aim of achieving higher plant availability by excluding plant outage caused by an SG tube leak as well. Although this concept is technically feasible, the adoption of an alternative concept is also considered for the demonstration JSFR by the project judgment in the FaCT Phase-I [2]. JSFRs are designed to be equipped with an SHTS and related subsystems (e.g., early leak detection, the steam-water side pressure release, rupture disks in the SHTS) that have the role of preventing core damage due to the sodium-water reaction postulated in case of an SG tube leak.

3. Safety Evaluations for DBE

3.1. Event Selections for DBEs. According to the current licensing practice in Japan, two event categories were set up within the frame of DBEs, namely, abnormal transients and accidents. Abnormal transients are defined events that lead to abnormal conditions due to anticipated failure or malfunction of a single component or a single erroneous operation. Accidents are defined unlikely events that might lead to the release of radioactive materials outside the facility. The prevention systems against the events to be classified into the accident were designed so as to limit the annual

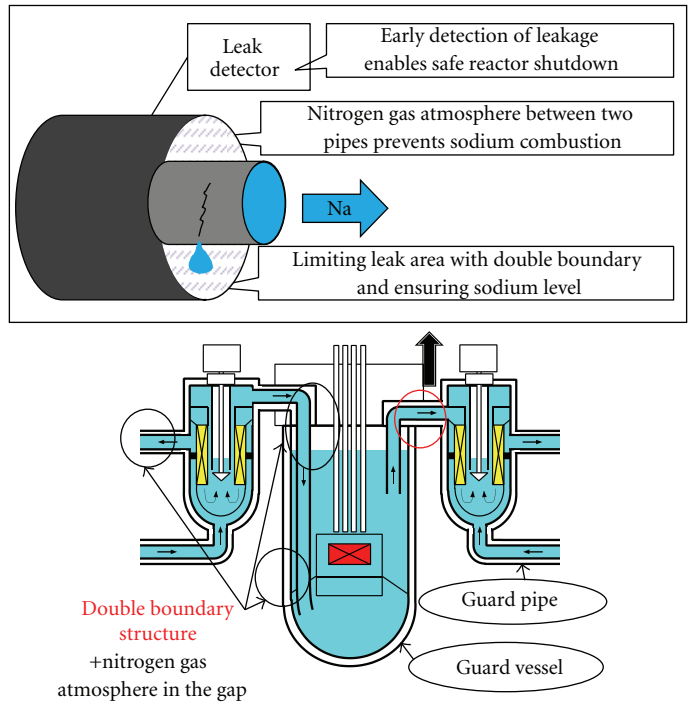

Figure 3: Schematic diagram of the double-wall structure.

occurrence frequency to the extent below 10^{-2}/ry that means the frequency less than once per a reactor lifetime.

In the current stage, it is important to choose and evaluate typical events, which are critical for determining the design conditions of the major safety function. In this paper, a loss-of-flow-(LOF-) type event was described to validate the RSS design. A loss-of-offsite power event was also described to validate the DHRS design. A comprehensive evaluation for all the selected DBEs will be conducted in the FaCT Phase-II.

3.2. Safety Criteria and Conditions for DBEs. Basic requirements for abnormal transients and accidents are the same as those of current LWRs in Japan. Namely, the requirement for abnormal transients is that recovery to normal operation is possible after the transient event is terminated. This means that fuel pin and plant damage are negligible. The requirement for accidents is that the core should be coolable without significant damage and provide no significant public exposure.

Along with these requirements, specific safety criteria for the hottest fuel pin in the core were tentatively defined in the FaCT Phase-I. The maximum temperature of fuel is limited by its melting temperature for both abnormal transients and accidents. In case of fuel melting, the radial expansion of fuel pellet induced by the internal pressure in the molten fuel cavity causes a mechanical load on the cladding tube. The failure of cladding tube could not occur under small melt fraction condition due to the lower fuel smear density of 82% [14]. Nevertheless, the criteria for accidents were conservatively taken because of no experimental data for fuel pins under a high burn-up condition, being aimed in the JSFR. The maximum cladding temperature is set tentatively, based on the developed austenitic stainless steel database as well as available data for oxide dispersion-strengthened steel, which is now under development for its use in the JSFR. According to the results of transient burst tests of cladding tube, where the temperature increase rate and the hoop stress of reactor case were simulated, the failure limit temperature with 95% reliability was obtained over 900°C. The maximum cladding temperature for accidents was determined at 900°C. For abnormal transients, it was set at 830°C with larger margin in order to make the damage negligible. Since the oxide dispersion-strengthened steel is expected to have higher strength comparing with austenitic steel, it is necessary to develop a database for the oxide dispersion-strengthened steel cladding tubes, especially for irradiated ones. The cumulative damage fraction of cladding, for which creep damage is taken into account, is calculated to be unity when the cladding tube failure occurs. The value for abnormal transients was provided as negligible contribution to cladding damage. For accidents, the value was obtained by subtracting the contribution of normal operation, abnormal transients, and fuel-handling from unity. The maximum temperature of coolant was limited to its boiling temperature in order to avoid both of significant cladding damage and rapid positive reactivity insertion due to coolant boiling.

The uncertainties of parameters and conditions in the evaluations were conservatively treated. A core burn-up state was selected so as to provide the most severe evaluation results, and sufficient uncertainties were considered in its reactivity coefficients. The single-failure criterion was applied to active components, of which failure provides the most severe result. Loss-of-offsite power was assumed when

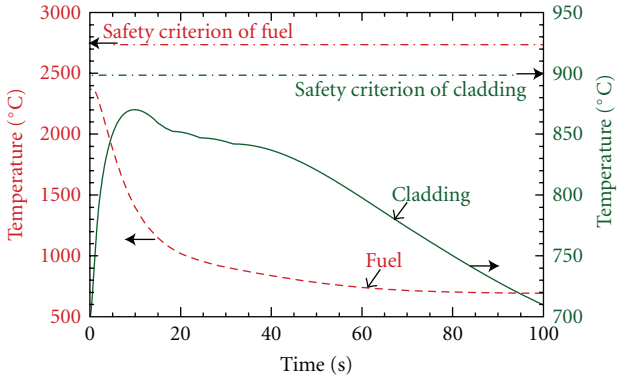

Figure 4: Primary pump seizure accident with primary RSS.

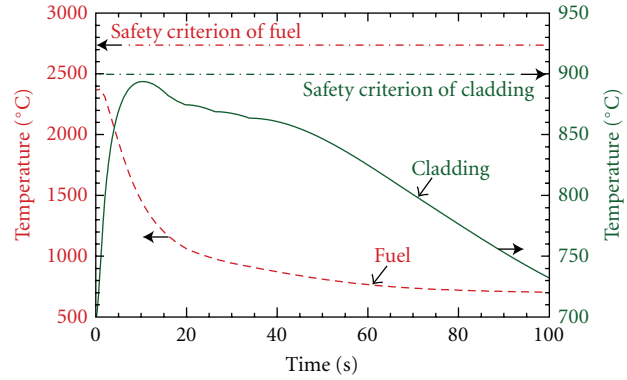

Figure 5: Primary pump seizure accident with backup RSS.

the mitigative systems, which require electric power for operation, were expected to activate. The effect of nonsafety grade systems was not counted in the evaluation.

3.3. DBE Analytical Results

3.3.1. Loss-of-Flow-(LOF-) Type Events. In general, the PHTS pump seizure accident in one loop tends to produce severe consequences in DBEs compared with conventional three- or four-loop design. Because of the two-loop system, this accident would become a critical safety issue in JSFR. However, some design adjustments described in Section 2.3.2 make it possible to restrict the maximum cladding temperature within the safety criterion. Each RSS was designed so as to independently shut the core down within the cladding temperature limit. The primary RSS can be activated by signals indicating "low ratio of primary pump speed to neutron flux" and "low ratio of primary flow rate to neutron flux." These signals can be adapted to a low power operation. The backup RSS is activated by another signal with different mechanism. A plant dynamics calculation method was used for this analysis in a similar way performed in the past [12]. In the analysis, the seizure is assumed instantaneously in the failed pump, whereas the flow having time was assumed 4.5 s with 1.0 s delay of pump trip in the intact pump after the actuation of trip signal. The response times of scram signals for primary and backup RSSs are set 0.45 s and 0.55 s, respectively.

Figure 4 shows calculated temperatures of fuel and cladding in the hottest pin for the primary RSS case in a full-power operation. The activation signal was the "low ratio of primary pump speed to neutron flux" signal. The calculated temperatures of fuel and cladding are 2373 and 870°C at maximum, respectively, which are less than the safety criteria.

The pump seizure accident has also been calculated assuming the activation of the backup RSS, as presented in Figure 5. The calculated maximum temperatures of fuel and cladding are 2375 and 893°C, respectively. These results satisfy the safety criteria, although the safety margin is small. It should be noted that the margin to the safety criteria can be enlarged by some design adjustments, such as the PHTS pump trip sequence and the PHTS flow rate halving time.

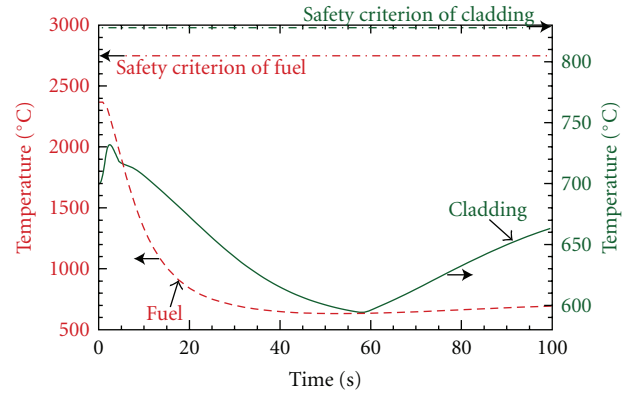

Figure 6: Loss-of-offsite power event (short term after the event initiation).

In the low power operation, the calculated maximum temperatures of fuel and cladding were lower than those in the full-power operation by approximately 200°C.

3.3.2. Decay Heat Removal. For the fully passive feature like this DHRS, the evaluation for abnormal transients is very important, especially from the viewpoint of fuel integrity during the slower transient events for the establishment of stable coolant circulation. A loss-of-offsite-power transient analysis has been done with the same calculation procedure as the pump seizure accident analysis mentioned above. In this event, the fully natural circulation capability of one-loop DRACS and two-loop PRACSs would be expected. In this calculation, the primary boundary temperature was assumed to mostly correspond to the coolant temperature at the exit of the reactor vessel.

Short-term calculated temperatures of fuel and cladding after the event initiation are shown in Figure 6. The calculated maximum temperatures of fuel and cladding are 2369 and 732°C, respectively. Figure 7 shows long-term calculated temperatures of fuel cladding and primary coolant boundary. Following the first peak of cladding temperature just after the reactor shutdown, the second and third peaks appear around 0.036 h (2.2 min.) and 0.32 h (19 min.), respectively. The second peak is governed by the primary

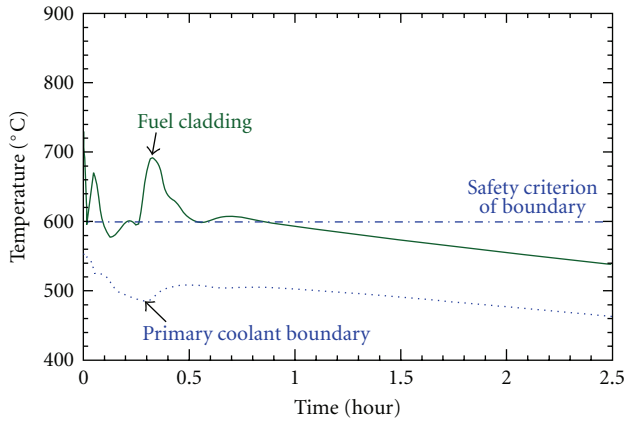

Figure 7: Loss-of-offsite power event (long term).

coolant flow rate that is determined by natural circulation capability based on a temperature difference in the PHTS before the core cooling using the DHRS is effective. After the establishment of natural circulation, the third peak is formed by the balance between the decay heat and the natural circulation capability of the DHRS itself. The calculated maximum temperatures of fuel cladding at second and third peaks are 679 and 693°C, respectively. The calculated maximum temperature of primary coolant boundary after the establishment of natural circulation is 509°C, which is lower than the initial reactor vessel exit temperature. After 0.7 h, the cladding temperature continuously decreases. These calculation results fulfill the safety criteria of fuel, cladding, and coolant boundary. The cumulative damage fraction is also less than the criterion for abnormal transients.

The other DBE analyses with regard to the decay heat removal also indicated that the natural circulation DHRS is effective.

4. Safety Evaluations for DEC

4.1. Event Selections for DECs. The DECs are additional conditions or events, where failure in fundamental prevention functions or more severe initiating-event conditions are assumed. Although the DECs are set up in a deterministic way, there should also be risk-based consideration in order to avoid too conservative design measures. The DECs of concern include classical initiators, such as ATWS. The event selection of DECs will be defined according to the progress of the design and PSA study. Along the DiD philosophy, the effectiveness of prevention and mitigation design measures against CDAs should be validated in the DEC category. Therefore, the safety evaluation should involve two categories for prevention and mitigation. In this paper, as representative DECs, we selected the ATWS, where the passive shutdown capability and mitigative measures against CDAs were evaluated.

4.2. Safety Criteria and Conditions for DECs. For DECs, the basic containment function and postaccident core cooling shall be maintained. The release level of radioactive materials shall be below the level at which offsite response is activated. In the JSFR, the following criteria were tentatively defined for the prevention and mitigation categories.

For the prevention category, the passive shutdown capability is assessed in this paper. The safety criterion was set below the boiling point of the coolant for a core outlet coolant temperature. The boiling point at the top of the core is 1020°C because the cover gas is slightly pressurized in the reactor vessel in the JSFR. As mentioned in Section 3.2, the failure limit of fuel cladding due to fuel melting is considerably high. The cladding failure limit for low smear density fuel is approximately 40% of areal melt fraction [14]. Hence, for the fuel pellet, the maximum melt fraction was conservatively limited to less than 30%. The melting temperature of fuel pellet is ~2740°C in the calculated core.

For the mitigation category, no significant mechanical and thermal impacts on the primary boundary are allowed because the JSFR aims at the IVR concept without any significant internal challenges on the containment function. Detailed description of the safety criteria is given in Section 4.3.2.

The DEC evaluations were conducted on a best-estimate basis. The influence of various uncertainties will be investigated in a future PSA study.

4.3. DEC Analytical Results

4.3.1. Passive Shutdown Capability Evaluation. The ATWS events are roughly divided to three types: LOF, transient over-power, loss-of-heat sink type. Thus far, we used to call "unprotected LOF (ULOF)" for the LOF-type ATWS. In the prevention evaluation category, however, the core can be protected by the passive shutdown feature. Such a terminology might create confusion, so we call "LOF without scram (LOFWS)" for the passive shutdown evaluation in this paper. Since the LOFWS event tends to produce the most severe consequence among three types of the ATWS events, an analytical result only for the LOFWS event is presented in this paper.

In the LOFWS analysis, a flow coastdown of all primary pumps was assumed without a reactor trip from a full-power operation. A one-dimensional plant dynamics analysis code with point kinetics and heat transfer models was applied to this event in a similar way performed in the past [10]. The maximum temperatures of fuel and coolant in the core were calculated for the nominal hottest channel, which represents the hottest fuel assembly in the core. The activation temperature of the SASS was set at 660°C, the feasibility of which was experimentally checked in selecting material components. A three-dimensional computational fluid dynamics (CFD) calculation was separately carried out to obtain a coolant transport time from the top of neighboring fuel assemblies around the backup control rod (BCR), where the SASS is installed, to the SASS temperature-sensing alloy at a nominal flow rate. Based on this CFD calculation, the transport time was set 1.3 s and only five-BCR insertion was assumed. In this event, this time becomes longer due to the reduction of flow rate. As the other parameter, the time constant of

the detachment, defined as a time difference between the time when a bulk coolant temperature around the SASS reaches the detachment temperature and the time when the SASS detaches, was also calculated by the CFD approach. To enhance the time constant, some design modification was necessary. This design modification depends on the locations of individual BCRs, so that the time constants for the core-center BCR and the four neighboring BCRs were set as 3.4 s and 1.0 s, respectively. The insertion time of the detached control rod was set as 1.5 s for 85% of the rod stroke, based on actual rod insertion test data. After the passive shutdown, although the natural circulation DHRS can be activated in the design, such a cooling mode is neglected in this analysis for simplicity.

Figure 8 shows a typical result of fuel, cladding, and coolant temperatures for the LOFWS, where the halving time of the coolant flow rate was 6.5 s. The calculated coolant temperature around the SASS armature at the four BCRs in the inner peripheral positions in the inner core reached 660°C of the SASS detachment temperature and detached at 11.9 s after the transient onset. This first BCR insertion mitigated a steep power increase. At another core-center BCR, the SASS detached the rod at 13.3 s. The calculated maximum temperatures of fuel and coolant are 2248 and 969°C, respectively, which are less than the safety criteria. Accordingly, the SASS averted bulk coolant boiling, so that the core cooling could be maintained. This analysis indicated the passive shutdown capability of the SASS against the typical ATWS.

4.3.2. CDA Evaluation. As the passive safety features are provided against fast sequences, such as ATWS, and redundant accident managements against slow sequences, the probability of a CDA becomes negligibly small. Nevertheless, the consequences of CDAs should be mitigated based on the DiD philosophy, since a recriticality potential in the course of CDAs has been regarded as one of the major safety issues in fast reactor cores and also as a potential candidate for early large-release sequences. Enormous effort has been dedicated to the clarification of accident scenarios and the consequences of CDAs. Once coolant boiling is assumed, a significant reactivity increase is possible because a typical SFR core has positive void reactivity feedback. Over the years, therefore, the ULOF scenario has particularly been investigated from the viewpoint of mechanical design margin against super-prompt excursion during the initiating phase and against energetic recriticality during the transition phase. The thermal design margin has been also investigated to ensure IVR [15].

As stated in Section 2.3.3, design measures are taken in the JSFR safety design approach so that severe power burst events with recriticality can be eliminated and core materials can be stably cooled in the reactor vessel for the long term. In developing the CDA scenario, the core degradation sequences were conveniently divided into four phases: initiating, early discharge, material relocation, and heat removal phases. To achieve the IVR, the following safety criteria were defined for the four phases:

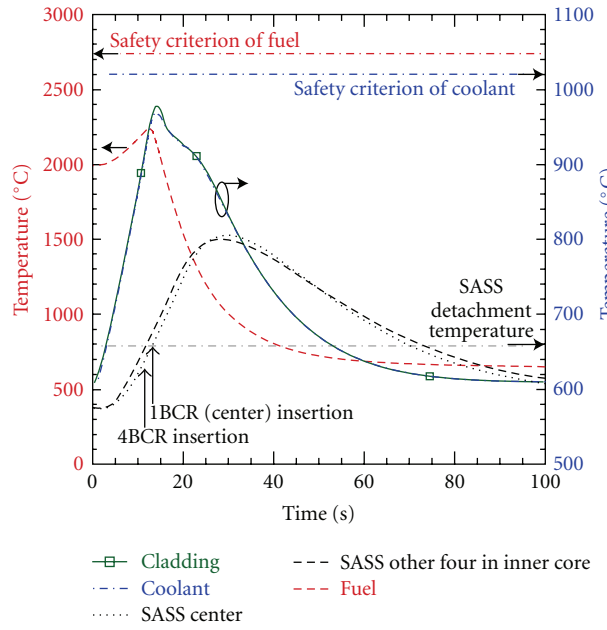

Figure 8: Loss-of-flow without scram accident with passive shutdown.

(i) no severe power burst for the initiating phase,

(ii) early fuel discharge from the core before the formation of the whole-core scale molten fuel pool for the early discharge phase,

(iii) relocation of disrupted core materials to the coolable geometry under the subcritical state for the relocation phase,

(iv) long-term stable cooling of disrupted core materials in the reactor vessel for the heat removal phase.

In order to avoid severe power burst during the initiating phase, the sodium void worth should be limited to a certain value. In the FaCT Phase-I, the reference value was determined as less than six dollars (6$) based on both theoretical consideration and the analytic experiences for various types of core design [16]. In general, it could be achieved by shortening the core height less than 1 m in a large-scale core. It was found that a power excursion driven by positive reactivity insertion due to sodium voiding in a ULOF sequence could be limited by negative Doppler reactivity insertion due to rapid fuel temperature increase and would be finally cancelled by negative reactivity insertion due to rapid fuel dispersal [17]. Before the FaCT Phase-I, ULOF initiating phase calculations were carried out for various core designs using the SAS4A code. In case of taller core height with larger-diameter fuel pins, the effect of negative fuel dispersal was slightly delayed. This was due to its lower fuel-power density and smaller axial fuel worth gradient. Therefore, additional reference values were created for an average fuel-specific heat and core height in the core design. These values are 40 kW/kg-fuel and 1 m, respectively. These design conditions were implemented into the current core design [18]. A fuel smear density is 82% theoretical

density in the JSFR design, so a high failure threshold is expected. This pin condition would allow a high axial level of fuel pin failure resulting in negative fuel motion reactivity just after the failure [19].

The SAS4A analysis showed mild power burst so as not to reach a prompt criticality during the initiating phase, as presented in Figure 9. Severe power burst has never been obtained even in parametric calculations [16]. These average core fuel enthalpies were less than the solidus temperature of oxide fuel. In these calculations, sodium voiding and its reactivity effect inside the inner duct were not taken into account because a separate calculation indicated that the sodium boiling inside the duct occurred in the early discharge phase; thus it does not affect the peak power level of initiating phase.

In the past, it was reported using the SIMMER-III computer code that an energetic recriticality occurred only by radial whole-core scale fuel motion [20]. To avoid such a recriticality, Japanese researchers have struggled to create measures enhancing axial fuel discharge, which is the most effective in reactivity decrease, before enlarging the molten region [21]. As one of measures, special fuel assemblies have been proposed to enhance the molten fuel discharge. The Fuel Assembly with Inner DUct Structure (FAIDUS) is a concept in which a steel duct is installed as a fuel escape path in every fuel assembly [21]. Considering both the superior fuel discharge capability of FAIDUS and its impact on other aspects, we additionally proposed a modified concept of FAIDUS, as shown in Figure 10. In this concept, a smaller-diameter inner duct with an opening at the upper end was installed [22]. In the modified FAIDUS design, the fuel escape path is shorter and hotter compared to that of conventional FAIDUS; therefore, the hydraulic diameter of the inner duct can be smaller. This is advantageous for limiting the impact of the safety feature on core performance. For the conventional FAIDUS, the development of a new grid spacer is required in order mainly to keep a clearance between the fuel pin bundle and the inner duct locating at the center of the fuel assembly. On the other hand, the conventional wire-spacer technique can be applied to the modified FAIDUS design because the inner duct is attached at a corner of the wrapper tube; hence, the fuel fabrication of this concept becomes more feasible with less R&D efforts. It should be noted that certain thermal hydraulic problems caused by the asymmetric arrangement of the modified FAIDUS must be resolved through some minor R&D.

The event sequence after termination of the initiating phase power transient in a relatively higher-power fuel assembly is explained as follows. The inner duct wall failed by the contact of hot liquid fuel/steel mixture. The fuel/steel mixture is ejected into the inner duct driven by the pressure build-up in the pin-bundle side due to fission gas released from melting fuel. Sodium voiding and its upward expansion inside the duct occur due to interaction between ejected fuel/steel and liquid sodium. The molten fuel is discharged upward through the voided duct driven by the gas pressure. The discharged fuel is dispersed into the upper sodium plenum of the reactor vessel. The dispersed fuel is relocated mainly on the intermediate isolation plate (top level of the core). The above key phenomena have been confirmed by experimental study [23].

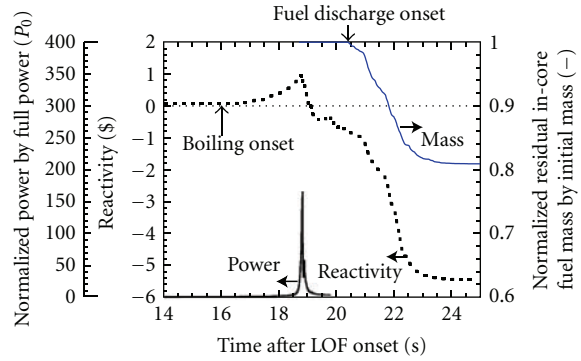

Figure 9: Initiating and early fuel discharge phases of unprotected loss-of-flow accident.

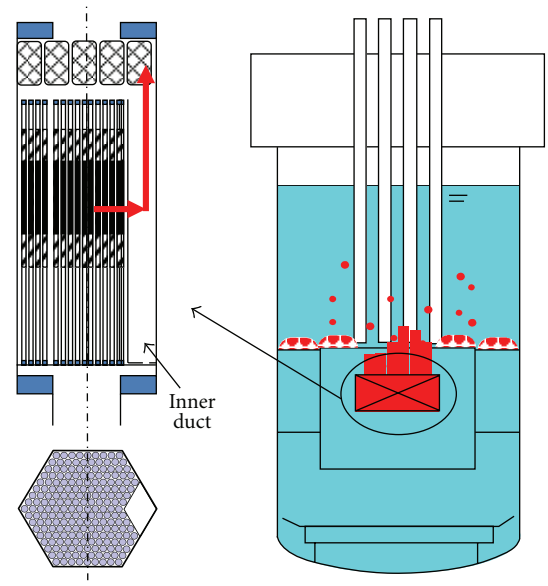

Figure 10: Fuel assembly with inner duct for enhancing molten fuel discharge.

Figure 9 shows the fuel discharge capability for the modified FAIDUS design during the early discharge phase, which was evaluated by the SIMMER-III code. In this calculation, the geometry of a single fuel assembly was used to investigate the phenomena in detail. The fuel assemblies in the core were divided into several groups depending on the power level, and fuel discharge phenomena in each representative fuel assembly were separately analyzed using a similar power history but different power level corresponding to each fuel assembly group. Although the power time history was given as the input obtained from the SAS4A result, the reactivity feedback due to fuel discharge was taken into account by means of an iterative calculation procedure. In each calculation of the representative fuel assembly, almost all the molten fuel in the assembly was discharged upward through the inner duct while the immobile solid fuel remained in the core region of the assembly. The total amount of fuel

discharged from the core, estimated as the summation of the discharged fuel from all the fuel assemblies in each group, was about 19% of the initial fuel inventory, and the core reached a subcritical condition.

Just after the early discharge of molten fuel, solid fuel without mobility would remain in the core in the decay heat level. The event sequence during this phase is explained as follows. Frozen fuel and remaining solid fuel around the upper part of the core fell and accumulated in the lower part of the core. Upper core structures inside the fuel assembly, such as axial fuel blanket, are collapsed as well as the intact fuel in the most-inner outer core. Based on a preliminary evaluation, the remaining fuel in the core region starts to melt by the decay heat at 150 to 200 s after the early fuel discharge phase. From a phenomenological point of view, it is expected that this molten fuel would move downward locally through the space in the primary control rod guide tube (CRGT) failed by the contact of materials molten by the decay heat. It should be noted that absorber-rod insertion could be assumed in backup CRGTs just at the beginning of the material relocation phase because the temperature of materials of the SASS would reach high enough to lose its magnetic property by contacting with molten fuel and sodium vapor generated during the early fuel discharge phase.

Based on the above event sequence, the reactivity change was evaluated by a series of static neutronic calculations. As a result, a significant reactivity insertion would be avoided by the enhancement of fuel discharge through the primary CRGTs; therefore the subcritical state would be ensured during the relocation phase.

Because the advanced loop concept has a relatively small reactor vessel compared with a large fuel inventory, a multilayer debris tray is basically required to hold the full inventory of core fuel without dryout and recriticality. Proper quenching and distribution as well as coolant convection are crucial points in this concept. A thermal hydraulic calculation was conducted for the coolability of fuel debris [24]. In this calculation, all of the fuel was uniformly relocated on the multilayer debris tray. The DHRS consisting of one DRACS and two PRACSs was available in a fully natural circulation mode. The calculation result showed that the decay heat balanced the removed heat around 30 min. after the start of the transient. The maximum coolant temperature in the debris bed was less than 900°C and steadily decreased after the peak temperature, so that sufficient cooling capability is provided for a long-term stable retention in the reactor vessel.

5. Probabilistic Safety Evaluation

It is required to implement the PSA in order to check whether the requirements of CDF and CFF are satisfied. At the early stage of drawing the design concept, it is also required to construct a well-balanced safe system so as to eliminate any weak points and/or remarkable cliff edge effects that can appear in the risk curve from the risk point of view. Therefore, our study aimed at comprehending systematically the safety characteristics of the system with respect to a risk potential and at making design improvement effectively in such a way as to appropriately control and minimize the risk using the PSA technique.

In SFRs, typical event sequences leading to core damage are categorized into three types: ATWS, LORL, and PLOHS. The point estimates of their frequencies have been evaluated by the preliminary PSA, focusing on internal events under normal operation. These point estimates were 1×10^{-8}/ry, 4×10^{-9}/ry, and 9×10^{-9}/ry for ATWS, LORL, and PLOHS, respectively [25]. The total CDF is about 2×10^{-8}/ry, which satisfies less than 10^{-6}/ry in the risk target. This value also meets less than 10^{-7}/ry of CFF.

The PSA activity is continued reflecting up-to-date plant design. A seismic PSA is also implemented because it is important for the seismic isolation system design in the JSFR. According to the preliminary result, the building and components in the JSFR have a sufficient safety margin even considering a current seismic design condition [25].

6. Conclusions

In the present study, the safety design concept for the JSFR has been established to fulfill the development target that would ensure a safety level comparable to future LWRs. Based on the DiD safety philosophy with the complementary use of the risk-informed approach, the JSFR adopts highly reliable systems that rarely cause abnormal conditions and specific design measures both for accident prevention and mitigation. In designing the JSFR, considering the superior safety characteristics of SFRs, three fundamental safety requirements were systematically investigated. The subsequent consideration provided as appropriate safety design measures: the SASS as the passive feature in addition to the two independent RSSs, the fully natural circulation DHRS that can remove the decay heat without the SHTS, the introduction of double-wall piping against sodium leaks, a core design limiting the sodium void worth, devisal of the special fuel assembly for attaining IVR under ATWS, and the leak-tight containment. Such passive and static measures that need not depend on operator actions can encompass high safety and reliability as well as being preferable from the physical protection point of view. The safety analyses and PSA revealed that the JSFR design fulfilled the safety criteria. Although some of them necessitate further R&D for their deployment in future commercialized reactors, we believe all are within reach. In the next phase, further design study will be steadily performed along with the several R&D efforts.

Acronyms

ATWS: Anticipated transient without scram
BCR: Backup control rod
CDA: Core disruptive accident
CDF: Core damage frequency
CFD: Computational fluid dynamics
CFF: Containment failure frequency
CRGT: Control rod guide tube
DBE: Design-basis event
DEC: Design extension condition

DHRS: Decay heat removal system
DiD: Defense in depth
DRACS: Direct reactor auxiliary cooling system
FaCT: Fast reactor cycle technology development
FAIDUS: Fuel assembly with inner duct structure
IHX: Intermediate heat exchanger
INPRO: Innovative nuclear reactors and fuel cycles
IVR: In-vessel retention
JAEA: Japan atomic energy agency
JSFR: Japan sodium-cooled fast reactor
LOF: Loss of flow
LOFWS: Loss of flow without scram
LORL: Loss of reactor level
LWR: Light water reactor
PSA: Probabilistic safety assessment
PHTS: Primary heat transport system
PLOHS: Protected loss of heat sink
PRACS: Primary reactor auxiliary cooling system
R&D: Research and development
RSS: Reactor shutdown system
SG: Steam generator
SHTS: Secondary heat transport system
UIS: Upper internal structure
ULOF: Unprotected loss of flow.

Acknowledgments

This paper includes the outcome of collaborative study between JAEA and JAPC (representing the nine electric utilities, Electric Power Development Co., Ltd. and JAPC) in accordance with "the agreement about the development of a commercialized fast breeder reactor cycle system".

References

[1] Y. Sagayama, K. Okada, and T. Nagata, "Progress on reactor system technology in the FaCT project toward the commercialization of fast reactor cycle system," in *Proceedings of the International Conference on the Fast Reactors and Related Fuel Cycles (FR '09)*, IAEA-CN-176-01-02, IAEA, Kyoto, Japan, December 2009.

[2] K. Aoto, N. Uto, Y. Sakamoto, T. Ito, M. Toda, and S. Kotake, "JSFR design study and R&D progress in the Fact project," in *Proceedings of the International Conference on the Fast Reactors and Related Fuel Cycles (FR '09)*, IAEA-CN-176-01-07, IAEA, Kyoto, Japan, December 2009.

[3] S. Kotake, Y. Sakamoto, T. Mihara et al., "Developement of advanced loop-type fast reactor in Japan," *Nuclear Technology*, vol. 170, no. 1, pp. 133–147, 2010.

[4] M. Ichimiya, T. Mizuno, and S. Kotake, "A next generation sodium-cooled fast reactor concept and its R&D program," *Nuclear Engineering and Technology*, vol. 39, no. 3, pp. 171–186, 2007.

[5] U.S. DOE, "Nuclear energy research advisory committee and the generation IV international forum, a technology roadmap for generation IV nuclear energy systems," Tech. Rep. GIF-002-00, U.S. DOE, 2002.

[6] IAEA, "Guidance for the evaluation of innovative nuclear reactors and fuel cycles: report of phase 1A of the International Project on Innovative Nuclear Reactors and Fuel Cycles (INPRO)," Tech. Rep. IAEA-TECDOC-1362, IAEA, 2003.

[7] INSAG, "Basic safety principles for nuclear power plant, 75-INSAG-3 rev. 1," International Nuclear Safety Advisory Group Report INSAG-12, IAEA, 1999.

[8] U.S. DOE Nuclear Energy Research Advisory Committee and the Generation IV International Forum, "Crosscutting risk and safety R&D scope report," Tech. Rep. GIF-011-00, 2002.

[9] U.S. DOE Nuclear Energy Research Advisory Committee and the Generation IV International Forum, "Technology goals for generation IV nuclear energy systems," Tech. Rep. GIF-019-00, 2002.

[10] S. Nakanishi, T. Hosoya, S. Kubo et al., "Development of passive shutdown system for SFR," *Nuclear Technology*, vol. 170, no. 1, pp. 181–188, 2010.

[11] M. Takamatsu, T. Sekine, T. Aoyama, M. Uchida, and S. Kotake, "Demonstration of control rod holding stability of the self actuated shutdown system in Joyo for enhancement of fast reactor inherent safety," *Journal of Nuclear Science and Technology*, vol. 44, no. 3, pp. 511–517, 2007.

[12] H. Yamano, S. Kubo, K. I. Kurisaka, Y. Shimakawa, and H. Sago, "Technological feasibility of two-loop cooling system in jsfr," *Nuclear Technology*, vol. 170, no. 1, pp. 159–169, 2010.

[13] H. Niwa, S. Kubo, and K. Kurisaka, "LMFBR design and its evolution: (3) Safety system design of LMFBR," in *Proceedings of the International Conference on the Advanced Nuclear Power Plants and Global Environment (GENES4/ANP '03)*, vol. 1154, AESJ, Kyoto, Japan, September 2003.

[14] I. Sato, T. Asaga, M. Mizuno, and K. Yamamoto, "Understanding on fuel pin behavior under the slow TOP condition based on in-pile test results," in *Proceedings of the IAEA/IWGFR Technical Committee Meeting on Material-Coolant Interactions and Material Movement and Relocation in LMFR*, pp. 499–518, Ōarai, Japan, June 1994.

[15] H. Endo, S. Takahashi, M. Ishida, and T. Hoshi, "A Study of the initiating phase scenario of unprotected loss-of-flow in a 600MWe MOX homogeneous core," in *Proceedings of the IAEA/IWGFR Technical Committee Meeting on Material-Coolant Interactions and Material Movement and Relocation in LMFR*, pp. 297–307, IAEA, Ōarai, Japan, June 1994.

[16] I. Sato, H. Yamano, and Y. Tobita, "Development of severe accident evaluation technology (Level 2 PSA) for sodium-cooled fast reactors, (2) identification of dominant factors in initiating phase of unprotected events," in *Proceedings of the International Congress on Advances in Nuclear Power Plants (ICAPP '09)*, AESJ, Tokyo, Japan, May 2009, Paper no. 9132.

[17] H. Niwa, "A comprehensive approach of reactor safety research aiming at elimination of recriticality in CDA for commercialization of LMFBR," *Progress in Nuclear Energy*, vol. 32, no. 3-4, pp. 621–629, 1998.

[18] M. Naganuma, T. Ogawa, S. Ohki, T. Mizuno, and S. Kotake, "Minor actinide-bearing oxide fuel core design study for the JSFR," *Nuclear Technology*, vol. 170, no. 1, pp. 170–180, 2010.

[19] I. Sato, Y. Tobita, and K. Konishi, "Elimination of severe recriticality events in the core disruptive accident of JSFR aiming at in-vessel retention of the core materials," in *Proceedings of the International Conference on the Fast Reactors and Related Fuel Cycles (FR '09)*, IAEA-CN-176-03-23P, IAEA, Kyoto, Japan, December 2009.

[20] Y. Tobita,, K. Morita, K. Kawada, H. Niwa, and N. Nonaka, "Evaluation of CDA energetics in the prototype LMFBR with latest knowledge and tools," in *Proceedings of the 7th International Conference on Nuclear Engineering. (ICONE '99)*, vol. 7145, JSME, Tokyo, Japan,, April 1999.

[21] H. Endo, S. Kubo, S. Kotake et al., "Elimination of recriticality potential for the self-consistent nuclear energy system," *Progress in Nuclear Energy*, vol. 40, no. 3-4, pp. 577–586, 2002.

[22] Y. Tobita, H. Yamano, and I. Sato, "Analytical study on elimination of severe recriticalities in large scale LMFBRS with enhancement of fuel discharge," *Nuclear Engineering and Design*, vol. 238, no. 1, pp. 57–65, 2008.

[23] K. Konishi, J. I. Toyooka, K. Kamiyama et al., "The result of a wall failure in-pile experiment under the EAGLE project," *Nuclear Engineering and Design*, vol. 237, no. 22, pp. 2165–2174, 2007.

[24] K. Koyama, Y. Yamada, S. Hayakawa, M. Watanabe, and O. Watanabe, "Development of severe accident evaluation technology (level 2 PSA) for sodium-cooled fast reactors, (4) identification of dominant factors in core material relocation and heat removal phases," in *Proceedings of the International Congress on Advances in Nuclear Power Plants (ICAPP '09)*, Paper no. 9126, AESJ, Tokyo, Japan, May 2009.

[25] K. Kurisaka and S. Okamura, "Preliminary evaluation of JSFR achievement level to risk target," in *Proceedings of the 19th International Conference on Nuclear Engineering (ICONE '11)*, JSME, Osaka, Japan, October 2011, ICONE19-43802, Suspended Makuhari, Chiba, May 2011.

Hindawi Publishing Corporation
Science and Technology of Nuclear Installations
Volume 2012, Article ID 351809, 13 pages
doi:10.1155/2012/351809

Research Article

Study on Detailed Calculation and Experiment Methods of Neutronics, Fuel Materials, and Thermal Hydraulics for a Commercial Type Japanese Sodium-Cooled Fast Reactor

Toshikazu Takeda, W. F. G. van Rooijen, Katsuhisa Yamaguchi, Masayoshi Uno, Yuji Arita, and Hiroyasu Mochizuki

Research Institute of Nuclear Engineering, University of Fukui, 1-2-4 Kanawa-cho, Tsuruga-shi, Fukui 914-0055, Japan

Correspondence should be addressed to Toshikazu Takeda, t_takeda@u-fukui.ac.jp

Received 4 November 2011; Accepted 12 January 2012

Academic Editor: Massimo Salvatores

This paper discusses the objectives and results of a multiyear R&D project to improve the modeling accuracy for the detailed calculation of the Japanese Sodium-cooled Fast Reactor (JSFR), although the preliminary design of JSFR is prepared using conventional methods. For detailed design calculations, new methods are required because the JSFR has special features, which cannot be accurately modeled with existing codes. An example is the presence of an inner duct in the fuel assemblies. Therefore, we have developed new calculational and experimental methods in three areas: (1) for neutronics, we discuss the development of methods and codes to model advanced FBR fuel subassemblies, (2) for fuel materials, modeling and measurement of the thermal conductivity of annular fuel is discussed, and (3) for thermal hydraulics, we describe advances in modeling and calculational models for the intermediate heat exchanger and the calculational treatment of thermal stratification in the hot plenum of an FBR under low flow conditions. The new methods are discussed and the verification tests are described. In the validation test, measured data from the prototype FBR Monju is partly used.

1. Introduction

Many scenarios of possible energy futures foresee an important role for nuclear power. Acceptance of nuclear power with large-scale contributions to the world's energy mix depends on satisfaction of key drivers to enhance sustainability in terms of economy, safety, adequacy of natural resources, waste reduction, and nonproliferation. Fast reactors with recycle significantly enhance the sustainability indices. Therefore, due to their flexibility to produce new fissile material and/or to reduce the amount of waste and its impact on the environment, fast reactors are needed to make nuclear power a truly long term option.

Japan has a long track record of maintaining a commitment to fast reactor technology. Considerable efforts have been focused on innovative design approaches to achieve optimal safety, waste minimization, enhanced proliferation resistance, and economical competiveness. Studies carried out over the past decade [1, 2] have concluded that these objectives could be achieved. All types of fast reactor designs were considered, including advanced loop and pool configurations, various fuel types and coolants, and complete costs over the entire life cycle. The system chosen in Japan for detailed design is a sodium-cooled fast reactor known as the Japan Sodium-cooled Fast Reactor (JSFR), a two-loop, oxide-fueled system rated at an electrical output of 1,500 MW [3–5]. In Figures 1 and 2 are illustrated a 3D view of the plant arrangement and a schematic of the primary and secondary sodium loops. In this JSFR, technical innovations such as a large fuel assembly using large-diameter fuel pins stacked with annular pellets, an inner duct to discharge molten fuel during a hypothetical core destructive accident, and a tall steam generator using straight, double-wall heat transfer tubes are adopted [6].

Technological innovation in the fields of safety and reliability is the key for commercialization of fast reactor for

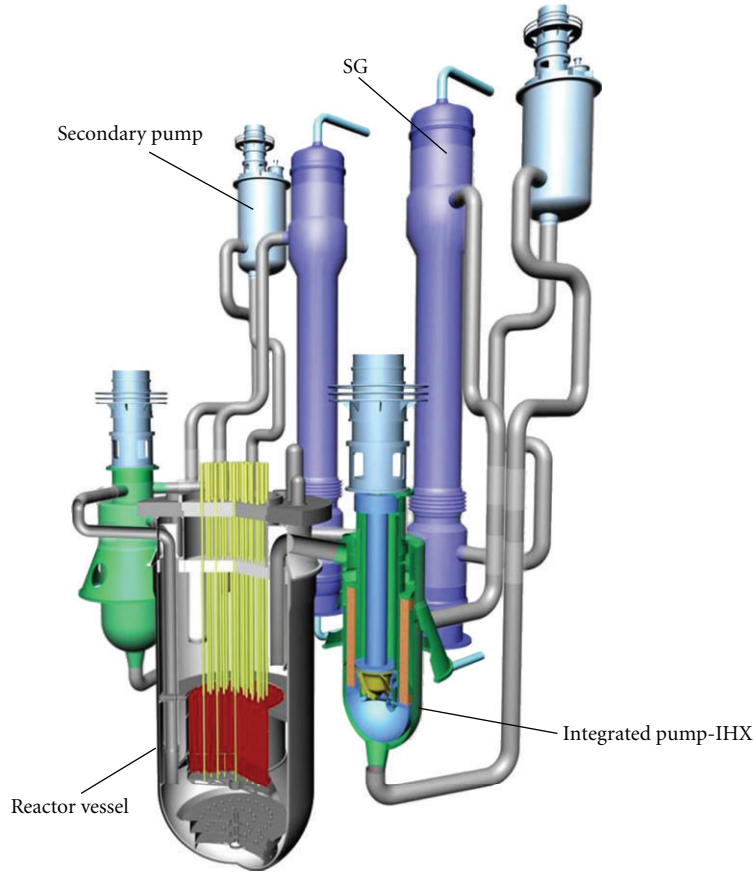

Figure 1: Schematic of JSFR-1500, showing the 2-loop arrangement with straight-tube heat exchangers, and with the primary pumps integrated into the Intermediate Heat Exchanger (IHX) (reproduced from [7]).

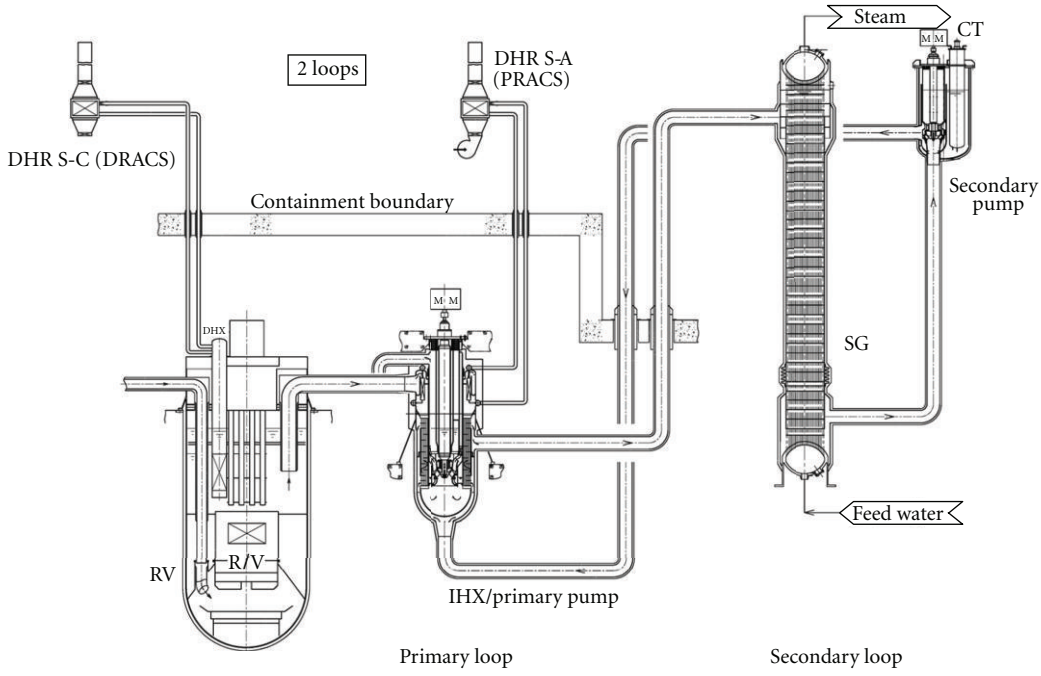

Figure 2: Primary and secondary circuits of JSFR-1500 (only 1 of 2 loops shown) (reproduced from [7]).

sustainable development. It is pursued in a wide range of scientific and technical area, including nuclear data, reactor physics, engineering design, and methods of validation and qualification.

Monju will produce a wealth of physics and performance as well as operational experience data. Efforts that make use of these data and provide the feedback needed to improve the designs of future fast reactors are a must. In particular, data and computer code Verification, Validation, and Uncertainty Qualification (V&V, UQ) with the help of theoretical and experimental studies will be most beneficial. In this paper, therefore, the development of calculation and experiment methods relevant to the reactor physics, fuel, and thermal hydraulics is described. Main focus is the application of the result to the design of an advanced commercial type sodium-cooled fast reactor.

To design the FBRs of the future, it is a requirement that one is able to calculate the physical characteristics accurately, that is, without the need of mock-up experiments. This requires advanced modeling tools. High-priority issues are the modeling of neutronics, fuel and structural materials, and thermal-hydraulics. In the present paper, these fields are introduced independently. However, in the future the models will be coupled to properly analyze and evaluate the overall behavior of the plant.

In the area of neutronics, the application of transport theory for full-core calculations requires accurate treatment of highly heterogeneous subassemblies. Therefore we are focusing on improvements of cell calculations: a hyperfine group treatment allows to explicitly treat all effects of cross-section resonances, while the use of advanced transport theory methods allows to explicitly treat highly heterogeneous subassemblies. In the area of fuel materials, we are focusing on the accurate modeling of advanced fuels in which particles are dispersed to improve material properties, especially the thermal conductivity. Furthermore, we are developing measurement technology for the pre- and postirradiation analysis of fuel pellets. Finally, in the area of thermal-hydraulics we are targeting several long-standing issues, that is, the poorly understood degradation of heat exchange in the Intermediate Heat Exchanger under low flow conditions, as well as the accurate 3D simulation of the temperature field in the hot plenum above the core from the standpoint of maintenance, reliability, component lifetime, and safety.

2. Neutronics Calculation Methods

The calculation methods for the commercial type Fast Breeder Reactor (FBR) have been developed based on deterministic methods. As the nuclear data we selected the JENDL-4.0 nuclear data set (Japan Evaluated Nuclear Data Library v4.0) since the core performance parameters of various fast reactor cores and critical assemblies calculated with JENDL-4.0 are closer to the measured data than the results of JENDL-3.3. Figure 3 shows the ratio of calculation to measurement (C/E ratio) of k_{eff} of several fast systems, comparing JENDL-3.3 and JENDL-4.0. In particular, JENDL-4.0 improves the underestimation of k_{eff} for uranium-fueled cores compared to

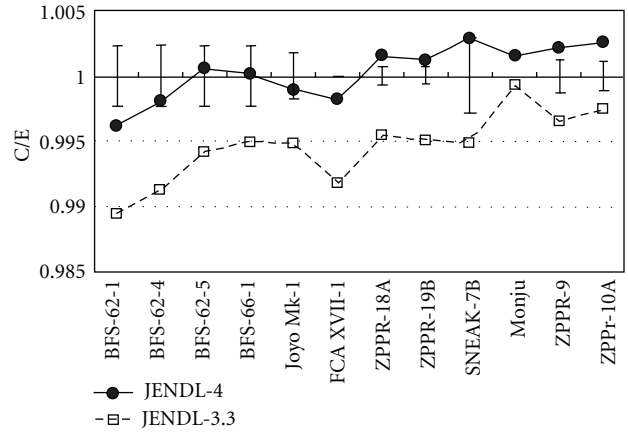

Figure 3: Comparison of the C/E ratio for k_{eff}, using JENDL-3.3 and JENDL-4.0 for several fast systems (reproduced from [8]). Vertical bars indicate experimental uncertainties. BFS: critical facility at IPPE (Russia, [9]); FCA: Fast Critical Assembly at JAEA Tokai; ZPPR: Zero Power Plutonium Reactor at Idaho National Lab, SNEAK: Schnelle Null-Energie-Anordnung Karlsruhe (Fast Zero-Power Facility Karlsruhe, Germany).

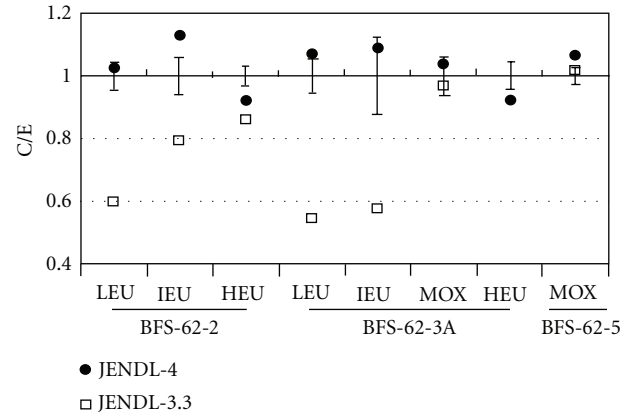

Figure 4: Prediction of SVR with JENDL-3.3 and JENDL-4.0 for several configurations of the BFS facility in IPPE (Russia [9]) (Reproduced from [8]). Vertical bars represent experimental uncertainties. HEU/IEU/LEU: High/Intermediate/Low Enriched Uranium; MOX: Mixed Oxide, that is, uranium–plutonium oxide fuel.

JENDL-3.3 (results of the BFS facility in Figure 3). Figure 4 shows the improvement of the prediction of the Sodium Void Reactivity (SVR) by JENDL-4.0 compared to JENDL-3.3 for several uranium-fueled configurations of the BFS facility. The prediction of the SVR is considerably improved. For other critical assemblies (e.g., ZPPR and SEFOR), a small improvement was found.

To obtain effective groupwise cross sections, the SLAROM-UF code has been selected. (SLAROM is a lattice analysis code developed by JAEA; UF stands for UltraFine.) Traditionally in Japan, effective cross-sections are calculated in 70 energy groups with the SLAROM and SRAC codes, using equivalence theory with a Dancoff factor (Standard Reactor Analysis Code, a modular code system for thermal reactor

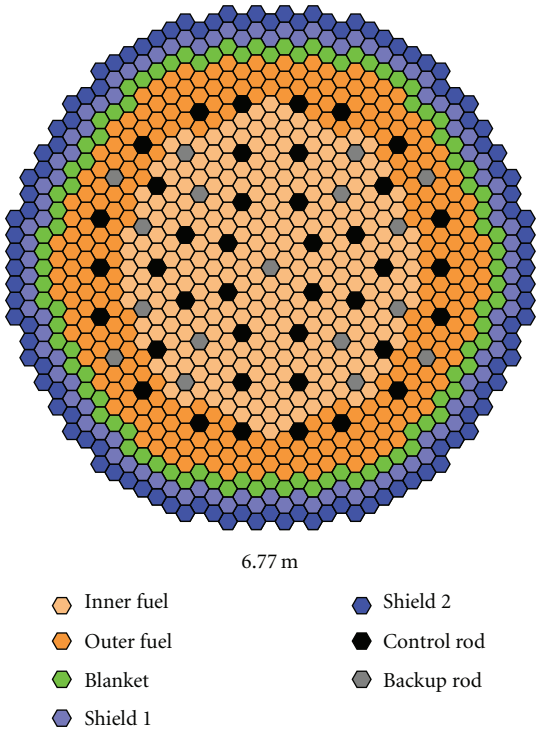

Figure 5: Core map of JSFR-1500 [6].

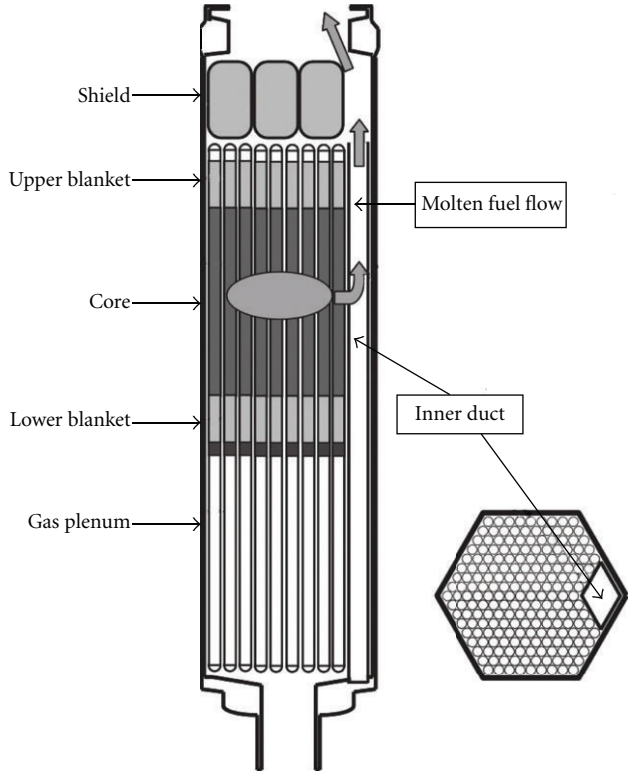

Figure 6: JSFR fuel assembly with internal duct (so-called modified FAIDUS concept, FAIDUS: Fuel Assembly with Inner DUct Structure) [13].

analysis developed by JAEA). In this kind of calculation, the problem-specific composition and geometry can only be taken into account partially, because the group cross-sections are calculated with a fixed neutron energy spectrum (weight flux) rather than a full problem-dependent neutron energy spectrum. Mutual self-shielding effects are also neglected.

The SLAROM-UF code has been developed by JAERI [10, 11] to treat ultrafine energy groups, using up to a hundred thousand groups below 50 keV. (JAERI: Japan Atomic Energy Research Institute, one of the predecessors of the present JAEA, Japan Atomic Energy Agency). The use of ultrafine energy groups leads to an improvement not only for the criticality calculations but also for the SVR [9, 12].

The commercial-size JSFR is a 1,500 MWe fast reactor with a core of 6.77 m diameter and 1.5 m height, as shown in Figures 5 and 6. In the case of a severe accident in a traditionally designed core the molten fuel may accumulate in some part of the core, and cause a recriticality. To prevent the occurrence of recriticality, there is an inner duct installed in each fuel assembly. In case of accidents, the molten fuel flows upward through the inner duct, and a recriticality is prevented.

Thus the JSFR fuel assembly has a complicated form, and the accurate description of the assembly should be taken into account when calculating assembly averaged cross-sections. To calculate the homogenized cross-sections, the Method of Characteristics (MOC) has been used because the complex geometry can be taken into account accurately. The effects of heterogeneities on the assembly-averaged cross-sections are taken into account by the MOC calculation.

For ultrafine group calculations, the modeling options in SLAROM-UF are limited to one spatial dimension (1D): the presence of the inner duct cannot be treated. For this reason, it was chosen to incorporate the BACH code (Beneficial Advanced Characteristics code for Hexagonal geometry [14]), a 2D MOC code for hexagonal geometry. In the new system, SLAROM-UF acts as a cross-section production module, producing effective cross-sections in a 70-group structure, while BACH is used to determine an accurate flux distribution and cross sections to be used in the core calculations (see Figure 7; more information about the codes mentioned in the figure is given later).

In order to verify the accuracy of the BACH code, we have compared the k_{eff} values and the intra-assembly reaction rate distributions. Figures 8 and 9 compare the U-238 capture rate distributions, calculated by the BACH code and the continuous-energy Monte-Carlo code MVP, in a fuel assembly of Monju and in a JSFR assembly, respectively. Good agreement is found for both assemblies, which shows the accuracy of the BACH code. In Figure 8, the fuel pins have been grouped into three groups labeled A, B, and C. This grouping is introduced to take into account the differences in self-shielding. The influence of the wrapper tube and the interassembly sodium is small for pins in group A, but larger for pins in groups B and C. Therefore, three sets of multigroup cross-sections were calculated representing three different levels of self-shielding.

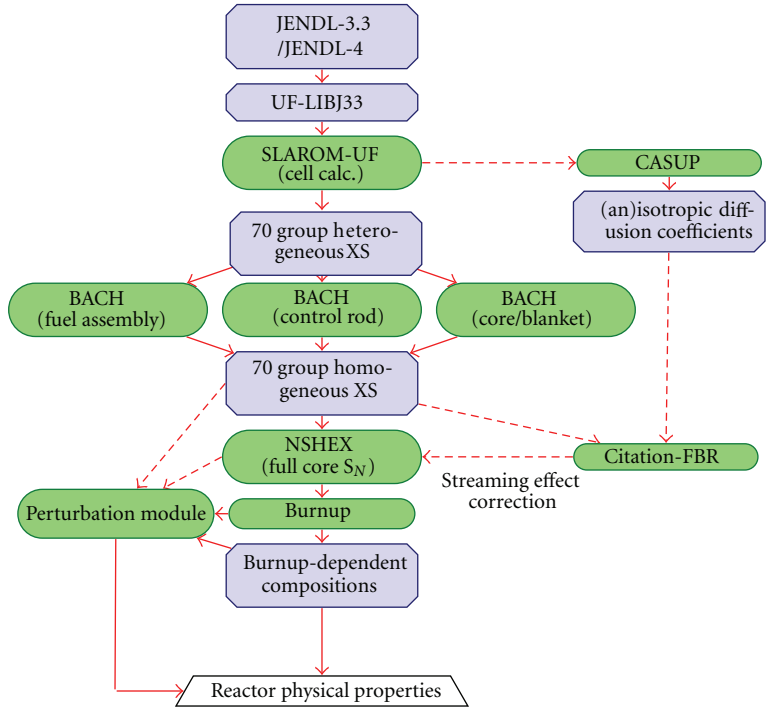

Figure 7: Flow chart of a reactor physics calculation.

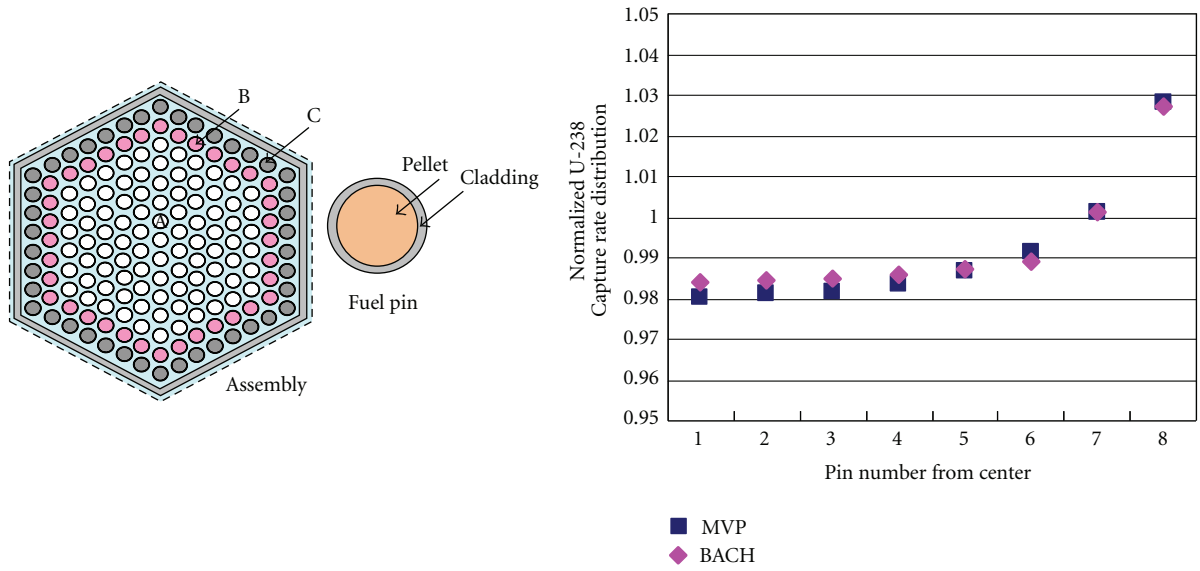

Figure 8: U-238 Capture Rate Distribution in a Monju fuel assembly. Fuel pins are grouped into three groups (A, B, and C) to take into account the difference in self-shielding between fully surrounded fuel pins and fuel pins near the wrapper tube and interassembly sodium channel.

By default, assembly averaged cross sections are calculated assuming an infinite lattice of repeating assemblies. For special assemblies, such as control rod assemblies, color set calculations are used, as shown in Figure 10.

After the preparation of homogenized cross sections, core calculations are performed with transport theory. The code NSHEX is a nodal Sn transport code, described in more detail in [15]. It is capable of treating Hexagonal-Z geometry with several options for the nodal expansion order and Sn quadrature sets. In this figure the diffusion code CITATION-FBR also appears. (An improved version for FBR applications of the traditional diffusion code CITATION; CITATION-FBR is developed by JAEA). This code is used in triangular-Z geometry. CITATION-FBR is capable of using anisotropic diffusion coefficients. This allows one to take into account effects of anisotropy in the case of a voided lattice, and so forth.

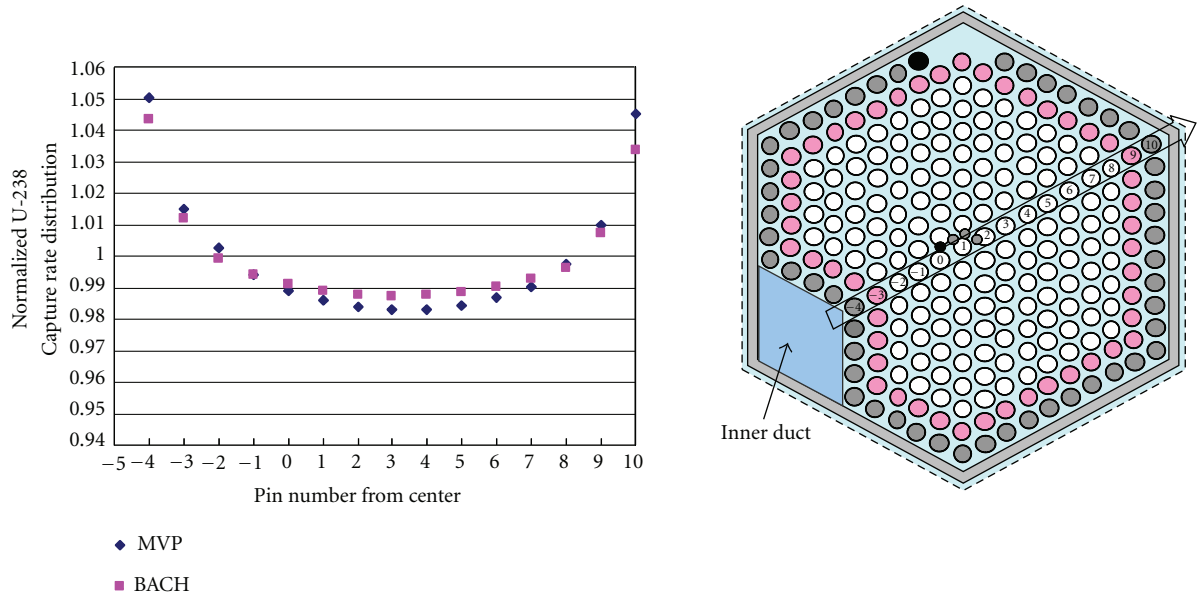

Figure 9: U-238 Capture Rate Distribution in a JSFR fuel assembly. Fuel assemblies are grouped into three groups to take into account the influence of the wrapper tube and sodium channels on the self-shielding.

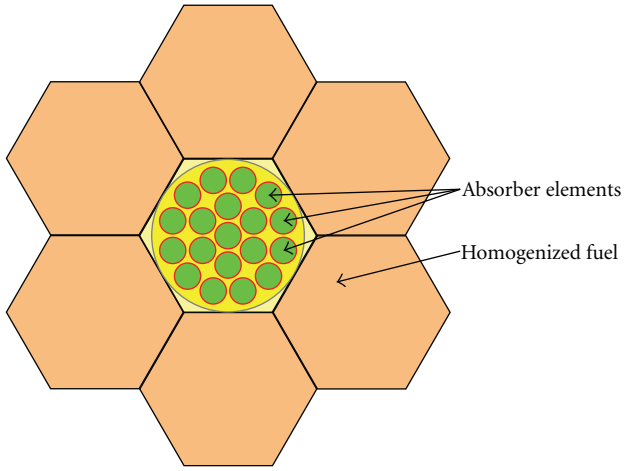

Figure 10: Color set calculation.

The code NSHEX can only treat isotropic scatter, while of course the angular flux in NSHEX can be anisotropic.

3. Calculation and Experiment Methods for Fuel

3.1. Calculation of the Thermal Conductivity of Particle Dispersing Fuels. The thermal conductivity of nuclear fuels is one of the most important properties concerning reactor safety. The Japanese code CEDAR [16] estimates the behavior of fast reactor fuels during irradiation using the thermal conductivity in addition to other material properties. In fast reactors, the centerline temperature of MOX fuel pellets increases up to the melting temperature of the MOX and a hole appears in the central part of the pellet early in the irradiation period. This is caused by the high heat flux and low thermal conductivity of the MOX fuel matrix [17–19]. The high heat flux combined with a steep temperature gradient has other effects, including the formation of cracks, redistribution of Fission Product (FP) and Trans-Uranium (TRU) atoms, the formation of precipitates of fuel and FP atoms in the middle part of the pellet, and the formation of a so-called Joint Oxide Gaine (JOG) at the pellet-clad interface. To improve the thermal conductivity, it has been proposed to disperse particles with a high thermal conductivity in the MOX matrix. In a previous study a Gd_2O_3-dispersed UO_2 fuel was proposed to improve the thermal conductivity of UO_2 pellets [20]. LWR fuel additives have many restrictions from the viewpoint of the capture of thermal neutrons; however, for FRs there are less limitations concerning additives, since the capture cross section of the concerned isotopes usually decreases with increasing neutron energy. In the present study, we investigated dispersion parameters such as particle size, shape, and concentration, in an effort to improve the thermal conductivity of the MOX fuel pellet in the early stages of irradiation. The particles are assumed to be randomly distributed. The effect of the dispersed particles after long irradiation is being investigated.

3.1.1. Calculation Procedure. The radial temperature distributions in pellets with dispersed particles were calculated using a FEM-based approach. The general FEM analysis for temperature distributions requires the solution of thermal transfer equations by considering several factors such as thermal diffusivity, heat capacity, material density, and heat generation [21].

In this study, systems containing distributed spherical particles, needle-like particles, and flat particles within the matrix were considered (see Figure 11). The MOX pellets are 10 mm in diameter and 10 mm in height. The dispersed

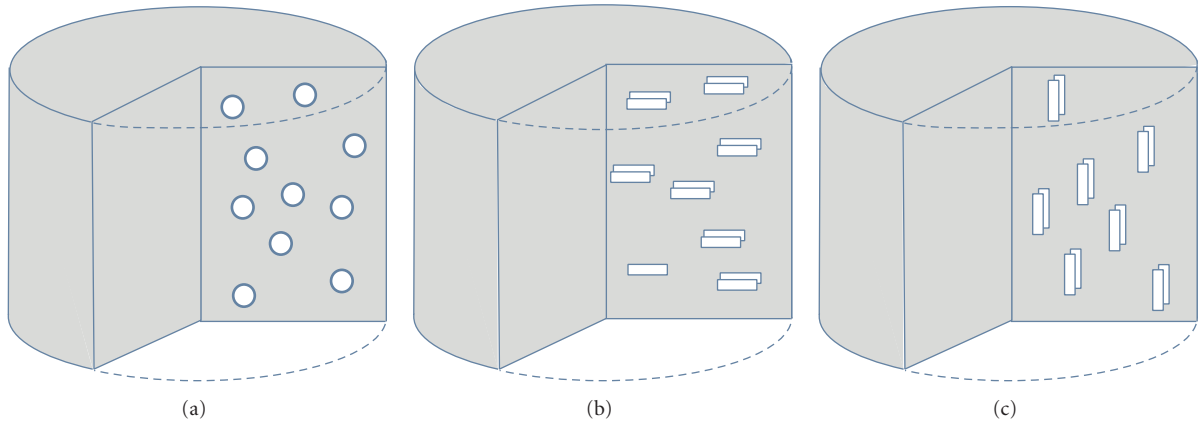

Figure 11: Dispersed particle shapes in the pellet matrix: (a) spherical balls, (b) needles, and (c) flat plates.

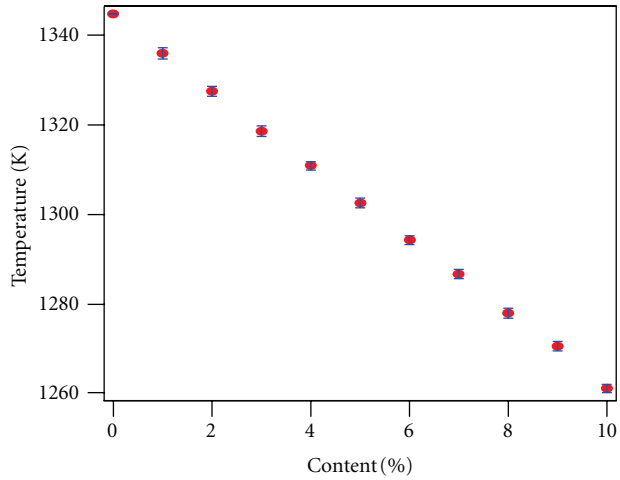

Figure 12: Centerline temperature as a function of particle content (spherical particles, 100 μm in diameter).

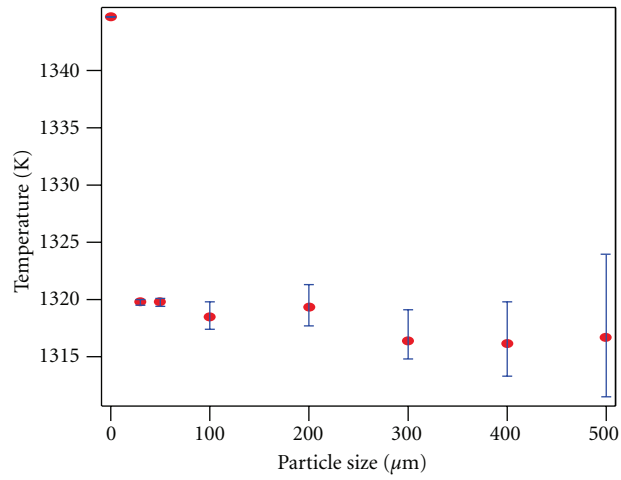

Figure 13: Centerline temperature as a function of the diameter of the spherical particles (3 vol% content).

particles are spherical balls of 30–500 μm in diameter, needles of $100 \times 100 \times 500\,\mu$m in dimension, and flat plates of $500 \times 500 \times 100\,\mu$m. The heat source for the MOX matrix and the external temperature of the pellet was fixed for the calculations. In the present study it is assumed that the thermal conductivity of the dispersed particles is ten times higher than that of the MOX matrix [17–19].

3.1.2. Results and Discussion. For the spherical particles the dependence of the pellet centerline temperature on the concentration of the particles was analyzed. Figure 12 shows the centerline temperature for pellets with a particle content ranging from 0 to 10 vol%. The centerline temperature decreases linearly with particle content. From this result the centerline temperature is effectively decreased by increasing the amount of dispersed particles. The amount to be used will be determined by the required performance of the fuel pellet.

The dependence of the centerline temperature on the size of the particles was investigated using a dispersion of spherical balls with diameters ranging from 30 to 500 μm. The result is illustrated in Figure 13, which shows the results for a total amount of dispersed particles of 3 vol%. At this volume fraction of particles, the pellet centerline temperature is more or less constant as a function of the size of the particles. This means that the contribution to the overall heat transfer of the pellet is determined by the volume fraction of the dispersed particles. However, the temperature distribution becomes less smooth as the diameter of a particle increases. As seen in Figure 14, the region near the particles has a low temperature and the area far from particles has a high temperature. Therefore, to minimize thermal stress and retain the integrity of the pellet, the size of dispersed particles must not be too large and 100 μm or less is recommended.

The centerline temperatures of pellets with dispersed spherical balls, needles, or flat plates were calculated. The differences in the centerline temperature upon the addition of spherical balls, needles, and plates were small. For the formation of particles, spherical dispersed particles are recommended.

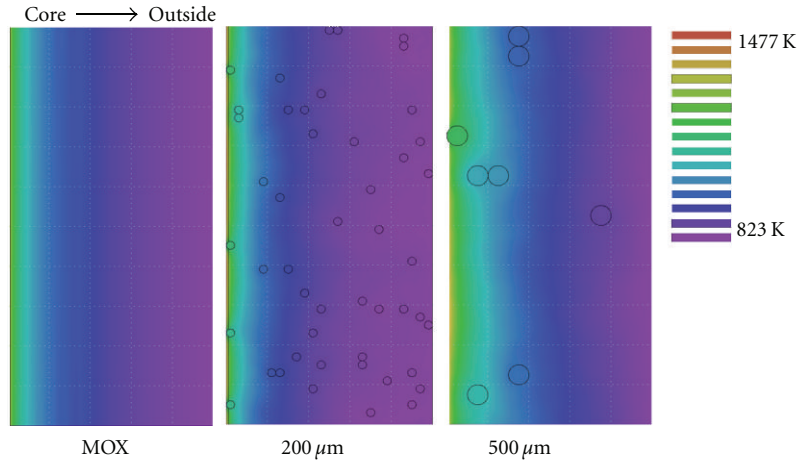

Figure 14: Temperature distribution inside a pellet cross with different sizes of the spherical dispersed particles (3 vol% content).

3.2. Measurement of the Thermal Conductivity of the Annular Pellet. The current fast reactor fuel pellet has a low smear density but the pellets to be used in a demonstration reactor will be annular with a high density. It is difficult to measure the thermal conductivity of an annular pellet with a thermal diffusivity measurement with a conventional laser flash method. The method is especially problematic in a hot cell, since it requires a disk-shaped sample with a surface cross section of 1 or 2 cm^2 and a thickness of about 1 or 2 mm. It is very difficult to prepare such samples for measurement from irradiated annular pellets. In the present study, the thermal conductivity of an annular pellet was measured using the hot disk method.

The hot disk method is one of the transient plane source methods developed by Gustavsson [21]. In this method, a flat sensor is placed between the plane surfaces of two measurement samples. The sensor is made of Kapton and uses embedded double spiral wires made of Ni. One of the wires is used to heat the sample and the other is used to measure the temperature of the sample. The temperature change is inferred from the change of the electrical resistance of one of the Ni wires, while the other wire provides a constant power supply. By analyzing the temperature change, the values of thermal conductivity and the heat capacity of the samples are obtained simultaneously. The merit of this method is that it provides a rapid and simultaneous measurement. The demerit is that it requires two samples, and the difficulty of high temperature measurements caused by the instability of the coated materials of the sensor. Sensors for liquid samples and large solid samples with hypothetically infinite axial dimensions have been developed, but a sensor for annular pellets has not yet been developed. The research presented here targets the development of a hot disk sensor for annular pellets.

3.2.1. Experimental Method. Simulated annular pellets of CeO_2 with an outside diameter of 8 mm and a central hole with a diameter of 2 mm were made using the SPS (Spark Plasma Sintering) method. After the SPS step, the sample was heated in air at 1873 K for 20 hours in order to compensate the reduction during the SPS step. Solid CeO_2 pellets were also made, and their thermal conductivity was measured using the hot disk method using a conventional sensor. For comparison, measurements were also made using the laser flash method. In the laser flash method, the thermal diffusivity of the sample was measured with the laser flash apparatus and the thermal conductivity was estimated from the following:

$$\lambda = \alpha \cdot C_P \cdot \rho, \tag{1}$$

where λ is the thermal conductivity, α is the thermal diffusivity, C_p is the heat capacity, and ρ is the density.

A hot disk sensor for annular pellets was developed. The sensor has two spiral Ni wires of 7.5 mm diameter with a central hole of 2 mm diameter as shown in Figure 15(a). After the surface of the samples was polished, the sensor was placed between two CeO_2 samples during the measurement as shown in Figure 15(b).

3.2.2. Results and Discussion. Table 1 shows the thermal conductivity of the samples measured with various methods as well as the literature value for comparison [22]. Since the thermal conductivity depends on the porosity of the sample, the measured values were normalized to those for 100% theoretical density (TD) using the Maxwell-Eucken equation [23]:

$$\lambda_P = \lambda_0(1 - P)/(1 + P\beta), \quad \beta = 0.5, \tag{2}$$

where λ_p is the thermal conductivity of porosity P ($= 1 - I/100$), and λ_0 is the thermal conductivity of the material at 100% TD.

Although all normalized values are a little lower than the literature values, the value of the thermal conductivity of the annular pellet obtained by the hot disk method using the annular sensor agrees well with those of normal pellets obtained by the hot disk method using a conventional sensor and by the laser flash method. This agreement shows the accuracy of

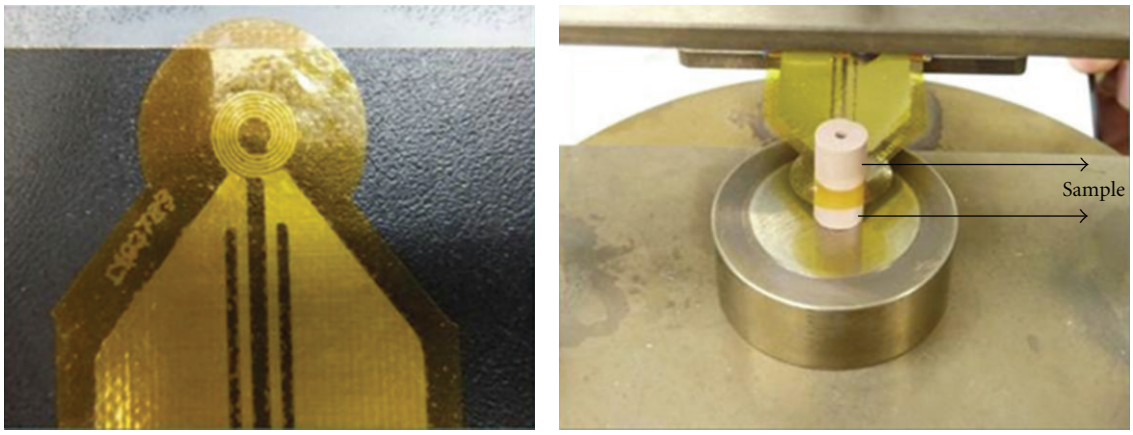

(a) (b)

Figure 15: (a) Hot disk sensor for annular pellets and (b) measurement of the CeO_2 annular pellets with the sensor.

Table 1: Thermal conductivity of CeO_2 pellets measured with several measurement methods.

Sample configuration Density method	Annular 89% TD hot disk method with the annular sensor	Normal 83% TD hot disk method with the normal sensor	Normal 83% TD laser flash method	Literature value (100%TD)
Thermal conductivity (W/mK) (as measured)	9.60	8.66	8.60	
Thermal conductivity (W/mK) (normalized to 100% TD)	11.4	11.3	11.2	12.6

the hot disk method with an annular sensor. As this method does not require cutting of the pellets, this method can be applied to the measurement of irradiated annular pellets in a hot cell.

4. Thermal Hydraulics

In order to apply the state-of-the-art technology in the area of thermal hydraulics to the design of the next generation reactor, thermal hydraulic calculations with CFD codes (Computational Fluid Dynamics) are used from the standpoint of V&V with Monju data; especially, calculations inside of the Intermediate Heat Exchanger (IHX) and the thermal stratification in the upper plenum are targeted. These are common key issues for the design of large sodium-cooled reactors. Since the IHX has a complex configuration with thousands of heat transfer tubes, the precise 3D calculation is very difficult. Heat exchange in the IHX under low flow conditions has been found to be difficult to predict. Thermal stratification should also be evaluated under low flow rate conditions (e.g., natural circulation).

4.1. Modeling of the IHX. The IHX of Monju is illustrated in Figure 16. The primary sodium enters the shell from a nozzle about halfway up the axial length of the IHX and flows upward in an annular space between the shell and the inner shroud. One flow window is provided in each 60-degree sector. High-temperature sodium should be distributed equally to these windows. For this reason, a flow distribution mechanism consisting of many small holes is provided about half-way up between the nozzle and the flow windows, as illustrated in Figure 17. The flow rate distribution through the different window positions is shown in Figure 18. Because of the distribution of the flow holes over the annulus, the flow distribution is almost uniform over a wide range of flow rates. After entering through the flow window, the sodium flows downward exchanging heat between the primary and the secondary side. There are more than 3000 heat transfer tubes, supported by 7 rectifying plates and 2 tube sheets. Therefore, there are 8 "steps" of the heat transfer regions in the IHX. The rectifying plate has holes through which the heat transfer tubes pass, as well as holes for the sodium flow.

Because of the aforementioned configuration, a CFD mesh of the whole IHX is very difficult. Therefore, a 1/6 sector model is discussed. The whole shell and two of the heat transfer regions are modeled based on the design. Calculations are performed to confirm the flow distribution in the heat transfer regions. The result of the calculation indicates that the primary sodium distribution is almost uniform.

The calculated result of one 60-degree sector with heat transfer tubes is shown in Figure 19. It is seen that the flow on the primary side of the IHX is rather uniform in low flow conditions. The next step is a corresponding calculation taking into account the heat transfer between the primary and the secondary side. This work is presently ongoing.

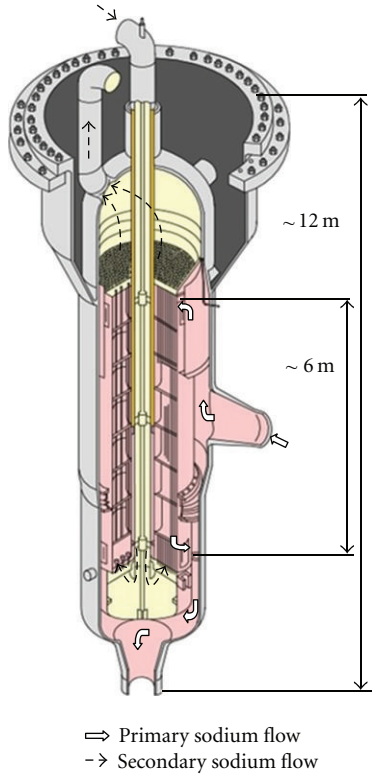

Figure 16: Schematic of the IHX of Monju.

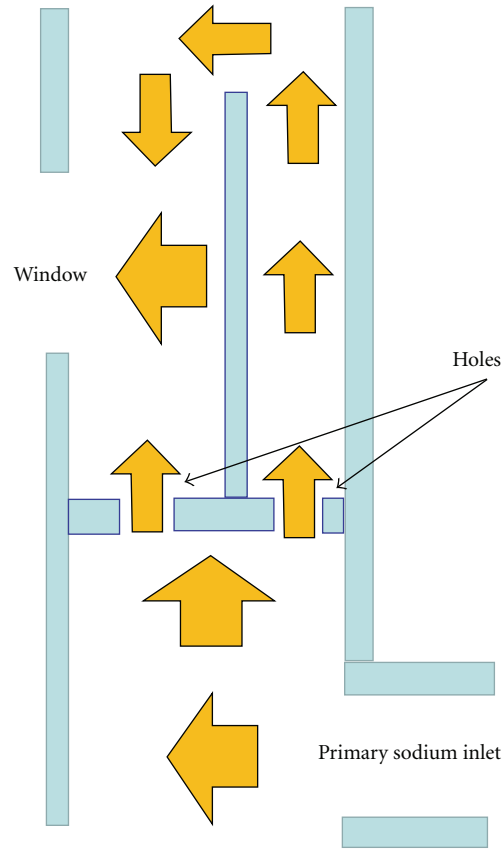

Figure 17: Flow distribution mechanism in the annulus of the IHX vessel.

4.2. Thermal Stratification Calculation in the Upper Plenum. The analysis of the occurrence of thermal stratification in the upper plenum of the Monju reactor is the subject of a Coordinated Research Program (CRP) organized by the IAEA. Temperature distributions in the upper plenum of the reactor vessel were measured at Monju when the plant was scrammed from a partial load condition during a turbine trip test at 40% of nominal electrical output (45% of nominal thermal output). The primary heat transport system (HTS) and the secondary HTS were cooled by the forced circulation after the reactor trip with small capacity motors, so-called pony motors. The flow rates in the three primary and secondary HTSs decreased to approximately 1/10 of the full power conditions. This test and its results are summarized in the report by Yoshikawa and Minami [23] as a document of the IAEA CRP.

There are two problems in the IAEA CRP benchmark. One is the total flow rate from the core to the upper plenum. The other problem is configuration of the flow-holes provided on the inner shroud in the reactor vessel. The total flow rate from each group of subassemblies specified in the IAEA benchmark calculation is approximately 97% of the measured flow rate at the Monju plant. This discrepancy was identified when the test data by Miyakawa [24] was investigated. The outlet temperatures from each group of subassemblies in the IAEA benchmark are measured, except for the shielding subassemblies, for which calculated temperatures are used. Therefore, the boundary conditions for the IAEA benchmark are somewhat hybrid (combination of calculated and measured data). The total amount of energy input into the upper plenum is underestimated if the total flow rate does not include the bypass flow rate. There is a possibility that this may be caused by the boundary conditions of flow rate and temperature, which are different from the actual situation.

In order to maintain consistency of the boundary conditions from the point of view of the amount of energy transferred into the upper plenum, a 1D analysis has been conducted using the NETFLOW++ code developed by Mochizuki [25]. NETFLOW++ was used to calculate the outlet flow rates and temperatures of all the assemblies in the core. This data was then used in a 3D CFD analysis of the hot plenum. The calculation was conducted using ANSYS FLUENT 12.0 [26]. The calculational mesh is shown in Figure 20, taking into account almost all internals of the Monju reactor and the configuration of the flow holes. Since the precise roundness of the edges of the flow-holes is not known, a rounded edge with a radius of 20 mm (R20) is assumed in the present study. The friction factor of a rounded flow hole saturates above a given roundness. Thus, it is expected that the calculated result is not very sensitive to the actual roundness of the flow holes. In earlier work, Mochizuki et al. [27] assumed that the flow-holes had a chamfered configuration. It was shown that the presence of chamfer has a considerable effect on the temperature distribution in the hot plenum.

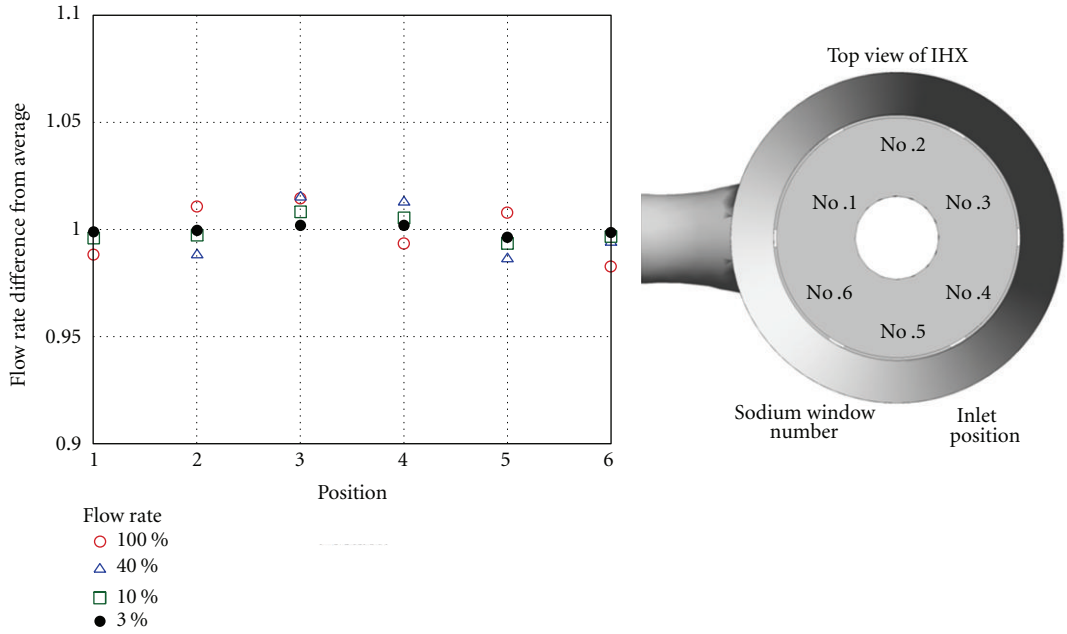

Figure 18: Flow rate distribution at the different window positions.

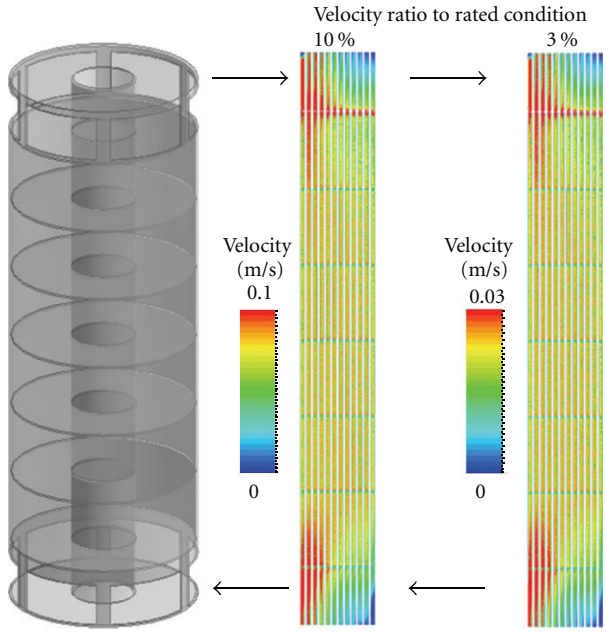

Figure 19: Flow pattern on the primary side of the shell of IHX.

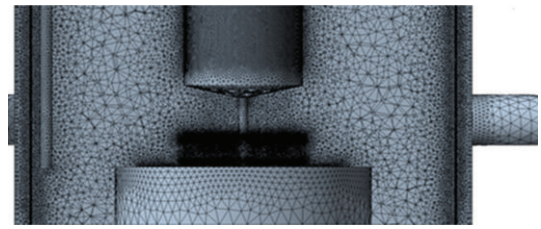

Figure 20: Tetrahedral mesh configuration in the plenum (25 million).

Table 2: Movement of the thermal stratification interface between measurement and calculation.

Elapsed time (sec)	Measured result (m)	Analytical result (m)
60	−5.38	−5.43
120	−4.82	−4.86
180	−4.51	−4.46
240	−4.37	−4.32
420	−4.09	−4.06
600	−4.06	−3.99

Figure 21 illustrates the behavior of the thermal stratification interface during the first 10 minutes of the transient. The temperature is distributed in three layers, that is, a low-temperature layer, a mixing layer, and a high-temperature layer. Although there are some parts where the temperature distribution does not completely match with the measured result, good agreement has been obtained in general. The thermal stratification interface is defined as the surface between material regions at different temperatures (the low temperature area below the interface and the mixing area above the interface). This interface moves up during the transient. A comparison of the elevation of the thermal stratification interface between calculation and measurement is shown in Table 2. As expected from the results in Figure 20, the movement of the thermal stratification interface is well predicted by the CFD model.

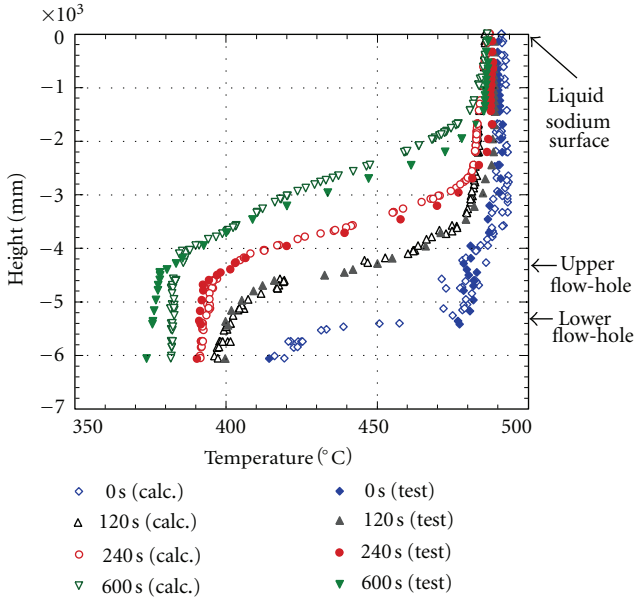

Figure 21: Comparison between measured results and calculation taking into account the flow-hole with rounded edge, heat capacity of UIS, and boundary conditions at the outlet of the subassemblies.

5. Conclusion

In this paper, we have given an overview of recent development work on calculational and experimental methods to support the design and analysis of the commercial size (Japanese) Sodium-cooled Fast Reactor (JSFR). This reactor has unique design features, and new methods have been developed to enable highly accurate modeling of JSFR. In the area of neutronics, methods have been devised to treat the complex fuel subassemblies, based on a hyper-fine group calculation for self-shielding and MOC for geometrical treatment. Modeling has been improved for particle dispersion MOX pellets, and for annular pellets, a special annular sensor has been developed to measure the thermal conductivity with a hot disk method. In the area of thermal hydraulics, calculation accuracy of difficult problems, for example, the intermediate heat exchanger and thermal stratification in the hot plenum under low flow conditions, has been improved by the combined use of 1D and 3D CFD models. In all cases, the trade-off between modeling accuracy and practical usability has been optimized. At present, Verification, Validation, and Uncertainty Qualification of all proposed methods is on-going, using measurement data from the prototype FBR Monju.

Acknowledgment

The presented work is the result of a part of the "Core R&D program for commercialization of the fast breeder reactor using Monju data," entrusted to the University of Fukui by the Ministry of Education, Culture, Sports, Science and Technology of Japan (MEXT).

References

[1] K. Aizawa, "R&D for fast reactor fuel cycle technologies in JNC," in *Proceedings of the Advanced Nuclear Fuel Cycles and Systems (GLOBAL '01)*, vol. 050, Paris, France, September 2001.

[2] K. Ito and T. Yanagisawa, "Last twenty years experiences with fast reactor in Japan," in *Proceedings of the International Conference on Fast Reactors and Related Fuel Cycles*, Kyoto, Japan, December 2009.

[3] Y. Chikazawa, S. Kotake, and S. Sawada, "Comparison of pool/loop configurations in the JAEA feasibility study 1999–2006," in *Proceedings of the International Conference on Fast Reactors and Related Fuel Cycles*, Kyoto, Japan, December 2009.

[4] Y. Sagayama, "Launch of fast reactor cycle technology development project in Japan," in *Proceedings of the Advanced Nuclear Fuel Cycles and Systems (GLOBAL '07)*, pp. 251–258, Boise, Idaho, USA, September 2007.

[5] H. Funasaka and M. Itoh, "Perspective and current status on fuel cycle system of Fast Reactor Cycle Technology development (FaCT) project in Japan," in *Proceedings of the Advanced Nuclear Fuel Cycles and Systems (GLOBAL '07)*, pp. 259–267, Boise, Idaho, USA, September 2007.

[6] K. Aoto, Y. Chikazawa, S. Kotake, and T. Ito, "Status of JSFR development in phase I FaCT project," in *Proceedings of the International Conference on Advanced Nuclear Fuel Cycles and Systems (GLOBAL '11)*, Makuhari, Japan, December 2011, Paper no. 471611.

[7] A. E. Waltar, D. R. Todd, and P. V. Tsvetkov, *Fast Spectrum Reactors*, Appendix C., Springer, 2011.

[8] G. Chiba, K. Okumura, K. Sugino et al., "JENDL-4.0 benchmarking for fission reactor applications," *Journal of Nuclear Science and Technology*, vol. 48, no. 2, pp. 172–187, 2011.

[9] T. Hazama, A. Shono, and K. Sugino, "Verification of a nuclear analysis system for fast reactors using BFS-62 critical experiment," *Journal of Nuclear Science and Technology*, vol. 41, no. 12, pp. 1145–1154, 2004.

[10] T. Hazama, G. Chiba, W. Sato, and K. Numata, "SLAROM-UF: Ultra Fine Group Cell Calculation Code for Fast Reactor—Version 20090113," JAEA-Review 2009-003, 2009.

[11] T. Hazama, G. Chiba, and K. Sugino, "Development of a fine and ultra-fine group cell calculation code SLAROM-UF for fast reactor analyses," *Journal of Nuclear Science and Technology*, vol. 43, no. 8, pp. 908–918, 2006.

[12] K. Aoto, N. Uto, Y. Sakamoto, T. Ito, M. Toda, and S. Kotake, "Design study and R&D progress on Japan sodium-cooled fast reactor," *Journal of Nuclear Science and Technology*, vol. 48, no. 4, pp. 463–471, 2011.

[13] T. Takeda, H. Imai, T. Kitada, H. Nishi, J. Ishibashi, and A. Kitano, "Development of 3-D detailed FBR core calculation method based on method of characteristics," in *Proceedings of the International Confernce Mathematics and Computation, Supercomputing, Reactor Physics and Nuclear & Biological Applications*, Avignon, France, September 2005.

[14] K. Sugino and T. Kugo, "Effect of polynomial expansion order of intranode flux treatment in nodal S_N transport calculation code NSHEX for large-size fast power reactor core analysis," *Journal of Nuclear Science and Technology*, vol. 48, no. 3, pp. 421–428, 2011.

[15] T. Mizuno and S. Shikakura, "Development of the fast reactor fuel performance code CEDAR," *PNC Technical Review*, no. 76, pp. 37–44, 1990 (Japanese), http://jolissrch-inter.tokai-sc.jaea.go.jp/pdfdata/PNC-TN1340-90-004.pdf.

[16] A. B. G. Washington, "UK atomic energy authority," Tech. Rep. TRG R-2236, 1973.

[17] Y. Philipponneau, "Thermal conductivity of (U, Pu)O_{2-x} mixed oxide fuel," *Journal of Nuclear Materials*, vol. 188, pp. 194–197, 1992.

[18] C. Duriez, J. P. Alessandri, T. Gervais, and Y. Philipponneau, "Thermal conductivity of hypostoichiometric low Pu content (U,Pu)O_{2-x} mixed oxide," *Journal of Nuclear Materials*, vol. 277, no. 2-3, pp. 143–158, 2000.

[19] K. Iwasaki, T. Matsui, K. Yanai et al., "Effect of Gd_2O_3 dispersion on the thermal conductivity of UO_2," *Journal of Nuclear Science and Technology*, vol. 46, no. 7, pp. 673–676, 2009.

[20] S. Humphries, *Field Solutions on Computers*, CRC Press, Boca Raton, Mass, USA, 1997.

[21] S. E. Gustavsson, "Transient plane source techniques for thermal conductivity and thermal diffusivity measurements of solid materials," *Review of Scientific Instruments*, vol. 62, no. 3, pp. 797–804, 1991.

[22] R. W. Rice, *Porosity of Ceramics*, Marcel Dekker, New York, NY, USA, 1998.

[23] S. Yoshikawa and M. Minami, *Data Description for Coordinated Research Project on Benchmark Analyses of Sodium Natural Convection in the Upper Plenum of the Monju Reactor Vessel under Supervisory of Technical Working Group on Fast Reactors, International Atomic Energy Agency*, Japan Atomic Energy Agency, 2008.

[24] A. Miyakawa, "System start up test of the prototype fast breeder reactor MONJU," *JAEAR&D Review*, p. 21, 2006.

[25] H. Mochizuki, "Development of the plant dynamics analysis code NETFLOW++," *Nuclear Engineering and Design*, vol. 240, no. 3, pp. 577–587, 2010.

[26] Ansys Inc., Ansys Fluent 12.0 User's Guide, 2009.

[27] H. Mochizuki, M. Takano, and H. Yao, "Analysis of thermal stratification in the upper plenum of the "Monju" reactor vessel-effect of chamfer of flow hole on thermal stratification," in *Proceedings of the 14th International Topical Meeting on Nuclear Reactor Thermalhydraulics (NURETH '11)*, Toronto, Canada, 2011.